

Capacity Approaching Coding Strategies for Machine-to-Machine Communication in IoT Networks

Boulos Wadih Khoueiry

A Thesis
In the Department
of
Electrical and Computer Engineering

Presented in Partial Fulfillment of the Requirements
For the Degree of
Doctor of Philosophy at
Concordia University
Montreal, Quebec, Canada

March 2016

© Boulos Wadih Khoueiry, 2016

**CONCORDIA UNIVERSITY
SCHOOL OF GRADUATE STUDIES**

This is to certify that the thesis prepared

By: **Boulos Wadih Khoueiry**

Entitled: **Capacity Achieving Coding Strategies for Machine-to-Machine
Communication in IoT Networks**

and submitted in partial fulfillment of the requirements for the degree of

DOCTOR OF PHILOSOPHY (Electrical and Computer Engineering)

complies with the regulations of the University and meets the accepted standards with respect to originality and quality.

Signed by the final examining committee:

_____Chair
Dr. C. Assi

_____External Examiner
Dr. F. Labeau

_____External to Program
Dr. H. Harutyunyan

_____Examiner
Dr. W. Hamouda

_____Examiner
D. Y. R. Shayan

_____Thesis Supervisor
Dr. M. R. Soleymani

Approved by

Dr. A. R. Sebak, Graduate Program Director

March 2016

Dr. A. Asif, Dean
Faculty of Engineering and Computer Science

Abstract

Capacity Approaching Coding Strategies for Machine-to-Machine Communication in IoT Networks

Boulos Wadiah Khoueiry, Ph.D.

Concordia University, 2016

Radio access technologies for mobile communications are characterized by multiple access (MA) strategies. Orthogonal MA techniques were a reasonable choice for achieving good performance with single user detection. With the tremendous growth in the number of mobile users and the new internet of things (IoT) shifting paradigm, it is expected that the monthly mobile data traffic worldwide will exceed 24.3 exabytes by 2019, over 100 billion IoT connections by 2025, and the financial impact of IoT on the global economy varies in the range of 3.9 to 11.1 trillion dollars by 2025. In light of the envisaged exponential growth and new trends, one promising solution to further enhance data rates without increasing the bandwidth is by increasing the spectral efficiency of the channel. Non-orthogonal MA techniques are potential candidates for future wireless communications. The two corner points on the boundary region of the MA channel are known to be achievable by single user decoding followed by successive decoding (SD). Other points can also be achieved using time sharing or rate splitting. On the other hand, machine-to-machine (M2M) communication which is an enabling technology for the IoT, enables massive multipurpose networked devices to exchange information among themselves with minor or no human intervention.

This thesis consists of three main parts. In the first part, we propose new practical encoding and joint belief propagation (BP) decoding techniques for 2-user MA erasure channel (MAEC) that achieve any rate pair close to the boundary of the capacity region without using time sharing nor rate splitting. While at the encoders, the corresponding parity check matrices are randomly built from a half-rate LDPC matrix, the joint BP decoder employs the associated Tanner graphs of the parity check matrices to iteratively recover the erasures in the received combined codewords. Specifically, the joint decoder performs two steps in each decoding iteration: 1) simultaneously and independently runs the BP decoding process at each constituent sub-graph to recover some of

the common erasures, 2) update the other sub-graph with newly recovered erasures and vice versa. When the number of erasures in the received combined codewords is less than or equal to the number of parity check constraints, the decoder may successfully decode both codewords, otherwise the decoder declares decoding failure. Furthermore, we calculate the probability of decoding failure and the outage capacity. Additionally, we show how the erasure probability evolves with the number of decoding iterations and the maximum tolerable loss. Simulations show that any rate pair close to the capacity boundary is achievable without using time sharing.

In the second part, we propose a new cooperative joint network and rateless coding strategy for machine-type communication (MTC) devices in the multicast settings where three or more MTC devices dynamically form a cluster to disseminate messages between themselves. Specifically, in the basic cluster, three MTC devices transmit their respective messages simultaneously to the relay in the first phase. The relay broadcasts back the combined messages to all MTC devices within the basic cluster in the second phase. Given the fact that each MTC device can remove its own message, the received signal in the second phase is reduced to the combined messages coming from the other two MTC devices. Hence, this results in exploiting the interference caused by one message on the other and therefore improving the bandwidth efficiency. Furthermore, each group of three MTC devices in vicinity can form a basic cluster for exchanging messages, and the basic scheme extends to N MTC devices. Furthermore, we propose an efficient algorithm to disseminate messages among a large number of MTC devices. Moreover, we implement the proposed scheme employing practical Raptor codes with the use of two relaying schemes, namely amplify and forward (AF) and de-noise and forward (DNF). We show that with very little processing at the relay using DNF relaying scheme, performance can be further enhanced. We also show that the proposed scheme achieves a near optimal sum rate performance.

In the third part, we present a comparative study of joint channel estimation and decoding of factor graph-based codes over flat fading channels and propose a simple channel approximation scheme that performs close to the optimal technique. Specifically, when channel state information (CSI) is not available at the receiver, a simpler approach is to estimate the channel state of a group of received symbols, then use the approximated value of the channel with the received signal to compute the log likelihood ratio. Simulation results show that the proposed scheme exhibits about 0.4 dB loss compared to the optimal solution when perfect CSI is available at the receiver.

To my wife Nancy, my sons Wadih Jr., and Christiano, and my daughter Zoé.

Acknowledgments

First and foremost, I would like to express my deepest gratitude to my supervisor, Prof. M. Reza Soleymani, for giving me the opportunity to work with his group. This dissertation could not have been written without Prof. Soleymani who not only served as my academic advisor but also as a Father who encouraged and supported me throughout my Ph.D. program. I extremely appreciate his guidance and approach to the fundamental problems of Communication. His knowledge, patience, enthusiasm and perfectionism made this thesis possible. I must admit that I learnt uncountable things from Prof. Soleymani, particularly, his research methodology and being independent. I would like to thank prof. Soleymani for always being available to listen and to provide insightful advice. Prof. Soleymani will remain a real friend for many years to come.

I also would like to express my sincere thanks to all members of my Ph.D. committee, Prof. Hovhannes A. Harutyunyan, Prof. Walaa Hamouda, and Prof. Yousef R. Shayan. I appreciate their valuable comments, advice and suggestions throughout my Ph.D. program and the valuable time they spent reading this thesis. My special thanks go to the external examiner, Prof. Fabrice Labeau from McGill University for thoroughly reading my thesis and providing many helpful comments and insights. I also would like to thank all current and previous members of the wireless and satellite communications laboratory at Concordia University for the fruitful discussion and support. Furthermore, I would like to thank NSERC CRD as well as InterDigital Canada LTD., and PROMPT.

This thesis is also dedicated to the memory of my Father Wadih, whom I lost during the first year of my Ph.D. program and would have been proud of me. I would like to thank my Mother Mounira for her constant, unconditional love and support.

Last but not least, I also would like to thank my beloved wife Nancy who is not only the love of my life, but also my best friend, for her unlimited support. I would have not been where I stand at the moment without her love, encouragement and limitless sacrifices. Furthermore, I would like to thank my sons Wadih Jr. and Christiano, and my daughter Zoé for being very patient with Dad who has been most of the time busy with his Ph.D. I promise you all a better life.

Contents

List of Tables	x
List of Algorithms	xi
List of Figures	xii
List of Symbols	xiv
List of Acronyms	xvii

1	Introduction.....	1
1.1	Motivation.....	1
1.2	Problem Statement.....	5
1.3	Literature Review.....	7
1.3.1	Multiple Access Erasure Channel.....	7
1.3.2	Machine-to-Machine Communication.....	8
1.3.3	Joint Channel Estimation and Raptor Decoding Over Fading Channel.....	11
1.4	Thesis Contributions	12
1.5	Thesis Outline	14
2	Background.....	16
2.1	Introduction.....	16
2.2	Single User communication Channel.....	16
2.3	Multiple Access Channel	18
2.3.1	Capacity Region for The Multiple Access Channel	19
2.3.2	Gaussian Multiple Access Channel	20
2.4	Successive Interference Cancellation	24
2.5	Relay Channel.....	25
2.5.1	Relaying Strategies	26
2.6	The Multi-Way Relay Channel.....	30
2.7	Network Coding and Physical Layer Network Coding	30
2.8	Low Density Parity Check Codes	31

2.9	Raptor Codes.....	36
2.10	Cognitive Radio	39
2.11	Internet of Things.....	41
2.12	Conclusion.....	44
3	Joint LDPC Decoding for the 2-User Multiple Access Erasure Channel.....	45
3.1	Introduction.....	45
3.2	System Model	47
3.3	Proposed Coding Strategy for 2-user Multiple Access Erasure Channel	48
3.3.1	Proposed Coding Scheme – Method 2.....	49
3.3.2	Outage Capacity.....	52
3.3.3	Simple Example of the Proposed Coding Scheme Using (7,4) Hamming Codes....	53
3.4	Implementation of The Proposed Coding Scheme	55
3.4.1	Encoding at the Sources.....	55
3.4.2	Decoding at the Destination.....	56
3.4.2	A Simple Example.....	58
3.5	Simulation Results and Discussion.....	60
3.5.1	Construction of Half-Rate LDPC matrix.....	61
3.5.2	Encoding Techniques for Both Methods	62
3.5.3	Decoding Algorithm for Method 1	64
3.5.4	Decoding Algorithm for Method 2	64
3.5.5	Simulation Results	67
3.5.6	Discussion	70
3.6	Conclusion	72
4	A Novel Machine-to-Machine Communication Strategy Using Rateless Coding for the Internet of Things.....	74
4.1	Introduction.....	74
4.2	System Model	75
4.3	Proposed Coding Strategy for MTC devices	78
4.3.1	Cluster with Three MTC Devices	78
4.3.2	Aggregated Cluster with N MTC Devices.....	83

4.4	DNF Relaying Scheme	89
4.4.1	A simple De-noising Strategy	89
4.4.2	Decision Regions and De-noise Mapping.....	90
4.5	Simulation Results and Discussion	91
4.5.1	Mechanism to Assign Transmission Rates for MTC Devices	93
4.5.2	System Performance in the Noiseless Scenario	94
4.5.3	System Performance in the Presence of Noise with AF and DNF Relaying Schemes	96
4.5.4	Performance Comparison of the Proposed Strategy with Existing Schemes	102
4.6	Conclusion and Future Work	107
5	Joint Channel Estimation and Raptor Decoding Over Fading Channels	109
5.1	Introduction	109
5.2	Channel and System Models.....	111
5.3	Channel Estimation Schemes.....	112
5.3.1	MAP and ML Channel Estimation Schemes	112
5.3.2	Proposed Channel Approximation Scheme	113
5.3.3	Time Complexity Analysis of Proposed and Existing Schemes	115
5.4	Simulation Results and Discussion	116
5.4.1	Performance Evaluation with LDPC Codes	116
5.4.2	Performance Evaluation with Raptor Codes	118
5.5	Conclusion and Future Work	121
6	Conclusion and Future Directions	123
6.1	Conclusion	123
6.2	Future Directions	127
	Bibliography	129

List of Tables

3.1	Four equally likely possible combinations at the destination	49
3.2	Recovered bits after each decoding iteration	61
3.3	Actual normalized degree distribution pairs for codeword length 10^4	63
4.1	Transmission rates configuration during phase one.....	81
4.2	Formation of basic and logical clusters of the example in Fig. 4.3	85
4.3	Adaptive rate transmission mechanism between MTC devices	92
4.4	Comparison between various schemes	105

List of Algorithms

3.1	Simulation Algorithm for Coding scheme Method 2	65
-----	---	----

List of Figures

2.1	AWGN channel.....	17
2.2	Gaussian and BPSK constellation constrained over the AWGN channel	18
2.3	Multiple Access Channel	19
2.4	Capacity region for the MAC	20
2.5	Gaussian multiple access channel.....	21
2.6	Capacity region for the GMAC with FDMA and TDMA	22
2.7	Successive interference cancellation technique for two sources	23
2.8	Capacity region for two user multiple access erasure channel with successive interference cancellation	24
2.9	Relay Channel.	25
2.10	De-noise and forward relaying scheme for two way relay channel.....	27
2.11	Bidirectional relaying schemes.....	29
2.12	Tanner Graph representation for the parity check matrix H	33
2.13	Raptor Codes.....	37
2.14	Smart city supported by MTC devices with interconnected users, surveillance systems, traffic lights, vehicles, roads, railways, sensor devices and servers via telecommunication infrastructures	42
3.1	System Model	47
3.2	Binary erasure channel with erasure probability ϵ , considering source 2	48
3.3	Probability of decoding failure as a function of the erasure in the channel ϵ	51
3.4	Outage Capacity.....	53
3.5	LDPC matrix for the half-rate code in the implementation example.....	57
3.6	Two-user decoding technique using both Tanner sub-graphs. Erasures are orange variable nodes	59
3.7	Sum rate as a function of probability of decoding failure	66
3.8	Outage Capacity.....	67
3.9	Erasure probability evolving with the number of decoding iterations.....	68
3.10	Threshold as a function of the design rate	69

4.1	Three MTC devices in proximity exchanging messages via a relay	76
4.2	Two phase proposed coding scheme for a cluster with three MTC devices.....	79
4.3	MTC strategy with clustering technique of dimension $N=27$	84
4.4	Logical cluster 1 of degree 2.....	86
4.5	Decision regions and de-noise mapping for the proposed DNF relaying strategy	90
4.6	BER vs. overhead for unit-rate and half-rate messages	94
4.7	Average rate as a function of simulation overhead ϵ_{sim}	95
4.8	Overhead as a function of the data block length k	96
4.9	BER as a function of the average SNR for various achievable rate R with AF and DNF relaying schemes.....	97
4.10	Sum rate as a function of the average SNR with AF and DNF relaying schemes.....	98
4.11	Overhead vs. SNR for half-rate and unit-rate messages	100
4.12	Traditional communication strategy over one TS.....	102
4.13	FDF coding scheme for three MTC devices	103
4.14	Performance comparison between different schemes.....	106
5.1	System Model	110
5.2	Complexity Analysis of Proposed and Existing Schemes	115
5.3	Joint channel estimation and LDPC decoding over block fading channel with $f_d T_s = 0.05$ and $K = 1320$ using Jakes' channel model	117
5.4	Joint channel estimation and Raptor decoding over block fading channel with $f_d T_s = 0.05$ and $K = 9800$ using Jakes' channel model	118
5.5	Joint channel estimation and Raptor decoding over block fading channel with $f_d T_s = 0.05$ and $K = 9800$ using AR(1) approximated channel model.....	119
5.6	Joint channel estimation and Raptor decoding over block fading channel with $f_d T_s = 0.01$ and $K = 9800$ using Jakes' channel model	120

List of Symbols

C	Channel Capacity
C_P	Rate of the pre-code
C_β	Outage Capacity
C_{BPSK}	BPSK Constrained Channel Capacity
C	Raptor Pre-code
d	Degree of a sub-cluster
D	Destination
$\Omega(x)$	LT Degree Distribution
I	Mutual Information
l_{avg}	LDPC Average variable degree
r_{avg}	LDPC Average Check degree
$\rho(x)$	LDPC Right Degree Polynomial
$\lambda(x)$	LDPC Left Degree Polynomial
$R(\lambda, \rho)$	LDPC Design Rate
(Λ, P)	LDPC normalized degree distribution pair from a node perspective
(λ, ρ)	LDPC normalized degree distribution pair from an edge perspective
p_l^{BP}	Probability of Erasure under BP algorithm after l iterations
$\epsilon^{BP}(\lambda, \rho)$	LDPC maximum Tolerable Loss
$\delta(\lambda, \rho)$	LDPC Multiplicative Gap
$E[.]$	Expected Value
E_s	Energy per Symbol
E_b	Symbol Energy
\mathcal{F}	Finite Field
$f_d T_s$	Normalized fade Rate
G	Generator Matrix
$g(X)$	Generator Polynomial
h	Channel fading coefficient

$\hat{h}_{i,MAP}$	MAP Estimation of the channel coefficient
$\hat{h}_{i,ML}$	ML Estimation of the channel coefficient
k	Source Message Length
α	Time Fraction
β	Probability of Decoding Failure Target
γ	Amplification Coefficient to Maintain Power Constraint at the Relay
ε	Raptor Overhead
$\varepsilon_{0.5}$	Half Rate Raptor Overhead
ε_1	Unit Rate Raptor Overhead
ε_{sim}	Simulation Raptor Overhead
ϵ	Erasure Probability
σ	Gaussian Noise Standard Deviation
H	Parity Check Matrix
L_c	Channel Reliability Value
m	Number of Parity Check equations
m_{io}	Message passed From Input to Output Nodes in BP
m_{oi}	Message passed From Output to Input Nodes in BP
m_r	Message at the relay
n	Codeword Length
P	Input Power Constraint
P_F	Probability of Decoding Failure
R	Achievable Rate
S	Binary Source
T	Decision Region Borderline
u	Encoded Message at Source 1
v	Encoded Message at Source 2
W	Channel Bandwidth
w_c	Column weight
w_r	Row weight
x	Channel Input

\hat{x}	Estimated Encoded Message
x_R^{DNF}	Channel Input when DNF relaying scheme is used in the BC phase
x_R^{AF}	Channel Input when AF relaying scheme is used in the BC phase
y	Channel Output
z	Circular Symmetric Complex Gaussian Noise
Z_o	Channel Output LLR

List of Acronyms

3GPP	Third Generation Partnership Project
AF	Amplify and Forward
AP	Access Point
AR	Autoregressive
AWGN	Additive White Gaussian Noise
BEC	Binary Erasure Channel
BER	Bit Error rate
BP	Belief Propagation
BPSK	Binary Phase Shift Keying
BS	Base Station
BSC	Binary Symmetric Channel
CADF	Combined Amplify and Decode Forward
CC	Constellation Constrained
CDMA	Code Division Multiple Access
CF	Compress and Forward
CR	Cognitive Radio
CSCG	Circular Symmetric Complex Gaussian
CSI	Channel State Information
D2D	Device to Device
DDP	Degree Distribution Pair
DE	Density Evolution
DF	Decode and Forward
DNF	De-Noise and Forward
DNF-AF	DNF and AF Selection Relaying Scheme
DoF	Degrees of Freedom
EB	Exabyte
FCC	Federal Communications Commission
FDF	Functional Decode and Forward

FDMA	Frequency Division Multiple Access
FEC	Forward Error Correction
FER	Frame Error Rate
GMAC	Gaussian Multiple Access Channel
HD	High Definition
IDMA	Interleave Division Multiple Access
IoE	Internet of Everything
IoT	Internet of Things
IoV	Internet of Vehicle
LDPC	Low Density Parity Check
LLR	Log Likelihood Ratio
LT	Luby Transform
LTE	Long Term Evolution
M2M	Machine-to-Machine
MA	Multiple Access
MAC	Multiple Access Channel
MAEC	Multiple Access Erasure Channel
MANET	Mobile Ad Hoc Networks
MAP	Maximum a Posteriori
MIMO	Multiple Input Multiple Output
ML	Maximum Likelihood
MMSE	Minimum Mean Square Error
MS	Mobile Station
MTC	Machine-Type Communication
MUD	Multi User Detection
MWRC	Multi Way Relay Channel
NC	Network Coding
NOMA	Non Orthogonal Multiple Access
OFDMA	Orthogonal Frequency Division Multiple Access
P2P	Peer to Peer
PNC	Physical-Layer Network Coding

PSK	Phase Shift Keying
Raptor	Rapid Tornado
RFID	Radio Frequency Identification
RRH	Remote Radio Head
SIC	Successive Interference Cancellation
SINR	Signal to Interference plus Noise Ratio
SNR	Signal to Noise Ratio
SD	Successive Decoding
TCMA	Trellis Coded Multiple Access
TDMA	Time Division Multiple Access
TS	Time Slot
UE	User Equipment
V2V	Vehicle to Vehicle
Wi-Fi	Wireless Fidelity
XOR	modulo 2 Addition

Chapter 1

Introduction

The internet of things (IoT) is a network that encompasses devices, physical objects, buildings, and other items which are equipped with sensing, processing and networked capabilities to collect and exchange data [1]. More precisely, IoT is the point in time when more things or objects were connected to the internet than people [2]. In this Chapter, we first present the motivation for the proposed research and present some projections over the next decade in terms of the number of connected devices, mobile data rates and the IoT global impact on the economy. Then, we define the problem that we try to tackle in this thesis, followed by a literature review on closely related work. Then, we illustrate the major contribution of the thesis and finally we conclude this chapter with the thesis outline.

1.1 Motivation

Wireless communication network is one of the fastest growing and most dynamic sectors worldwide. IoT is an emerging and promising subject from social, economic and engineering perspectives. IoT was born between 2008 and 2009 [2]. IoT will be the largest and most widely spread global network where consumer electronics, vehicles, wearable micro devices, sensors and other multipurpose devices with powerful data processing capabilities are being connected to each

other or to central servers via the internet or/and telecommunication operators. The advancements in pervasive computing power, electronic miniaturization and networking have made the implementation of IoT closer to reality more than ever. Researchers have anticipated a potential impact of IoT on the existing internet and telecommunication operators' infrastructures and the economy worldwide over the next few years. While Cisco [2] projects more than 24 billion connected devices to the internet by 2019, Huawei [3] predicts 100 billion IoT connections by 2025. Economically, McKinsey Global Institute [4] forecasts that the financial impact of IoT on the global economy varies in the range of 3.9 to 11.1 trillion dollars by 2025. Furthermore, Cisco [2] predicts that the monthly global mobile data traffic will surpass 24.3 Exabyte (EB) by 2019, the average global mobile connection speed will surpass 2 Mbps by 2017, and more traffic will be offloaded from cellular networks by 2017.

Mobile applications are continuously evolving and growing, leading to a large demand for higher data rates which also implies increasing requests for spectrum resources. A quick review of the spectrum bands shows that some bands are underutilized or unoccupied most of the time [5]. Cognitive radio (CR) technique [6] has been proposed as a potential solution to enhance spectrum usage efficiency.

On the other hand, with this tremendous growth every day in wireless devices, the IoT biggest network will comprise a massive number of heterogeneous machine-to-machine (M2M) namely machine-type communication (MTC) devices [7-10] worldwide with low or no mobility that attempt to exchange data between themselves or to deliver them to business servers. These intelligent devices will be equipped with networked and real time processing capabilities to reduce the burden of gathering large amount of data and processing delay.

Furthermore, the increasing demand for mobile popular applications, like social networking, peer-to-peer (P2P) file sharing, video streaming or multicasting, and so on, requires an enormous traffic flow and puts tremendous pressure on long term evolution (LTE) core networks and air interface resources. Device-to-device (D2D) communication has evolved as a promising key technology in the next generation of LTE networks [11]. D2D communication in the LTE framework is a potential and reliable candidate to develop the IoT largest network. D2D communication offers several performance benefits [12-15]. Firstly, due to the fact that devices are naturally in vicinity, it is more efficient for these devices to communicate directly with each other instead of going through the central station. This way, users' equipment (UEs) save energy, reduce latency, enhance resource utilization, offload traffic from central station, enhance frequency reuse factor and increase network capacity. Secondly, devices can transmit at higher data rates due to the short range direct communication (excellent channel quality) underlying the central station and also can extend the service coverage. Thirdly, D2D communication opens a brand new market for novel P2P services including social networking applications, local advertisement and so on.

Additionally, perfect CSI availability at the receiver is necessary for iterative decoders [16-18] in order to achieve near Shannon capacity limit performance over Rayleigh flat fading channels. Practically, receivers do not possess perfect CSI and consequently some estimation/approximation for CSI is required. The optimum technique is to jointly perform channel estimation and decoding. However, this approach exhibits high complexity and delay at the receiver. With the recent advances in iterative decoding algorithms, iterative receivers have been designed to properly perform with reasonable computational complexity on factor graphs [19]. Such graphical models enable efficient computation of marginal distributions through the sum product algorithm [20-22]. One way to estimate the channel is by transmitting known pilot symbols at a specific period. This

allows the receiver to estimate the channel and eventually to compute the log likelihood ratio (LLR) at the decoder. The drawback of such a technique is the overhead incurred from transmission of dummy data known at both sides of the communication link.

In this thesis, we will show that the interference resulting from coexistence of radio devices can be exploited to improve the overall bandwidth efficiency of a communication channel. Interference management techniques are mainly divided into the following categories: 1) avoiding interference by using orthogonal channels, 2) treating the interference as noise, 3) exploiting interference by decoding it. The first technique is used when the power of interference is equivalent to the wanted signal. This results in dividing the degrees of freedom (DoF) of the channel among the users. The second technique is used when the level of interference is weak. Then single user decoding is applied. When treating interference as noise, the information contained in the interference is lost. This reduces the overall throughput. The first two techniques, which are conventionally used in practice, result in an inefficient use of resources. Alternatively, exploiting interference is used when the interfering signal is stronger than the desired signal. Decoding the interfering signal first, then applying successive interference cancellation (SIC) [23], the desired signal is then decoded interference free [24].

The main motivation behind this thesis is to propose coding strategies that exploit the interference in the channel to increase the spectral efficiency and therefore the data rates. Those strategies employ state of the art efficient coding techniques to achieve any rate pair close to the capacity boundary region. Another core motivation is the unstoppable future of IoT where a massive number of MTC devices seek connectivity to exchange information. In this context, the LTE network is an existing infrastructure and a potential communication technology for IoT framework. Therefore, we aim to propose several coding strategies that increase the efficiency of the channel.

1.2 Problem Statement

In light of the above new communication shifting paradigm, some fundamental solutions are required to increase rates without increasing spectrum band regardless the promising efficiency of CR technology. The common approach to increase data rates without increasing spectrum band is by increasing the bandwidth efficiency of the traditional communication channel where another source is allowed to simultaneously transmit using the same channel bandwidth. This idea although looks simple, exhibits many challenges. The main challenge is the interference caused by one source on the other which results in more complex decoding techniques [25-26]. The channel model where two sources simultaneously transmit to the same destination is called 2-user MA channel (MAC) [23]. In this channel each source has an independent message to transmit to the destination. It is assumed that the sources are also independent. In the uncoded and noiseless case, the destination receives both streams from the two sources simultaneously. In this scenario, the channel is called 2-user MAEC. In a MAEC and with the fact that each source transmits equally likely binary data $\{0, 1\}$, the combined stream at the destination contains three possible values $\{0, 1, 2\}$ with respective probabilities $\{1/4, 1/2, 1/4\}$. When the received signal is in the subset $\{0, 2\}$, the destination knows that both sources transmitted similar binary data. However, when received signal is in the subset $\{1\}$, the destination knows that both sources have transmitted opposite binary data and cannot identify what each source sent. Therefore, 50 % of the received stream on average is erased or lost. To solve this problem, a half rate code is required to recover the erased data.

The basic coding scheme for the two-user MAEC is to independently encode each data source with a half-rate code, then at the destination, the receiver also independently decodes both codewords. This scheme achieves a sum rate of at most 1. An alternative and more efficient approach is to encode one of the data sources at half-rate while the other source transmits at unit-rate (uncoded

stream). At the destination, the receiver decodes the half-rate codeword first, then applies successive decoding (SD) [23] to recover the uncoded stream interference free [24]. This scheme achieves the two corner points of the capacity region and other points can be also achieved using time sharing [23]. What if any source i for $i = \{1,2\}$ wants to transmit at any rate $0.5 < R_i < 1$ such that $R_1 + R_2 \leq 1.5$ to achieve any point on the capacity region without time sharing no rate splitting [27]. The response to this question is in the proposed coding strategy in Chapter three.

On the other hand and in the IoT framework, MTC devices exchange messages with other nearby devices or servers. Devices can be any radio frequency identification (RFID) devices, fixed or mobile sensors, and mobile cellular users and so on. In the LTE context, an interesting application on mobile devices is the download of popular videos. In a group of a few mobile cellular users, each user equipment (UE) can download part of the popular video, then the rest of the group exchange their parts between each other by establishing D2D communication links, so at the end, each UE gets the full video. This reduces the traffic on the downlink and creates load balancing where each part of the popular video is downloaded once by a different UE. In a broader scope, MTC devices exchange short length messages between nearby MTC devices with possible in-network processing to reduce the amount of gathered data transferred to hosting servers. Therefore, efficient coding strategies in the multicast settings are required for M2M communication devices. Consider the scenario where a group of three MTC devices in a cluster want to exchange their messages. In the conventional approach, one MTC device is active at a time while the other two MTC devices are silent. So the conventional scheme requires three time slots (TSs) to multicast 3 bits, hence this scheme is not efficient. Instead, we propose, in Chapter four, an efficient cooperative coding strategy for a large number of MTC devices in the multicast setting where devices in proximity may exchange messages with each other via a relay.

On the other hand and in the context of channel estimation, the approximation of the CSI at the receiver can be alternatively performed using the received information symbols instead of sending additional known redundant pilot symbols which reduces the overall rates. In this framework, we propose, in Chapter five, a new simple and robust approach to approximating channel coefficients at the receiver without using pilot-aided techniques. The main advantage of this method is that it does not need transmission of pilot symbols, nor extra coded bits for yielding the same performance compared to other techniques.

1.3 Literature Review

1.3.1 Multiple Access Erasure Channel

The binary erasure channel (BEC) which was introduced by Elias [28] in 1954 models a binary source transmitting data over an imperfect channel in which some of the bits are erased or completely lost. Because of several reasons, packets may be lost or erased over the network and never reach the final destination. Erasure correcting codes [29-30] made reliable communication possible over BEC. Specifically, the source is encoded with a linear erasure code. If some bits are lost during transmission, the decoder is able to recover the erased bits. The capacity of the BEC [28] with erasure probability ϵ is $1 - \epsilon$. Elias showed that random codes with rates arbitrarily close to capacity are achievable with small error probability using Maximum likelihood (ML) decoding. In a single user communication, regular and irregular Turbo and low density parity check (LDPC) codes are investigated on the BEC in [17], [31-34]. Nested code, which is a coding approach for multi-user communication, consists of first encoding each message independently, then applying network coding (NC) to all encoded codewords. Nested codes were first introduced in [35] as a new joint network and channel coding approach to communication networks using convolutional codes.

The nested codes resulting from this technique can be decoded at various rates depending on the amount of prior knowledge each receiver possesses. While the nested encoder consists of XORing all the individually encoded codewords, the decoder calculates the LLR for each bit by simply applying the flipping operation.

The capacity of the 2-user MAEC is 1.5 bits per channel use [23]. The common decoding technique for 2-user MAEC is when one user transmits encoded data at half-rate while the other user transmits uncoded stream. At the destination, using single user decoding, the receiver decodes first the half-rate encoded codeword, then using SD to recover the uncoded stream interference free. This technique achieves the two corners on the capacity region. Other points can also be achieved using time sharing [23]. In this regards, Hagh et al. [36] showed that the two corners of the capacity region are achieved by encoding one source at half-rate using rateless codes while the other source transmits uncoded bits, then performing SIC can recover both data streams. They further showed that the other points on the boundary region can be achieved using time sharing.

1.3.2 Machine-to-Machine Communication

M2M has emerged as a promising technology enabling billions of multipurpose MTC devices to communicate with each other without human intervention [8-9], [37-38]. Another flavor of M2M communication is the device-to-device (D2D) communication which similarly refers to establishing direct communication links between devices. In the sequel, D2D or MTC will be used interchangeably.

D2D communication as an underlay to cellular networks raises many technical challenges, for example intra-cell interference management, device discovery, signaling overhead, clustering and multicasting cooperative schemes [39-40]. The authors in [41] discuss the recent advances in D2D from synchronization, discovery and communication perspectives and review the standardization

progress of D2D in 3GPP. Recent progress on channel modeling and measurements is discussed in [41-42]. A fundamental difference between D2D communications and mobile ad hoc networks (MANETs) is that D2D communications can be assisted by the central station for synchronization, device discovery, resource allocation and other overhead consuming functions that are extremely costly in a MANET. Additionally, D2D communication is an opportunistic, local and single hop communication where MANET consists of multi hop routing which degrades the overall performance. For comparison of short range wireless transmission techniques, we refer the reader to [43, Table 1].

Several works have been done on D2D cluster based cooperative communications [44-48]. In [44], authors indicate that it is possible to enhance system capacity with D2D communications. Furthermore, they show that the more the cluster members are in vicinity to each other, the better is the performance. In [45], the authors propose an intra-cluster D2D transmission scheme with optimized resource utilization. They show that by iteratively partitioning clusters, the system throughput can be maximized. In [46], the authors propose a clustering strategy for D2D multicast communications. They derive the outage capacity of a single cluster and show that the proposed clustering strategy lowers the average transmission time effectively. In [47], the authors propose a dynamic D2D retransmission scheme which can adaptively select retransmission algorithm according to the network device's density. They show that this scheme achieves a good performance in terms of resource efficient utilization and interference avoidance. In [48], the authors propose a cooperative scheme to dynamically activate D2D links in order to select the optimal relay node while minimizing the number of active devices. They show that the number of necessary resources for multicast service delivery in the downlink reduces which results in offloading the downlink spectrum.

Resource allocation is an efficient technique to control and reduce interference caused by two or more wireless communication devices operating on the same channel [49-51]. In [49], the authors propose a joint CR based resource allocation and power control scheme for D2D communication underlying LTE networks in the multicast setting to improve system capacity. In [50], the authors propose two resource allocation schemes to mitigate interference among coexistent D2D pairs and improve system performance. In [51], the authors study the dynamic resource allocation technique for D2D communication and propose a service time prediction-based dynamic resource allocation mechanism for LTE networks.

Nested codes [35] are an effective channel coding technique to multicast information over multiple devices. The resulting nested codes can be decoded at different actual rates by different receivers that depend on the prior knowledge possessed by each receiver. In [52], the authors propose nested codes to improve D2D communication in the multicast settings.

Destination cooperation in interference channels is another flavor of D2D communication where one device can act as a relay for another device. In [53], the authors propose a cooperative communication scheme for two mobile users located in a common cell edge area. The main idea of the scheme is that both mobile users are opportunistically able to receive and decode each other's messages based on the signal-to-interference-plus-noise ratio (SINR). If one user has correctly decoded both own and other user messages, the user can cooperate by relaying the other user message. It was shown that this scheme achieves a diversity order of 2. The same authors propose an extension to this scheme [54] where cooperation may occur not only when both own and other device messages are received correctly, but when just own message is decoded correctly by relaying own message. This own message is considered as an interference from the other device's perspective. Due to the short distance between devices, the other device receives and decodes the

other device's message correctly, then removes it from the main received signal to recuperate its own message. It has been shown that the extended scheme achieves additional gain while maintaining the same diversity order of 2. The authors in [55] propose a cooperative coding scheme for three mobile users in vicinity underlaying LTE networks with raptor coding and amplify and forward (AF) relaying scheme.

1.3.3 Joint Channel Estimation and Raptor Decoding Over Fading Channel

Joint channel estimation and LDPC decoding over fading channels based on factor graphs are investigated in [56-59]. Jin et al. [56] consider a low complexity algorithm to iteratively estimate the continuous values of the fading levels and apply the density evolution (DE) method [60] to analyze its performance with LDPC decoding over a block fading channel. They show that using ML and maximum a posteriori (MAP) techniques, a threshold enhancement of 0.6-1.1dB is achieved for different sub-block lengths. Niu et al. [57] investigate two methods to handle continuous variables trying to overcome the high complexity updates based on Kalman filtering. 1) The first approach is used to approximate the complexity of message updates. 2) The second approach retains the message passing rules, but approximates the correlated Rayleigh fading channel by a first order autoregressive (AR) channel model. They show that soft decision feedback outperforms hard decision by about 0.8 dB for the filtering approach. They also compare optimal Wiener filtering with low pass filtering and Kalman smoothing. The latter approach reduces complexity at the expense of performance. Similar work is also investigated in [61] in the presence of interference. On the other hand, normalized min-sum algorithm can be used to reduce complexity in iterative channel estimation process [58]. In [58], Lin et al. show that by choosing an optimal normalization factor, the min-sum algorithm performs similar to the sum-product and is slightly worse compared to the case when perfect CSI is available.

Root-LDPC codes are specially designed for transmission over block-fading channels with sub-blocks, which results in full diversity property. Andriyanova et al. [59] propose joint channel estimation and decoding scheme for root-LDPC codes when CSI is not available at the receiver. They showed that full diversity can still be preserved when CSI is not available. Other techniques for estimating channel information at the receiver are based on pilot-assisted symbols where pilot symbols are inserted into the data stream [57, 62-63]. Valenti et al. [62] address pilot-aided iterative decoding and channel estimation for turbo codes BPSK system over Rayleigh fading channels. They showed that by iteratively estimating the channel and turbo decoding, significant enhancements can be achieved. They also showed the fact that the frequency of the pilot symbols determines the overall performance of the system. Kwon et al. [63] propose a method to encode the pilot symbols along with the information symbols using systematic encoding. They show the positive gain achieved from coded pilot symbols in contrast with uncoded pilot symbols. Majumder et al. [64] consider a joint Raptor decoding and channel estimation scheme based on the iterative decoding scheme for LDPC codes [56]. Their scheme performs about 0.7-1dB from the optimal case which behaves almost similarly to the ML scheme [56].

1.4 Thesis Contributions

With the above motivation and challenges, we propose in this thesis a number of coding strategies and relaying schemes for improving the bandwidth efficiency of MACs. The contributions to the thesis are summarized as follows:

- In the MAC framework, we propose a new practical encoding and joint belief propagation (BP) decoding techniques for the 2-user MAEC that achieve any rate pair close to the capacity region without time sharing nor rate splitting. While at the encoders, the corresponding parity

check matrices are randomly built from a half-rate matrix, the joint BP decoder employs the associated Tanner graphs of the parity check matrices to iteratively recover the erasures in the received combined codewords. Specifically, the joint decoder performs two steps in each decoding iteration: 1) simultaneously and independently runs the BP decoding process at each constituent sub-graph to recover some of the common erasures, 2) update the other sub-graph with newly recovered erasures and vice versa. When the number of erasures in the received combined codewords is less than or equal to the number of parity check constraints, the decoder may successfully decode both codewords, otherwise the decoder declares decoding failure. Furthermore, we calculate the probability of decoding failure and the outage capacity. Additionally, we show how the erasure probability evolves with the number of decoding iterations and the maximum tolerable loss.

- In the IoT perspective, we propose a new cooperative joint network and rateless coding strategy for MTC devices in the multicast settings where three or more MTC devices dynamically form a cluster to disseminate messages between themselves. Specifically, in the basic cluster, three MTC devices transmit their respective messages simultaneously to the relay in the first phase. The relay broadcasts back the combined messages to all MTC devices within the basic cluster. Given the fact that each MTC device can remove its own message, the received signal in the second phase is reduced to the combined messages coming from the other two MTC devices. Hence, this results in exploiting the interference caused by one message on the other and therefore improving the bandwidth efficiency. Furthermore, each group of three MTC devices in vicinity can form a basic cluster for exchanging messages, and the basic scheme extends to N MTC devices. The extended scheme is described in details in Chapter 4. Furthermore, we implement the proposed scheme employing practical Raptor codes with the

use of two relaying schemes namely AF and de-noise and forward (DNF). We show that with very little processing at the relay using DNF relaying scheme, performance can be further enhanced. We show that the proposed scheme achieves a near optimal sum rate performance.

- In the context of channel estimation, we propose a simple channel approximation scheme to estimate the CSI at the receiver. Specifically, when CSI is not available at the receiver, a simpler approach is to estimate the channel state of a group of received symbols, then use the approximated value of the channel with the received signal to compute the LLR.

1.5 Thesis Outline

The rest of the thesis is organized as follows:

In Chapter 2, we present a brief background about enabling techniques used in the proposed schemes. We start with an introduction to a single user communication channel, MAC channel, relay channel and multi-way relay channel, and then we define each of the used techniques and the related work that was done in the literature. We then introduce the concept of SD, NC and physical-layer NC. We also introduce LDPC codes and Raptor codes. We present the concept of CR. We then present the notion of device-to-device communications and the IoT and finally conclude the chapter.

In Chapter 3, we present the proposed coding scheme for 2-user MAEC. Specifically, we calculate the upper bound on the probability of decoding failure, and we show that if the number of erasures in the received combined codewords is greater than the number of parity check constraints, the decoder declares failure. Furthermore, we calculate the probability of decoding failure and the outage capacity. Additionally, we present an efficient encoding and joint decoding scheme based on the half-rate parity check matrix code. Using joint BP decoding at the destination, during each

iteration, two tasks are performed: 1) each constituent decoder is able to resolve some of the erasures in the received combined codewords, 2) the recovered bits by one decoder are automatically recovered at the other decoder. We also present the implementation of the coding scheme using LDPC codes. We also present the simulation results and we show that this scheme achieves any rate pairs close to the boundary region using joint decoding, without using SD nor time sharing and rate splitting.

In Chapter 4, we present the proposed coding strategy that considerably increases the efficiency of the channel in the multicast setting. Specifically, we consider a scenario where three M2M communication devices want to exchange their messages via a low cost relay or another device in proximity. The main advantage of the proposed scheme is twofold: 1) use of joint channel and physical-layer NC where MTC devices simultaneously transmit their messages, 2) no decoding at the relay, where relaying can be as simple as AF or DNF. Additionally, we present an efficient and scalable technique to disseminate information among a large group of MTC devices. Furthermore, we present the simulation results using practical rateless codes and we show that the proposed scheme achieves a near optimal sum rate performance.

In Chapter 5, we first present a comparative study of joint channel estimation and decoding of factor graph-based codes over flat fading channels. We also propose a simple channel approximation scheme to estimate the channel state at the receiver before carry on with iterative decoding. Using LDPC and Raptor codes, we present the simulation results and show that the proposed scheme performs close to the optimal solution when perfect channel state information is available at the receiver.

In Chapter 6, we conclude our work with a brief summary about the proposed coding strategies and their major advantages. Then, we suggest some potential extensions for future research directions.

Chapter 2

Background

2.1 Introduction

In this Chapter, we give a brief introduction about some concepts which will be used in later chapters. First we overview the basic single user communication channel, the MAC, the relay channel and the multi-way relay channel. Then, we take a look at some communication concepts which include SD, NC and physical-layer NC. Then, we explain some modern coding techniques including LDPC and Raptor codes. Later, we describe the concept of CR, and we explain the concept of (IoT) including the various communication models for the IoT, and finally, we conclude the chapter.

2.2 Single user communication Channel

The basic and fundamental channel model is the single user additive white Gaussian noise (AWGN) channel as depicted in Fig. 2.1. The i th output symbol y_i of this channel is the sum of the i th input symbol x_i and the i th Gaussian noise z_i .

$$y_i = \sqrt{P}x_i + z_i \quad (2.1)$$

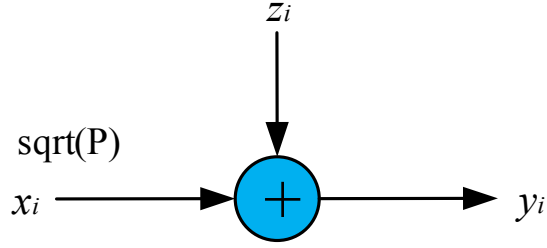


Fig. 2.1 AWGN channel

where P is a power constraint at the transmitter and z is a circular symmetric complex Gaussian random variable, $z \sim \text{CSCG}(0, \sigma^2)$ where $\frac{\sigma^2}{2}$ is the variance of the AWGN in each dimension.

The capacity of the AWGN channel with power constraint P and noise variance σ^2 is defined as [23]

$$C = \max_{E[X^2] \leq P} I(X; Y) \quad (2.2)$$

where I is the mutual information [65] between the input and the output of a Gaussian channel.

The solution of the maximization function gives the information capacity as [23]

$$C = \frac{1}{2} \log_2 \left(1 + \frac{P}{\sigma^2} \right). \quad (2.3)$$

When the input constellation is finite in size and the symbols from the input constellation are chosen with uniform distribution, I is referred to as Constellation Constrained (CC) capacity of the channel.

The capacity is achieved with Gaussian inputs to the channel. However in practice, this is not achievable. For instance, let us assume that the BPSK modulation is used with $P = 1$ and $\sigma^2 = 1$.

Then with the given power constraint, the channel input with equal probability is $x = \{-1, +1\}$.

Hence, the BPSK CC capacity of the channel is given by

$$C_{BPSK} = 1 - \frac{1}{2\sqrt{\frac{2\pi}{\sigma^2}}} \int_{-\infty}^{+\infty} \log_2(1 + e^{-u}) e^{-\frac{(u-2/\sigma^2)}{2/\sigma^2}} du. \quad (2.4)$$

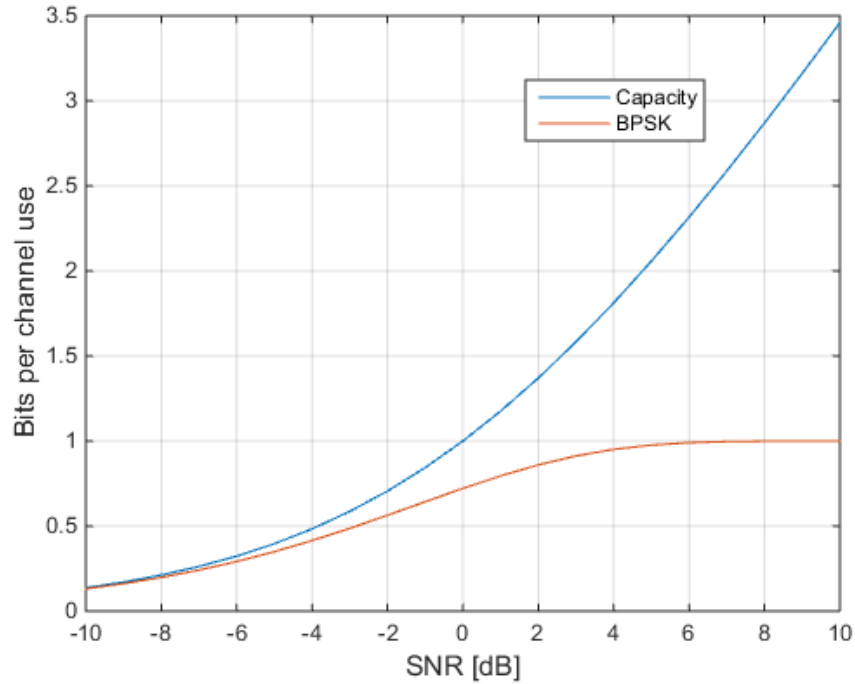


Fig. 2.2 Gaussian and BPSK constellation constrained over the AWGN channel

The capacity plot of the CC and Gaussian inputs over AWGN channel is illustrated in Fig. 2.2.

2.3 Multiple Access Channel

One of the most fundamentally interesting and widely encountered in real life scenarios is the MAC. MAC models a scenario where two or more users want to send messages to a common destination as illustrated in Fig. 2.3. Some practical examples include a group of independent mobile users communicates with a base station (BS), or a group of wirelessly equipped devices communicates with a common receiver, or various ground stations communicate with a satellite receiver. In general, MA techniques are classified into orthogonal and non-orthogonal methods [66]. In orthogonal schemes, signals from different users are orthogonal to each other and their cross correlation is zero. Several techniques have been used in practice to achieve orthogonality. i.e., time

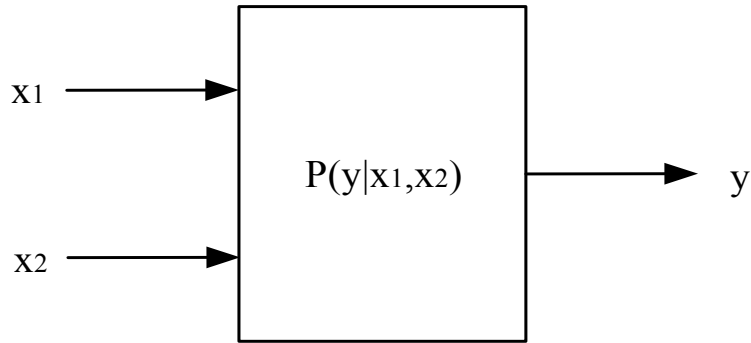


Fig. 2.3 The Multiple Access Channel where x_1 , x_2 , and y are channel inputs at source 1 and 2 and channel output respectively. $P(y|x_1, x_2)$ represents the probability transition matrix

division multiple access (TDMA), frequency division multiple access (FDMA), and orthogonal frequency division multiple access (OFDMA). The main advantage of the orthogonal approaches is the avoidance of co-channel interference. On the other hand, non-orthogonal methods allow a certain degree of non-zero cross correlation among signals from different users. These schemes include random waveform code division multiple access (CDMA) [67], trellis coded multiple access (TCMA) [68], and interleave division multiple access (IDMA) [69]. With the recent progress in multi-user detection (MUD) [25], it is demonstrated [66] that non-orthogonal methods have a spectral-power efficiency advantage over orthogonal techniques by exploiting the information contained in the interfered signals.

2.3.1 Capacity Region for the Multiple Access Channel

The capacity of a MAC is the closure of the convex hull of all achievable rate pairs (R_1, R_2) satisfying [23]

$$R_1 < I(X_1; Y|X_2) \quad (2.5)$$

$$R_2 < I(X_2; Y|X_1) \quad (2.6)$$

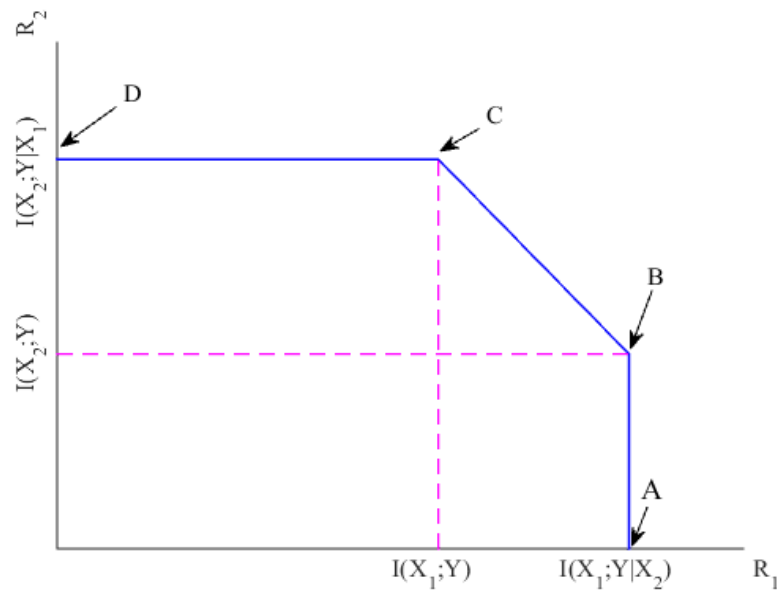


Fig. 2.4 Capacity region for the MAC

$$R_1 + R_2 < I(X_1, X_2; Y) \quad (2.7)$$

where X_1 , X_2 and Y are the channel input from user 1, the channel input from user 2, and the channel output, respectively. Fig. 2.4 shows the achievable region of a MAC for a fixed input distribution.

Point A corresponds to the maximum achievable rate from user 1 to the destination when user 2 is not sending any information. The point B corresponds to the maximum rate at which user 2 can send information as long as user 1 sends at his maximum rate. This is the rate that is obtained if X_1 is considered as noise for the channel from X_2 to Y . The receiver decodes X_2 codeword first, then can subtract its effect from the channel. Similarly for points C and D. The non-corner points between point B and point C can be achieved by time-sharing.

2.3.2 Gaussian Multiple Access Channel

The 2-user Gaussian MAC (GMAC) is depicted in Fig. 2.5 where two users communicate to a single destination. The i th received signal at the destination is given by

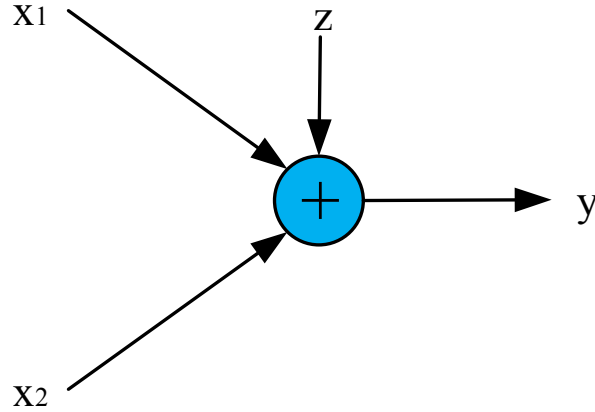


Fig. 2.5 Gaussian multiple access channel

$$y_i = \sqrt{P_1}x_{1i} + \sqrt{P_2}x_{2i} + z_i \quad (2.8)$$

where P_j is the power constraint at the j th transmitter for $j = \{1,2\}$ and z_i is the i th circular symmetric complex Gaussian random, $z_i \sim \text{CSCG}(0, \sigma^2)$ where $\frac{\sigma^2}{2}$ is the variance of the AWGN in each dimension. The capacity region of the GMAC is illustrated in Fig. 2.6 and similarly computed as the above general case which is the convex hull of the set of rate pairs satisfying (2.5)-(2.7) for some input distribution $f_1(x_1)f_2(x_2)$ and the total power constraints $E[X_1^2] \leq P_1$ and $E[X_2^2] \leq P_2$.

We define the channel capacity function as

$$C(u) \triangleq \frac{1}{2} \log_2(1 + u) \quad (2.9)$$

corresponding to the channel capacity of a Gaussian white noise channel with signal to noise ratio (SNR) u . Therefore, the upper bound on individual rates R_1 , R_2 and sum rate $R_1 + R_2$ are written as

$$R_1 \leq C\left(\frac{P_1}{\sigma^2}\right) \quad (2.10)$$

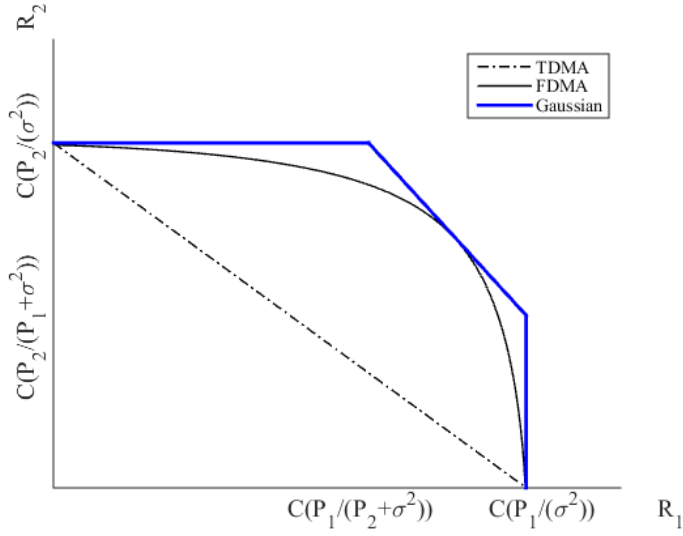


Fig. 2.6 Capacity region for the GMAC with FDMA and TDMA

$$R_2 \leq C\left(\frac{P_2}{\sigma^2}\right) \quad (2.11)$$

$$R_1 + R_2 \leq C\left(\frac{P_1 + P_2}{\sigma^2}\right) \quad (2.12)$$

These upper bounds are achieved when the input distributions are Gaussian. i.e., $X_1 \sim N(0, P_1)$ and $X_2 \sim N(0, P_2)$. The two corner points are achieved by means of single user decoding and SIC. In other words, the receiver first decodes the second user, considering the first user as part of the noise. Then, the second user is subtracted out and the first user can be decoded interference free. This process is called onion peeling [23]. In the general case when the number of users is N , the sum rate is $C\left(\frac{NP}{\sigma^2}\right)$ and the average rate per user is $\frac{1}{N}C\left(\frac{NP}{\sigma^2}\right)$. When the number of users N is very large, the sum rate is also large, however, the rate per individual user goes to zero.

In FDMA, the rates depend on the bandwidth allocated to each user. Consider the 2-user scenario with powers P_1 and P_2 using nonintersecting frequency bands with bandwidths W_1 and W_2 , where $W_1 = \alpha W$ and $W_2 = (1 - \alpha)W$ for $\alpha \in [0, 1]$. From the single user band limited channel capacity, the following rate pairs are achievable

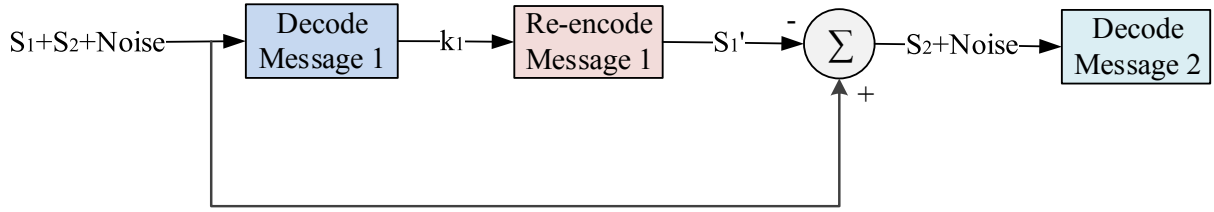


Fig. 2.7 Successive interference cancellation technique for two sources

$$R_1 = W_1 \log_2 \left(1 + \frac{P_1}{\sigma^2 W_1} \right) \quad (2.13)$$

$$R_2 = W_2 \log_2 \left(1 + \frac{P_2}{\sigma^2 W_2} \right) \quad (2.14)$$

As α varies from 0 to 1, the curve is plotted in Fig. 2.6. Note that the FDMA curve touches the boundary of the capacity region at one point corresponding to allocating bandwidth to each channel proportional to the power in that channel. Therefore, the bandwidth allocation is optimal when the allocated powers are proportional to the bandwidths.

In TDMA, each user is allocated a TS during which only that user is active. Consider the 2-user scenario, each with power P . The rate at which each active user transmits is $C \left(\frac{P}{\sigma^2} \right)$. If users have equal length and number of TS, the average achieved rate per user is $\frac{1}{2} C \left(\frac{P}{\sigma^2} \right)$. This system is called naïve TDMA. Since each user is silent half of the time on average, the power used on average is half. Therefore, we can allocate double the power to each active user and maintain the average power constraint P . With this modification, the average achieved rate per user is $\frac{1}{2} C \left(\frac{2P}{\sigma^2} \right)$. Furthermore, by varying the length of the slot and the instantaneous power allocated to each user, the same capacity region as FDMA can be achieved with different bandwidth allocations. On the other hand, CDMA achieves the entire capacity region, and in addition, allows new users to be added easily without changing the codes of the current users.

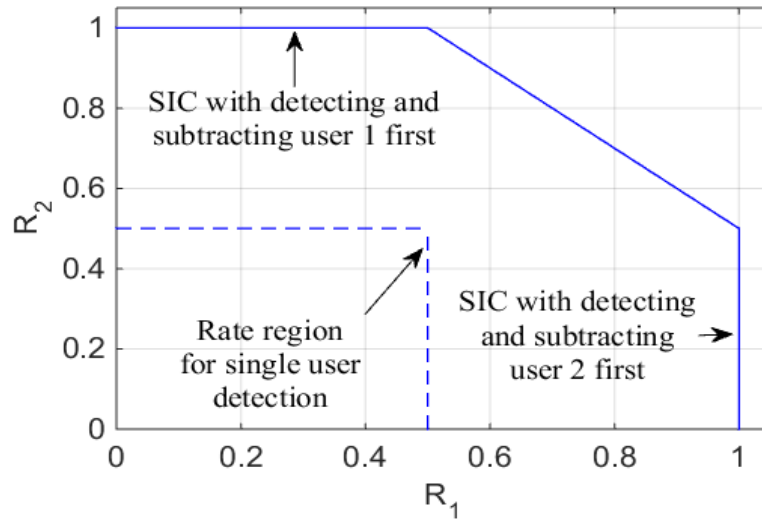


Fig. 2.8 Capacity region for two-user multiple access erasure channel with SIC.

2.4 Successive Interference Cancellation

SIC [23] is an iterative process that starts with the strongest coded signal first, decodes it and then re-encodes it. The second step is to subtract the re-encoded message from the original received signal, and then decode the remaining message interference free [24] as shown in Fig. 2.7. In other words, the decoding process consists of several single user decoders where the strongest signal is first decoded using single user decoding technique while considering the other interfering signals as noise. Then the decoded message is re-encoded and subtracted from the original message to remove its effect and so on, until the last message which is decoded interference free. Fig. 2.7 illustrates the SIC technique for the 2-user MAC where it is assumed that the power level of source 1 coded signal is higher than the power signal of source 2 coded signal. First, the source 1 message is successfully decoded, then re-encoded and subtracted from the original signal to get source 2 coded message with noise. Assuming that source 1 transmit at rate $R_1 = 1$, source 2 can send at a

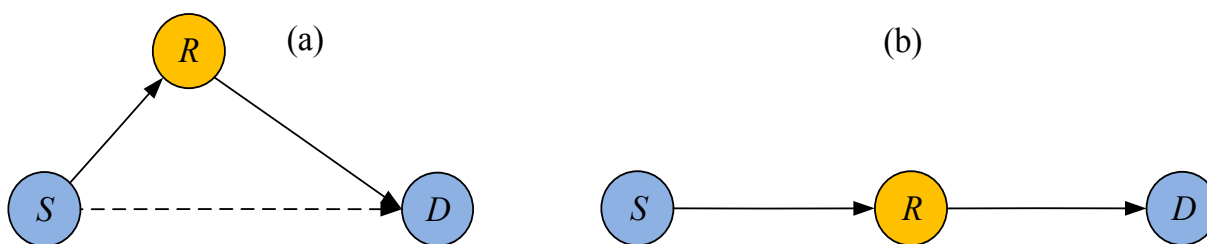


Fig. 2.9 Relay Channel. (a) Relay channel where dashed line represents the direct communication link. (b) A two-hop communication channel

rate R_2 up to 0.5 as shown in Fig. 2.8. At the destination, the decoder first applies SIC to decode the half-rate message and then decode the unit-rate message. Actually, this is the maximum achievable rate on such a channel. We have shown the capacity region for this scheme in Fig. 2.8. However, for the purpose of comparison, we have also added the region for single user detection.

2.5 Relay Channel

The three-terminal relay channel was introduced by van der Meulen [70] where lower and upper bounds on the capacity were discovered. Later, the bounds in [70] were significantly improved by Cover and El Gamal [71] where several coding strategies were introduced. These coding strategies are referred to as Decode-and-Forward (DF), Partial Decode-and-Forward (Partial-DF), and Compress-and-Forward (CF). Cover and El Gamal derived the cut-set upper bound on the capacity of the relay channel and established the capacity for the cases of degraded and reversely degraded relay channels. Cover and El Gamal also obtained a general lower bound on the capacity of the relay channel by combining partial DF and CF schemes. Capacity of the relay channel with feedback from the receivers to the transmitters is also studied in their work. Fig. 2.9 depicts the relay channel with and without direct communication link.

2.5.1 Relaying Strategies

In cooperative communication systems [72], the relay plays a central role in the performance of the overall system. The relay can be full or half duplex. In full duplex, the relay simultaneously transmits and receives communication signals, whereas in half duplex (more practical), the relay can either transmit or receive. The relaying strategies vary from amplifying and forwarding [73] the signal without any processing to completely regenerating the data and applying further processing [71]. Next, we briefly describe the relaying strategies.

Amplify and Forward

This is the simplest and traditional scheme that does not require processing at the relay. AF strategy was proposed for the Gaussian parallel or diamond relay channel by Schein and Gallager for the first time in [74] and in details in [75]. In their work an achievable rate region for diamond relay networks was presented using the combination of AF and DF. Performance of AF in wireless Gaussian channels is studied in [73]. A new achievable rate region for the Gaussian parallel relay channel is obtained in [76] using Combined Amplify-and-Decode Forward (CADF) scheme and it is shown that this scheme outperforms all previous techniques for their proposed network. In AF relaying scheme, the received signal is scaled by γ before is transmitted to the next hop. γ is the amplifier gain to maintain the average power constraint at the relay [73].

Decode and Forward

In DF, the relay first tries to decode the received signal to regenerate the original message [71]. If this process is successful, the relay re-encodes the recovered message to produce the original codeword. The relay then transmits the encoded message to the destination. Otherwise, the relay remains silent. Hence, the DF scheme retransmits reliable information to the next hop.

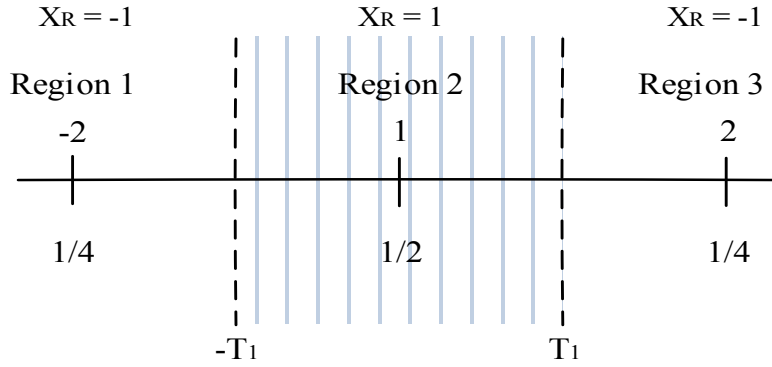


Fig. 2.10 Decision regions for the DNF relaying scheme in the case of a two-way relay channel

Compress and Forward

The CF scheme is mainly used when the relay destination link is bandwidth limited [71]. Similarly to the DF scheme, the CF scheme decodes first the received codeword to recover the original message. If the original message is correctly decoded, then the codeword is compressed or quantized before being transmitted.

De-Noise and Forward

The DNF scheme is a useful relaying strategy when the relay is not interested in decoding individual messages. DNF process detects the superposition of multiple signals at the relay and it does not decode individual messages, instead it removes completely the AWGN. The de-noising strategy [77], which was first introduced for wireless multi hop network, follows a certain mapping function to re-map the superposed signal into a symbol of the same constellation (that was used at the sources) instead of using joint decoding. Fig. 2.10 illustrates a simple example [77] of DNF for two communication devices with BPSK modulation where $X_1, X_2 = \{-1, 1\}$ are the modulated signals at each device, respectively. In AWGN channel, the received signal at the relay is $Y_R = X_1 + X_2 + Z_R$, where Z_R is the noise at the relay. In the noiseless scenario and in the MA phase, the received signal at the relay has three possible values $\{-2, 0, 2\}$. If $Y_R = \pm 2$, the relay knows

what each communication device has transmitted, however, if $Y_R = 0$ the relay cannot jointly decode both messages. Yet, the relay can apply DNF by mapping the received signal as follows. If $Y_R = \pm 2$, then $X_R = -1$, otherwise $X_R = 1$. The communication device interprets the received signal during the BC as follows. If the received signal is -1, this means that the other communication device has sent the same symbol as his. If the received signal is 1, the other device has sent the opposite of what this device has sent during the MA phase. The MAP optimal threshold T_1 in Fig. 2.10 is given by

$$T_1 = 1 + \frac{\sigma_R^2}{2} \ln(2) \quad (2.15)$$

Functional Decode and Forward

The idea of FDF scheme was first introduced in [78-79] for the two-way relay channel. Consider a two-way relay system where two users want to exchange messages via a relay. It is assumed that all nodes are half-duplex and therefore direct communication between users is not possible. The transmission strategy is over two stages. In the uplink stage, both users 1 and 2 simultaneously transmit their linearly encoded messages to the relay. The relay receives a noisy version of the sum of both codewords, i.e., $X_{12} = X_1 \oplus X_2$ where the sum is modulo 2. X_{12} is another codeword. Using error correcting codes [29-30], the relay decodes X_{12} and broadcasts it back to both users. Each user first removes its own message from the received codeword to recover the other user's message. The FDF scheme is also extended to more than two users [80] using TDMA.

The capacity results for the relay channel are only known for a few special cases. In [81] the capacity of a deterministic discrete memoryless relay channel where the relay's channel output is a deterministic function of the source's and its own channel inputs is presented. In [82] and [83] the capacity results for the degraded relay channel [71] are extended to multi-relay setup scenarios.

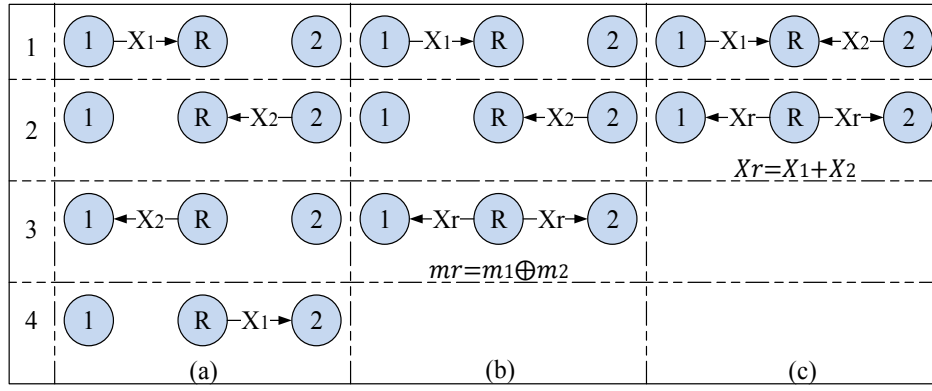


Fig. 2.11 Bidirectional relaying schemes: (a) Conventional relaying, (b) relaying with NC, (c) relaying with physical-layer NC

Results on the capacity of the relay channels with orthogonal transmit channels are presented in [84]. In [85] a new CF lower bound is presented. The authors used Wyner-Ziv [86] coding to reduce the rate required to transmit the information from the relay to the destination. A lower bounds on the capacity of Gaussian relay channel with orthogonal receive components is obtained in [87]. Upper and lower bounds on the outage capacity and ergodic capacity of the wireless relay channels in Rayleigh-fading environment is studied in [88]. A comprehensive study of DF and CF coding schemes for single and multi-user wireless relay networks can be found in [89]. Cover and Kim [90] and Kim [91] investigated the capacity of a class of relay channels called primitive relay channels. In these channels the relay can reliably communicate with the destination via a separate link at any rate up to a fixed rate of R_0 . The relay-destination channel is assumed separate so that communication over this link does not interfere with the source-destination communication. This assumption is useful in two phase communication protocols used in half-duplex relay channels [92 and references therein]. In [90] they established the capacity for the deterministic case where the relay's output is a deterministic function of the source's input and the destination's output of the channel using Hash-and-Forward (HF) technique and showed that CF coding scheme can also achieve the capacity. In [91] Kim used Slepian-Wolf theorem [93] and time-sharing to achieve the capacity.

2.6 The Multi-Way Relay Channel

The multi-way relay channel (MWRC) [94] is a promising building block for relay networks in the multicast setting where more than two users communicate with each other through a relay. Due to the half-duplex constraint, neither user can receive the other user in the MA phase. The MWRC can model several interesting practical communication scenarios. In satellite communications, multiple co-channel terminals exchange their messages through a gateway which acts as a relay in the multi-way relay channel. In cellular networks, a group of people can form a social network and exchange messages through the BS which acts as a relay in the multi-way fashion. Furthermore in the cellular context, a group of users in vicinity can establish a device-to-device communication and share messages through a simple repeater in proximity which acts a multi-way relay channel. In ad hoc networks, several users can contribute in building a distributed file sharing database through a central access point (AP). In sensor networks, several sensors can cooperatively pass their data to a central location. The two-way relay channel [95] is the simplest case of multi-way relay channels where two users exchange their messages with the aid of a relay. Fig. 2.11(a) illustrates the conventional two-way relaying scheme over four phases. In the first two phases, each user transmits individually its message to the relay whereas in the last two phases, the relay separately applies AF or DF scheme and transmits the signal intended to the other user.

2.7 Network Coding and Physical-Layer Network Coding

NC, which is the notion of coding at the packet level, has changed the model under which communication networks are designed. While in the traditional scheme, the intermediate network nodes route a packet from the incoming link to the outgoing link without any additional processing, NC combines packets, for example, by simply bit-wise XOR'ing them. NC was originally

introduced [96] to increase the throughput over wired networks. However, given the unreliability and broadcast nature of wireless networks, NC can provide a natural solution for the characteristic of wireless communication that affects routing [97]. NC was applied to the two-way relay channel in [98] where messages from both users are decoded first, then broadcast modulo two summation of both messages to both users as depicted on Fig 2.11(b). With the fact that each user has its own exchanged message, each user removes this effect and is able to fully recover the other user message.

Physical-layer NC was independently and concurrently proposed by three groups [77, 99-100] to exploit the natural operation of NC that occurs from the broadcast of two or more non-orthogonal signals. Nazer et al. [101] proposed a reliable physical-layer NC by removing the noise at each communication stage using appropriate error correcting codes. Fig 2.11(c) illustrates the physical-layer NC where in the MA phase both users transmit their messages then, the relay broadcasts the superimposed signal in the second phase. There are two main advantages from employing this scheme. Firstly, this scheme requires half the number of phases to communicate the messages compared to the conventional scheme, hence, doubling the throughput. Secondly, the less number of transmissions at the relay to communicate the same amount of information saves the power at the relay.

2.8 Low Density Parity Check Codes

LDPC codes originally proposed by Gallager [17] in 1960 were largely forgotten due to computational demands and implementation complexity at that time until mid-nineties when Gallager's work was re-investigated by Mackay and Neal [102]. Richardson, Shokrollahi and Urbanke designed capacity approaching irregular LDPC codes [103] which outperforms Turbo

codes [104-106]. LDPC codes, which are capacity approaching codes are a class of linear codes. LDPC codes are basically represented via two techniques namely matrix and graphical representations.

Matrix representation

LDPC codes are represented by a sparse parity check matrix H which forms the nullspace of the code with dimension $m \times n$. Given a binary row vector message containing k bits, H consists of $m = n - k$ parity check equations. An example of half-rate LDPC matrix is illustrated in (2.16) where $n = 10$ and $k = 5$

$$H = \begin{pmatrix} 1 & 0 & 0 & 0 & 1 & 1 & 1 & 0 & 0 & 0 \\ 0 & 0 & 0 & 1 & 1 & 0 & 1 & 0 & 1 & 0 \\ 1 & 1 & 1 & 1 & 0 & 0 & 0 & 0 & 0 & 0 \\ 0 & 1 & 0 & 0 & 0 & 0 & 0 & 1 & 1 & 1 \\ 0 & 0 & 1 & 0 & 0 & 1 & 0 & 1 & 0 & 1 \end{pmatrix}. \quad (2.16)$$

The code consists of the n -tuples codewords u such that the following equation is satisfied

$$uH^T = 0. \quad (2.17)$$

The matrices for LDPC codes are sparse. The sparsity of H allows for efficient practical iterative decoding algorithms [17]. However, optimal ML decoding for linear block codes is almost impossible due to complexity, particularly, for large codeword lengths. On the other hand, iterative decoding, which achieves near optimal performance, is used for LDPC codes due to the sparsity feature of H . The matrix in (2.16) is not sparse due to a small codeword length. Regular LDPC codes also called Gallager codes [17], have constant column and row weights w_c and w_r , respectively. The design rate of the code in this case is

$$R = \frac{n - m}{n} = 1 - \frac{m}{n} = 1 - \frac{w_c}{w_r}. \quad (2.18)$$

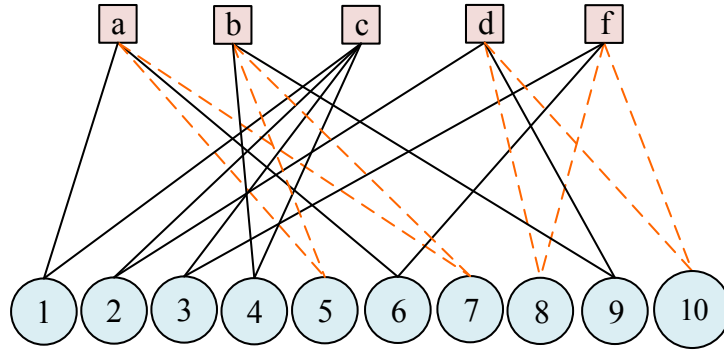


Fig. 2.12 Tanner Graph representation for the parity check matrix H in (2.16)

Graphical representation

An alternative representation of LDPC codes is via a Tanner graph [107]. The girth of a Tanner graph is the length of the shortest cycle in the graph. Girths in Tanner graphs prevent the BP algorithm from converging [102-103]. The Tanner graph associated with H is a bipartite graph with n variable nodes corresponding to the codeword bits and m check nodes corresponding to the parity check constraints. A check node j is connected to a variable node i if $H_{ji} = 1$. A cycle in a Tanner graph refers to a finite set of connected edges such that an edge starts and ends at the same node and no node appears more than once except the initial and final node. Length-4 cycles consist of a cycle of four nodes, two of which are on each side of the Tanner graph. The bipartite graph of the parity check matrix in (2.16) is illustrated in Fig. 2.12 where the red dashed edges represent the length-4 cycles. In this example, each variable node has degree 2 and every check node has degree 4. This code is called (2, 4) regular LDPC code.

Factor graphs are bipartite graphs representing the factorization of a function. The two main message passing algorithms on factor graphs are the max-product [107] and the sum-product algorithms [17]. We refer the reader to [20] for a tutorial paper on factor graphs and sum product algorithms. The LLR update rules for decoding the LDPC code are as follows [113]

$$m_{v,c}^{(l)} = \begin{cases} m_v, & \text{if } l = 0, \\ m_v + \sum_{c' \neq c} m_{c',v}^{(l-1)}, & \text{if } l \geq 1. \end{cases} \quad (2.19)$$

$$m_{c,v}^{(l)} = \ln \left(\frac{1 + \prod_{v' \neq v} \tanh \left(\frac{m_{v',c}^{(l)}}{2} \right)}{1 - \prod_{v' \neq v} \tanh \left(\frac{m_{v',c}^{(l)}}{2} \right)} \right) \quad (2.20)$$

where $m_{v,c}^{(l)}$ represents the message passed from message node v to the check node c at the l^{th} round of the algorithm. Similarly define $m_{c,v}^{(l)}$. At round 0, $m_{v,c}^{(0)}$, denoted as m_v , is the LLR of the message node v conditioned on its observed value, which represents the a priori LLR coming from the LT belief propagation decoder.

On the other hand, the performance of LDPC codes can substantially be improved by allowing nodes of various degrees. This code is called irregular LDPC code [100] for which the degrees of nodes are generated from a degree distribution. If the graph has only one degree on the right hand side, this graph is called right regular [108]. For an LDPC code of length n , denote the number of variable nodes of degree i by Λ_i , so that $\sum_i \Lambda_i = n$. Similarly, denote the number of check nodes by P_i , so that $\sum_i P_i = m$. In polynomial notation, this is equivalent to

$$\Lambda(x) = \sum_{i \geq 1} \Lambda_i x^i, \quad P(x) = \sum_{i \geq 1} P_i x^i. \quad (2.21)$$

(Λ, P) is called the normalized degree distribution pair (DDP) from a node perspective. Hence, the design rate is as follows

$$R(\Lambda, P) = 1 - \frac{P(1)}{\Lambda(1)}. \quad (2.22)$$

For the DE analysis, an alternative approach to construct H from a DDP (λ, ρ) is from an edge perspective. Define

$$\lambda(x) = \sum_{i \geq 1} \lambda_i x^{i-1} = \frac{A'(x)}{A'(1)}, \quad \rho(x) = \sum_{i \geq 1} \rho_i x^{i-1} = \frac{P'(x)}{P'(1)} \quad (2.23)$$

where λ_i and ρ_i are the fraction of edges that connect to variable and check nodes of degree i . The average variable and check degrees denoted by l_{avg} and r_{avg} are given respectively by

$$l_{avg} = \frac{1}{\int_0^1 \lambda(x) dx}, \quad r_{avg} = \frac{1}{\int_0^1 \rho(x) dx}. \quad (2.24)$$

The design rate is given by:

$$R(\lambda, \rho) = 1 - \frac{l_{avg}}{r_{avg}} = 1 - \frac{\int_0^1 \rho(x) dx}{\int_0^1 \lambda(x) dx}. \quad (2.25)$$

Density evolution analysis

In the BEC, DE describes how the probability of erasures evolves as a function of the iteration number [30]. Consider a DDP (λ, ρ) , let $\epsilon \in [0, 1]$ be the channel parameter and let $P_{-1}^{BP} = 1$, the probability of erasure under BP algorithm after l iterations and for $l \geq 0$, is defined as

$$P_l^{BP} = \epsilon \lambda \left(1 - \rho(1 - P_{l-1}^{BP}) \right). \quad (2.26)$$

Threshold

The threshold ϵ^{BP} associated with a DDP (λ, ρ) is defined as the maximum tolerable loss [108] for which the information can be reliably transmitted over the $BEC(\epsilon)$. i.e., if $\epsilon < \epsilon^{BP}$ the probability of erasures $P_l^{BP} \rightarrow 0$ as $l \rightarrow \infty$. The threshold is given by

$$\epsilon^{BP}(\lambda, \rho) = \min \left(\frac{x}{\lambda(1 - \rho(1 - x))} \right), \quad \text{for } x \in [0, \epsilon^{BP}]. \quad (2.27)$$

An upper bound on threshold can be also found from the stability condition which is given by

$$\epsilon^{BP}(\lambda, \rho) \leq \frac{1}{\lambda'(0)\rho'(1)}. \quad (2.28)$$

Multiplicative Gap

The multiplicative gap $\delta(\lambda, \rho)$ associated with a DDP (λ, ρ) is defined as the fraction loss of the capacity that is not achievable. The multiplicative gap vanishes when $\epsilon^{BP}(\lambda, \rho) + R(\lambda, \rho) = 1$.

Therefore, $\delta(\lambda, \rho)$ is given by

$$\delta(\lambda, \rho) = 1 - \frac{R(\lambda, \rho)}{1 - \epsilon^{BP}(\lambda, \rho)} \quad (2.29)$$

2.9 Raptor Codes

Fountain codes [109] are rateless channel codes with unknown rates a priori. i.e., the encoder produces an endless stream of output symbols from a given set of input symbols. The receiver attempts to decode the codeword every time a new symbol is received. This process continues until the destination successfully decodes the codeword and acknowledges the source to terminate the transmission. Each transmitted output symbol is produced by adding up a randomly chosen subset of the input symbols. The decoder of an optimal fountain code can recover with high probability the original k input symbols from any set of t output symbols with error probability at most inversely polynomial in k . The overhead is defined as the ratio $\frac{t}{k}$.

On the other hand, Tornado codes [110] are fixed rate codes, i.e., the codeword length n is fixed beforehand based on the initial channel erasure rate estimation. Tornado codes are derived from sparse irregular random bipartite graphs [103]. The edge degree distribution of such graphs are carefully chosen leading to successful decoding with high probability by simple BP decoder. Tornado codes are constructed using concatenation at different levels. At the first layer, the input symbols are XOR'ed into coded symbols. Then these coded symbols are XOR'ed into coded symbols at the second layer and so on.

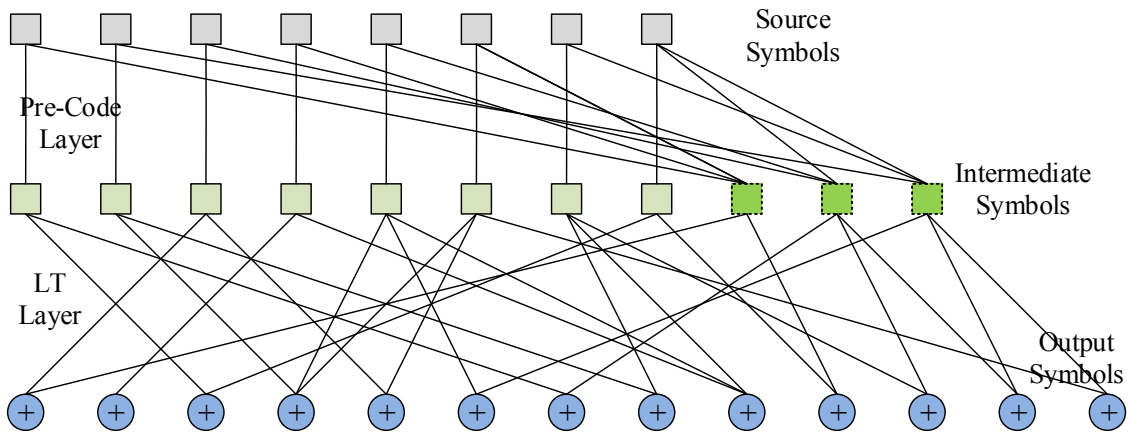


Fig. 2.13 Raptor Codes: Pre-code appends redundant symbols to source symbols in the case of systematic pre-code to form intermediate symbols. LT code with optimized degree distribution generates output symbols from intermediate symbols

In contrast, Luby Transform (LT) codes [111] are the first class of universal fountain codes. Based on a realization d of a specific degree distribution, for instance Soliton distribution, each output symbol is produced from summing up d input symbols. LT coding is performed over two steps. First, generate the value of d from a degree distribution. Second, uniformly select d input symbols to produce the output symbol by performing modulo 2 sum on these symbols. The decoding of LT codes is performed by back substitution. The decoder looks for degree one output symbols to decode first after each decoding round. This process continues until enough output symbols are received and codeword is successfully decoded. The LT codes do not have a fixed encoding cost. Raptor (Rapid Tornado) codes [112] are a special and new class of Fountain codes with optimized degree distribution and another layer of high rate codes called the pre-code layer. The core idea of Raptor coding is to relax the condition that all input symbols have to be recovered by the LT code. i.e. only a fraction of source symbols are decoded by the LT code [111] layer and the remainder is decoded by the pre-code layer. Raptor codes consist of two layers, namely the pre-code and the LT code layers, as shown in Fig. 2.13. The pre-code layer is a high rate block code whereas the second layer is an LT code with an optimized degree distribution for Raptor codes [18].

A Raptor code is characterized by the parameters $(k, C_p, \Omega(x))$ where k is the input symbols to the pre-code layer, C_p is the rate of the erasure correcting block code referred to as the pre-code and $\Omega(x)$ is the generator polynomial of the optimized degree distribution of the LT layer [18]. A raptor code encodes k input symbols to possibly limitless number of output symbols over Galois field F_2 . The destination acknowledges the source to stop generating symbols once the receiver successfully decodes the codeword. Hence, the output codeword length n is not known a priori. The pre-code is in general chosen as a high rate right regular LDPC code [108]. The LDPC code [113] layer produces the intermediate symbols from k input symbols. Whereas the LT layer produces the output symbols from the intermediate symbols based on an optimized degree distribution $\Omega(x)$. The distribution is characterized by the generator polynomial $\Omega(x) = \sum_i^t \Omega_i x^i$, where Ω_i is the probability that i is chosen. The encoding process of the LT layer consists of first sampling a degree d from the distribution $\Omega(x)$, then d intermediate symbols are chosen according to a uniform distribution from all intermediate symbols. The d chosen intermediate symbols are then modulo 2 summed up to produce the output symbol.

The number of transmitted output symbols n (which is not known a priori) by the Raptor code can be written as

$$n = \frac{k(1 + \varepsilon)}{C_p} \quad (2.30)$$

where ε is the overhead. Therefore, the rate for Raptor code can be written as

$$R = \frac{k}{n} = \frac{C}{(1 + \varepsilon)} \quad (2.31)$$

The LLR update rules for the decoding of LT code are as follows [114]

$$\tanh\left(\frac{m_{o,i}^{(l)}}{2}\right) = \tanh\left(\frac{Z_o}{2}\right) \prod_{i' \neq i} \tanh\left(\frac{m_{i',o}^{(l)}}{2}\right) \quad (2.32)$$

$$m_{i,o}^{(l+1)} = \sum_{o' \neq o} m_{o',i}^{(l)} \quad (2.33)$$

where i stands for the input / intermediate nodes, o stands for the output node, $m_{i,o}^{(l)}$ represents the message passed from input node i to output node o at iteration l and similarly for $m_{o,i}^{(l)}$, Z_o is the LLR corresponding to output symbol o .

In the BPSK case, $Z_o = L_c y$, where y is the received symbol from the channel and $L_c = 2 \frac{E_s}{\sigma^2}$, and E_s is the symbol power and σ is the standard deviation of the Gaussian noise. Hence,

$$Z_o = 2 \frac{E_s}{\sigma^2} y \quad (2.34)$$

After running the decoder for sufficient number of iterations, the LLR of each intermediate node v is calculated as $LLR(v) = \sum_o m_{o,i}^{(l)}$. This a posteriori LLR is sent to the LDPC belief propagation decoder as a priori LLR of the respective symbols. The source symbols LLRs are the output of this stage of decoding, which then pass through a hard decision stage to complete the decoding procedure.

2.10 Cognitive Radio

Wireless communications are constantly evolving leading to more demand in spectrum resources. Although different spectrum bands are allocated to particular services, it was identified that these bands are underutilized most of the time [5-6]. CR was proposed as a promising technique to improve the spectrum usage efficiency. CR is an adaptive radio that modify its transmission parameters based on some sensed information from the environment in which it operates [5]. Several strategies are proposed depending on the ability of the secondary user (SU) to coexist with the primary user (PU).

2.10.1 Interweave Cognitive Radio

In interweave CR systems, also called opportunistic access systems, SUs are only allowed to use the spectrum when PUs are not active. Thus, no interference is tolerated by the PU. In opportunistic spectrum sensing, SUs exploit the spectrum holes that are unused by the PU. This technique is not efficient particularly in a highly dynamic PUs

2.10.2 Underlay Cognitive Radio

In underlay CR systems, also called spectrum sharing systems, the SU and PU can coexist simultaneously on the same spectrum as long as the SU ensures that interference caused to the PU is below a certain threshold. The SU has to transmit at low power and therefore secondary transceiver must be able to operate in low SNR. This technique is restricted to low power applications or short range communications (D2D) and has been adopted in LTE standard [11] (cognitive femtocells).

2.10.3 Overlay Cognitive Radio

In the overlay CR technique, the SU tradeoffs some resources to enhance the primary signal and help PU to correctly decodes its message. In return, the SU can access the PU spectrum. In this approach, the SU can operate at higher SNR and thus, achieves better performance compared to underlay approach. The overlay method is more efficient and lead to higher performance at both PU and SU.

2.11 Internet of Things

Introduced by Ashton in 1999 [1], the IoT is an emerging and promising subject from social, economic and engineering perspectives. IoT is the global biggest network where consumer electronics, vehicles, wearable micro devices, sensors and other multipurpose devices with powerful data processing capabilities are being connected to each other or to central servers via the internet or/and telecommunication operators.

The large scale implementation of IoT affects many practical and promising applications, some of which are: 1) smart grids [115] for intelligent monitoring, control and efficient delivery of electricity to consumers. 2) Smart cities [116] for increasing security, green energy, smart traffic monitoring and intelligent parks. 3) Smart homes [117] for enhancing security and efficient energy consumptions through home automation components. 4) Smart healthcare systems [118] for efficient continuous monitoring of people with disabilities and the elderly, enabling improved level of independence [119]. 5) Intelligent transportation systems [120] for building smarter infrastructure and toward smart logistics systems. 6) Smart tracking and tracing [121]. 7) Public safety systems. Fig. 2.14 illustrates the idea of a large number of wirelessly equipped devices connected together in a smart city.

On the other hand, M2M communication has developed as a promising technology enabling billions of multipurpose devices to communicate with each other without human intervention [8-9], [37-38, [115]. MTC refers to existing and future autonomous networked sensing devices which gather and exchange information over the network.

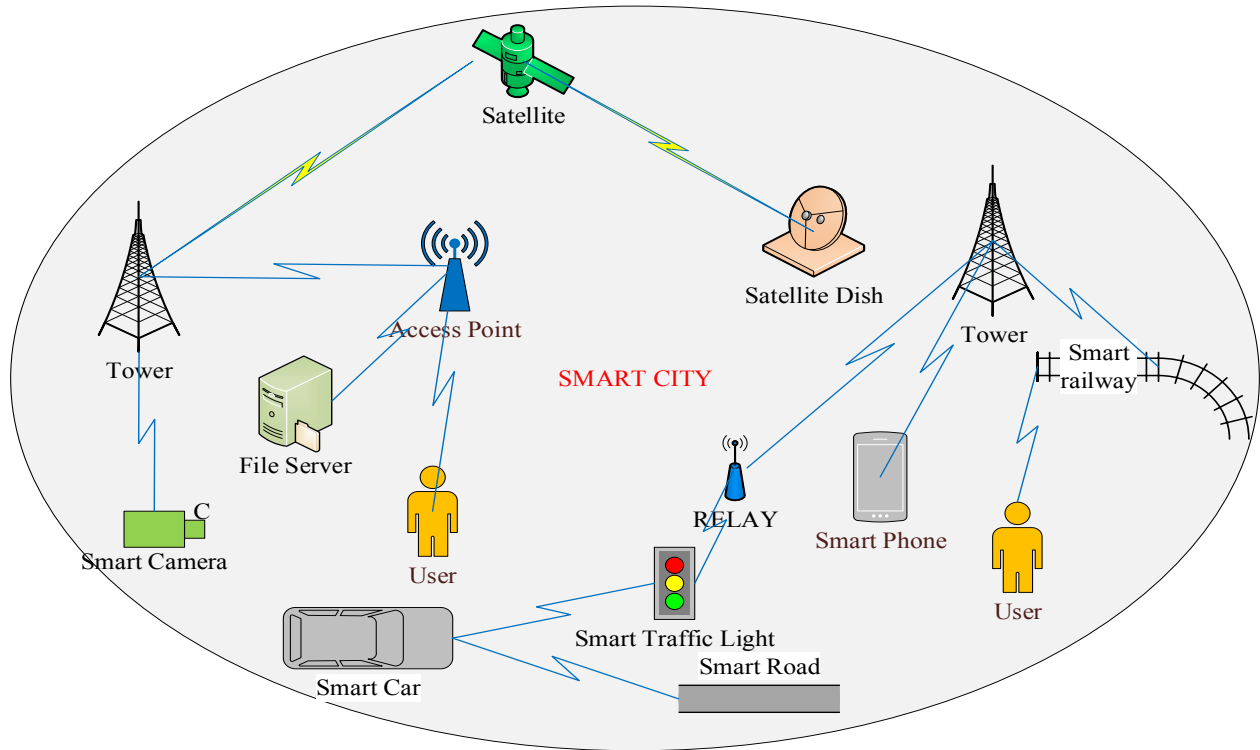


Fig. 2.14 Smart city supported by MTC devices with interconnected users, surveillance systems, traffic lights, vehicles, roads, railways, sensor devices and servers via telecommunication infrastructures

2.11.1 Communication Models for the IoT

Earlier this year, the internet architecture board (IAB) released an architectural guide for networking of smart objects (RFC 7452) [122] which outlines the framework of communication models used by IoT devices. The IoT common communication models are categorized into four patterns which will be summarized next.

Device-to-Device Communication patterns

D2D communication models a scenario where two or more devices establish direct communication links between one another to exchange information, rather than going through a centralized controller or an application server. D2D communication uses many existing protocols and

infrastructures. D2D is a promising key technology for the next generation of mobile networks where mobile devices establish D2D sessions underlying LTE networks [11]. Furthermore, in the context of smart homes, D2D communication utilizes protocols like Bluetooth [123], ZigBee [124], or Z-Wave [125] networks to establish D2D sessions. This communication model is commonly used in home automation systems where information is exchanged between devices small data packets with relatively low data rate requirements. For example, in a home automation setup, light bulbs and switches, thermostats, door locks and possibly other domestic devices transmit messages to each other.

Device-to-Cloud Communication patterns

D2C communication models a scenario where an MTC device establish a direct communication link to a cloud server over the internet to exchange all types of messages. Using the IP based protocol, WiFi links connect the MTC devices to the cloud. For example, a smart thermostat transmits data to a cloud database server where the data can be gathered for statistics or other analysis purposes. Home users can activate or deactivate the heating system from their smart phones via the cloud. Therefore, D2C enhances user capabilities to extend their controls beyond home environment.

Device-to-Gateway Communication patterns

In D2G, MTC devices communicates with a local gateway where some processing occurs before transmitting the data to the cloud server. A home automation system or any portable smart device can act as a local gateway. D2G is mainly used for interoperability purpose where a new non compatible MTC device wants to join the network. However, D2G communication method requires an additional application layer gateway software which increases complexity and cost.

Back End Data Sharing patterns

In back end data sharing, multiple application server providers (ASP) exchange information over the cloud for several purposes. For example, in a big complex, the data that is collected from MTC sensors is gathered in a standalone data silo. Back end data sharing architecture allows other ASP to access, analyze the data and possibly sharing it with another ASP.

2.12 Conclusion

In this chapter, we presented some background about concepts and techniques that are related to our work and mainly used in the rest of the thesis. More precisely, we first presented few classical channel models which include point to point channel, MAC, relay channel, and multi-way relay channel. Then, we presented the concept of physical-layer NC and SIC. We also explained LDPC and Raptor coding techniques. Finally, we presented the concept of the IoT and M2M communication devices.

In the next chapter, we present our first contribution to the thesis where we propose coding schemes for the 2-user non-orthogonal MAC. Moreover, we show that the interference resulting from coexistence of radio devices can be exploited to improve the overall bandwidth efficiency of a communication channel. Using LDPC codes, we also show that the proposed scheme achieves any rate pairs on the capacity region without time sharing nor rate splitting.

Chapter 3

Joint LDPC Decoding for the 2-User Multiple Access Erasure Channel

3.1 Introduction

With the tremendous demand for higher data rates and the scarcity in spectrum band, the traditional fixed and orthogonal channel allocation do not cope with the most increasingly developed wireless network worldwide. One promising key solution to further enhance data rates without increasing the bandwidth is by increasing the spectral efficiency of the channel. Non orthogonal multiple access (NOMA) techniques are promising candidates for the future wireless communication big network. In the two user NOMA techniques, the two corner points on the boundary region are known to be achievable by single user decoding followed by SIC. Other points can also be achieved using time sharing or rate splitting.

In this chapter, we firstly propose a joint belief propagation LDPC decoding technique namely method 2 for the two-user NOMA channel. This method exploits the fact that resolution of an erasure in one decoder means the resolution at the other decoder since at the erasure locations, the bits from two sources are complement of one another. Our algorithm consists of independently and

simultaneously using single user BP decoding technique at each sub-graph followed by communicating the results between the two decoders at the end of each iteration. Furthermore, we calculate the probability of decoding failure and the outage capacity. Additionally, we show how the erasure probability evolves with the number of decoding iterations and the maximum tolerable loss using DE analysis. Simulation results show that any sum rate point close to the capacity boundary is achievable.

Secondly, we propose an encoding technique at the sources that randomly splits a half-rate full rank parity check matrix H of dimensions $m \times n$ into the corresponding parity check matrices H_1 and H_2 , respectively, of dimensions $m_1 \times n$ and $m_2 \times n$ where $m_1 + m_2 = m$. Furthermore, we compute an upper bound on the recoverable erasures in a 2-user MAEC. Additionally, we compare the proposed method 2 with the single user decoding and SIC (method 1). It is clear that both methods achieve similar performance, however, method 2 achieves any rate point on the capacity boundary without using time sharing nor rate splitting. Furthermore, we show that a properly constructed half-rate parity check matrix achieving rates close to the capacity region on the BEC results in an efficient code achieving any rate point close to the capacity region on the 2-user MAEC.

The rest of the chapter is organized as follows. In Section 3.2, we present the system model and define some notations. In section 3.3, we describe the coding strategy, calculate the probability of decoding failure and evaluate the outage capacity. In section 3.4, we present the implementation of the proposed coding scheme. In section 3.5, we present the simulation results and Section 3.6 concludes the chapter.

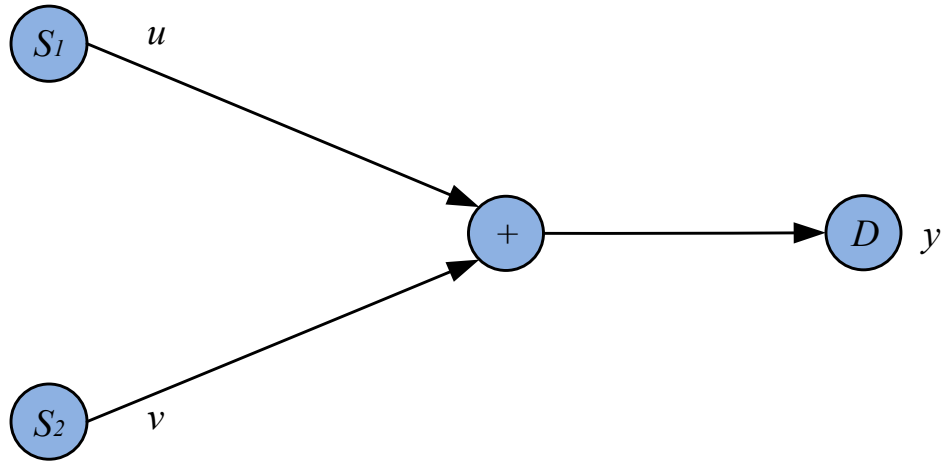


Fig. 3.1 System Model

3.2 System Model

Consider two binary sources denoted by S_j for $j = \{1,2\}$ that want to simultaneously communicate with a destination D at rates $R_j = \frac{k_j}{n}$, where k_j denotes the data length of source j and n denotes the codewords length, respectively. The communication occurs in the same band and on the same channel. i.e., non-orthogonal multiple access. We assume that the transmitters are symbol synchronized. In a noiseless scenario, the i th received symbol at the destination is the superposition of both source symbols and is given by

$$y_i = u_i + v_i, \quad (3.1)$$

where u_i and v_i are the i th transmitted symbols from S_1 and S_2 , respectively. With the fact that each source generates equally likely binary bits, half of the combined bits on average get erased in the received codeword. Fig. 3.1 illustrates the two source MAEC with binary input and ternary output. Hence, the channel output is $y_i = \{0,1,2\}$ as illustrated in Table 3.1 with respective probabilities $\left\{\frac{1}{4}, \frac{1}{2}, \frac{1}{4}\right\}$. When $y_i = \{0,2\}$, the decoder knows that the i th bit in the received combined codewords is a reliable information, i.e., $u_i = v_i$ and the decoder can decide what both

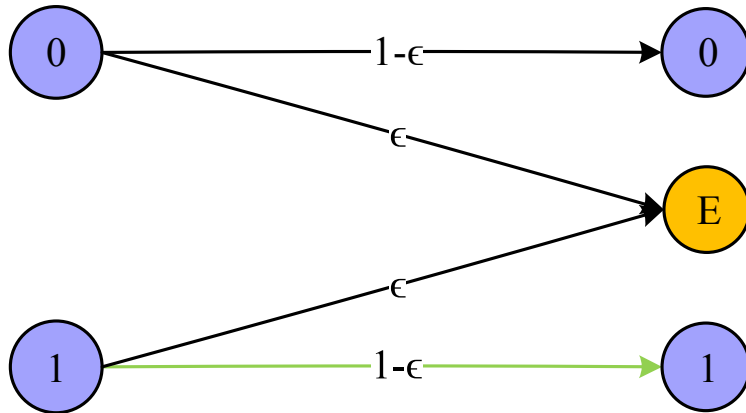


Fig. 3.2 Binary erasure channel with erasure probability ϵ , considering source 2

sources sent. On the other hand, when $y_i = 1$, the decoder knows that sources have sent opposite bits, i.e., $u_i = v_i + 1$ and cannot decide what each source sent. Assume source 1 transmits at rate $R_1 = 1$ bit per channel use (uncoded stream). Source 2 can transmit at rate $R_2 \leq 0.5$ bit per channel use (coded stream). At the destination considering user 2, this channel is equivalent to a BEC as depicted in Fig. 3.2 with erasure probability $\epsilon = 0.5$. Therefore, the capacity of this channel is $1 - \epsilon = 0.5$ and in fact this is the maximum sum rate $R_1 + R_2 \leq 1.5$ that can be achieved on this channel.

3.3 Proposed Coding Strategy for 2-User Multiple Access Erasure Channel

In this section, we first describe the proposed coding scheme namely method 2, then we calculate the probability of decoding failure and the outage capacity. We also illustrate a simple example to clarify the idea of the proposed coding scheme.

Table 3.1 Four equally likely Possible Combinations at the destination

u	v	Y
0	0	0
0	1	1
1	0	1
1	1	2

3.3.1 Proposed Coding Scheme - Method 2

The main idea of the proposed coding scheme is to exploit the existing information resulting from an erased bit in combined codewords, i.e., the location of the erased bits and the fact that the bits transmitted by two sources are opposite in these locations. Next, we describe the encoding and decoding processes.

Encoding process

The primary idea of the encoding at both sources is to exploit the fact that a half-rate full rank parity check matrix H can be randomly divided between both individual parity check matrices H_1 and H_2 with corresponding rates R_1 and R_2 resulting in a sum rate $R_1 + R_2 \leq 1.5$ very close to the capacity. Each individual parity check matrix can be represented in a Tanner sub-graph. To fully exploit all the parity bits produced at both encoders, each parity check equation has to be linearly independent. Hence, the individual parity check matrix H_j at the j th encoder must not be rank deficient. We assume that the rank property is met and the structure of each encoder is unique. Let G_j be the generator matrix of size k_j by n at the j th encoder that characterizes the (n, k_j) code C_j for $j = \{1, 2\}$. The corresponding codewords produced by encoders 1 and 2 are given by $u = s_1 G_1$ and $v = s_2 G_2$, respectively where s_j is a 1 by k_j message vector at the j th source. We illustrate the encoding and decoding process through a simple example later in this section.

Decoding process

The decoding technique mainly consists of first forming H from the individual parity check matrices H_i , then solving the system of linear equation in (3.5) to recover the erased bits in codeword u , then v is automatically recovered following the fact that a recovered erased bit in one codeword implies that the corresponding bit in the other codeword is the inverse. The main result of this subsection is presented in the following proposition.

Proposition

Let n , k_1 and k_2 be the length of: the codeword, the message at source 1 and source 2, respectively. It is easy to show that when the number of erasures does not exceed $2n - k_1 - k_2$, we can recover both transmitted codewords.

Proof: Assume that there are e erasures in a received combined codeword y , i.e., places where $u_i = v_i + 1$. Overall, we have $2e$ unknowns. However, given e equations of type $u_i = v_i + 1$, the number of unknowns is reduced to e . $uH_1^T = 0$ and $vH_2^T = 0$ provide us with $n - k_1$ and $n - k_2$ equations, respectively. The e unknowns can be found if e does not exceed the number of equations $(n - k_1) + (n - k_2) = 2n - k_1 - k_2$, i.e.

$$e \leq 2n - k_1 - k_2 \quad (3.2)$$

■

The probability of failure to recover the erasures in the 2-user MAEC is

$$P_F = P[e > 2n - k_1 - k_2] = \frac{1}{2^n} \sum_{l=2n-k_1-k_2+1}^n \binom{n}{l}. \quad (3.3)$$

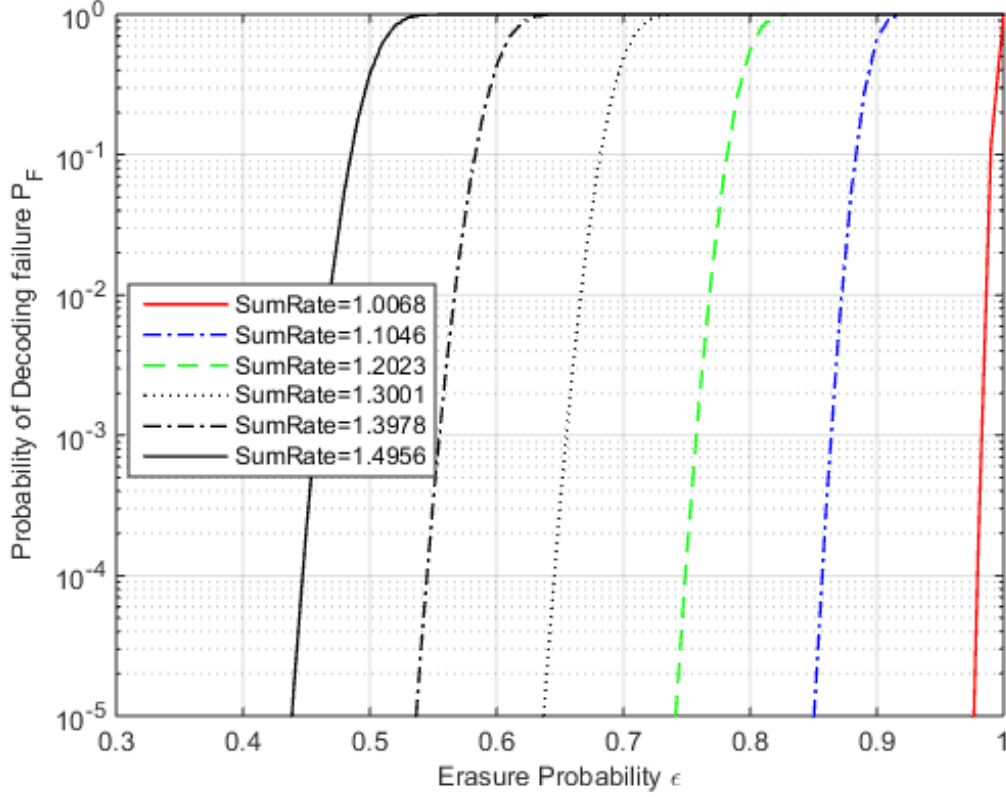


Fig. 3.3 Probability of decoding failure as a function of the erasure in the channel ϵ for various sum rate

Fig. 3.3 shows the probability of decoding failure P_F as a function of the erasure probability ϵ of the channel for various sum rates $R = R_1 + R_2$. Note that as ϵ increases the sum rate decreases for a specific P_F target.

Since in an erasure channel of this type, almost half of the bits get erased, we have $e \approx \frac{n}{2}$. Hence,

(3.2) can be written as

$$\frac{n}{2} \approx 2n - k_1 - k_2 \quad \Rightarrow k_1 + k_2 \approx \frac{3n}{2} \quad \Rightarrow R_1 + R_2 \approx 1.5. \quad (3.4)$$

That is the coding scheme 2 can achieve the capacity of the 2-user MAEC.

Given a binary row vector message containing k bits, the LDPC matrix H of dimensions $m \times n$ consists of $m = n - k$ parity check equations. Therefore, the code consists of the n -tuples codewords u such that the following equation is satisfied.

$$uH^T = 0. \quad (3.5)$$

Necessary Solvability Conditions of (3.5)

The e unknowns in (3.2) can be recovered provided that the available known equations resulting from the merged parity check matrix H are linearly independent. Therefore, the parity check matrix H must have full rank, i.e., $\text{rank}(H) = 2n - k_1 - k_2$. We propose a simple technique at the sources that preserves the rank property of H . Once both sources have agreed on the codeword block length n and the individual transmission rates R_1 and R_2 , respectively, the first step is to generate a full rank half-rate parity check matrix H of dimension $\frac{n}{2}$ by n . We explain in details the implementation of this technique in Section 3.4. Let $H = \begin{pmatrix} H_1 \\ H_2 \end{pmatrix}$ be a parity check matrix of dimension $\frac{n}{2}$ by n . If the rank of H is $r = \frac{n}{2}$, then $r_1 + r_2 = \frac{n}{2}$ where r_1 and r_2 are the ranks of H_1 and H_2 , respectively. It is easy to see that $r_1 + r_2 = \frac{n}{2}$. Let θ be an integer between 0 and $\frac{n}{4}$. Assume that $r_1 \leq \frac{n}{4} - \theta$, if $r_2 < \frac{n}{4} + \theta$, then $r_1 + r_2 < \frac{n}{4} - \theta + \frac{n}{4} + \theta = \frac{n}{2}$. This contradicts the fact that the rank of H is $\frac{n}{2}$.

3.3.2 Outage Capacity

The outage capacity C_β is defined as the largest achievable sum rate R such that the probability of decoding failure P_F is less than β [17]. Fig. 3.4 shows the outage capacity C_β for various probability of decoding failure target β .

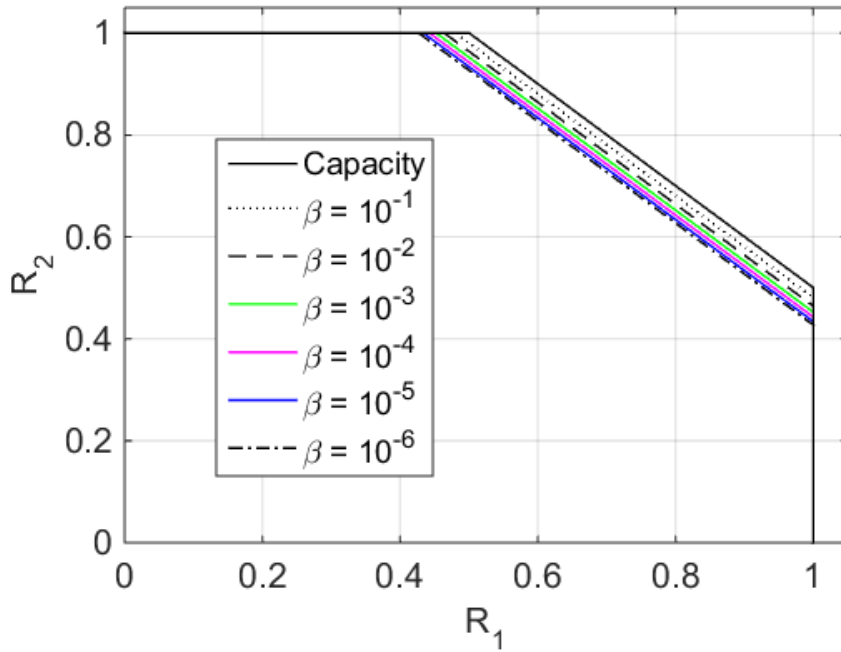


Fig. 3.4 Outage Capacity

3.3.3 A Simple example of the proposed coding scheme using (7,4) Hamming Codes

To further capture the idea of the new coding scheme, a simple example is explored in this section. Consider the (7,4) Hamming codes generated by the generator polynomials $g_1(X) = 1 + X + X^3$ and $g_2(X) = 1 + X^2 + X^3$ at user 1 and 2, respectively. Assume that the message vectors at source 1 and 2 are $s_1 = 1100$ and $s_2 = 0101$, respectively. The resulting encoded vectors are $u = s_1G_1 = 1011100$ and $v = s_2G_2 = 0100111$, respectively. At the destination $y = u + v = EEEE2EE$. Since the number of erased bits in the received erasure pattern y is $e = 6 \leq 2n - k_1 - k_2 = 6$, the decoder is able to separate both codewords by solving the system of linear equations

$$uH_1^T = 0, \quad (3.6)$$

$$vH_2^T = 0. \quad (3.7)$$

Define q such that

$$q_j = \begin{cases} 1 & \text{if } u_j \neq v_j \\ 0 & \text{elsewhere} \end{cases} \quad (3.8)$$

then, $v = u + q$. Substituting in (3.7) $vH_2^T = uH_2^T + qH_2^T = 0$ or $uH_2^T = qH_2^T$ and

$uH^T = u \begin{pmatrix} H_1 \\ H_2 \end{pmatrix}^T = \begin{pmatrix} 0 \\ qH_2^T \end{pmatrix}^T$. For this example, we have

$$qH_2^T = (1 \ 1 \ 1 \ 1 \ 0 \ 1 \ 1) \begin{pmatrix} 1 \ 0 \ 0 \\ 1 \ 1 \ 0 \\ 1 \ 1 \ 1 \\ 0 \ 1 \ 1 \\ 1 \ 0 \ 1 \\ 0 \ 1 \ 0 \\ 0 \ 0 \ 1 \end{pmatrix} = (1 \ 0 \ 1) \quad (3.9)$$

Now, the remaining part is to merge H_1 and H_2 then solve the system of equations to find the vectors u and v .

$$Hu^T = \begin{pmatrix} H_1 \\ H_2 \end{pmatrix} u^T = \begin{pmatrix} 1 \ 0 \ 1 \ 1 \ 1 \ 0 \ 0 \\ 0 \ 1 \ 0 \ 1 \ 1 \ 1 \ 0 \\ 0 \ 0 \ 1 \ 0 \ 1 \ 1 \ 1 \\ 1 \ 1 \ 1 \ 0 \ 1 \ 0 \ 0 \\ 0 \ 1 \ 1 \ 1 \ 0 \ 1 \ 0 \\ 0 \ 0 \ 1 \ 1 \ 1 \ 0 \ 1 \end{pmatrix} \begin{pmatrix} u_1 \\ u_2 \\ u_3 \\ u_4 \\ u_5 \\ u_6 \\ u_7 \end{pmatrix} = \begin{pmatrix} 0 \\ 0 \\ 0 \\ 1 \\ 0 \\ 1 \end{pmatrix}, \quad (3.10)$$

then by using elementary row operations (upper triangle conversion), (3.10) simplifies to

$$\begin{pmatrix} 1 \ 0 \ 1 \ 1 \ 1 \ 0 \ 0 \\ 0 \ 1 \ 0 \ 1 \ 1 \ 1 \ 0 \\ 0 \ 0 \ 1 \ 0 \ 1 \ 1 \ 1 \\ 0 \ 0 \ 0 \ 1 \ 0 \ 1 \ 0 \\ 0 \ 0 \ 0 \ 0 \ 1 \ 1 \ 0 \\ 0 \ 0 \ 0 \ 0 \ 0 \ 1 \ 1 \end{pmatrix} \begin{pmatrix} u_1 \\ u_2 \\ u_3 \\ u_4 \\ u_5 \\ u_6 \\ u_7 \end{pmatrix} = \begin{pmatrix} 0 \\ 0 \\ 0 \\ 1 \\ 1 \\ 0 \end{pmatrix}. \quad (3.11)$$

From (3.10) and using the equations from (3.7), the decoder first separates both codewords, then decodes s_1 and s_2 . Now assume that the received combined codeword is $y = EEEEEEE$. Since the number of erased bits in the received erasure pattern is $e = 7 > 2n - k_1 - k_2$, the decoder declares decoding failure. Hence, the probability of decoding failure in this case is given by $P_F = \frac{1}{2^7}$.

3.4 Implementation of the Proposed Coding Scheme

With the fact that both sources transmit equally likely data bits, on average half of the received bits get erased. One possible solution (basic method) to this problem is to have a standalone LDPC code of half-rate at each source. At the destination, each source independently tries to recover its corresponding transmitted codeword from the received corrupted stream by using single user detection. This coding scheme achieves a sum rate of at most $R_1 + R_2 \leq 1$. An alternative solution (method 1) is to also have a standalone LDPC code of half-rate at one of the sources and the other source transmits at unit-rate (uncoded stream). At the destination, we decode the half-rate codeword first, then apply SIC to remove its effect from the received codeword and then recover the uncoded stream by using single user detection. This coding scheme achieves the two corners of the capacity region (0.5, 1) and (1, 0.5) and using time sharing technique to achieve the other points on the boundary region. Hence, the sum rate is $R_1 + R_2 \leq 1.5$. Next, we illustrate the proposed coding scheme (method 2) where any source may transmit at rates $0.5 < R_i < 1$ such that $R_1 + R_2 \leq 1.5$ to achieve any point on the capacity region without time sharing. We evaluate the performance of method 2 using LDPC codes. The implementation key features of method 2 are: 1) Encoding process at the sources, 2) joint decoding process at the destination's side.

3.4.1 Encoding at the Sources

Firstly, both users agree on the codeword length n and their transmission rates $R_1 < 1$, and $R_2 < 1$ such that $R_1 + R_2 \leq C = 1.5$. Then the half-rate parity check matrix H is constructed with dimension $m \times n$ from an optimized DDP (λ, ρ) . The design rate of the code is given by $R =$

$$\frac{n-m}{n} = 1 - \frac{\int_0^1 \rho(x) dx}{\int_0^1 \lambda(x) dx} \leq \frac{1}{2}. \text{ From } H, \text{ we construct } H_1 \text{ and } H_2 \text{ by randomly selecting } m_1 \text{ and } m_2 =$$

$m - m_1$ rows, respectively. Hence, the individual transmission rates are $R_1 = 1 - \frac{m_1}{n}$ and $R_2 = 1 - \frac{m_2}{n}$, respectively. In other words, $R_1 + R_2 = 2 - \frac{(m_1+m_2)}{n} = 2 - \frac{m}{n} \leq 1.5$, where $\frac{m}{n}$ is the ratio between the number of rows and columns of H i.e., the check and variable nodes on the equivalent Tanner graph. In the optimal situation where H is exactly a half-rate parity check matrix, i.e., $\frac{m}{n} = 0.5$, and with large enough codeword length n , the probability of erasures is almost zero. Therefore, the achievable sum rate is the capacity C . However, in practice, this upper bound on R is not exactly achievable but rate points very close to capacity boundary are achievable. In the next section, we show these achievable points on the boundary region of the MAC. Once H_1 and H_2 are formed, each source encodes its data bits to form its corresponding codeword. Let u and v denote the generated codewords at source 1 and 2 respectively. The encoding process [102] produces the codewords that satisfies (3.6) and (3.7).

Assume that $u = [c_1|s_1]$ and $v = [c_2|s_2]$ where c_i and s_i represent the parity bits and the message bits at the i^{th} user, respectively, for $i = \{1,2\}$. Also assume that $H_i = [A_i|B_i]$, where A_i and B_i are $m_i \times m_i$ and $m_i \times (n - m_i)$ matrices, respectively. By substituting H_1, H_2, u and v in (3.6) and (3.7), the check bits at the i th users are given by

$$c_i = A_i^{-1}B_i s_i, \quad (3.12)$$

where A_i has to be non-singular matrix to have a solution for c_i . If A_i is singular, columns in H_i can be rearranged (swapped) such that A_i is non-singular. Note that the sparseness of the matrix is maintained since operations are done on the columns.

3.4.2 Decoding at the Destination

The joint decoder employs an independent single user BP decoding algorithm at each sub-graph. The single user BP decoding algorithm at any sub-graph performs two rounds of computation in

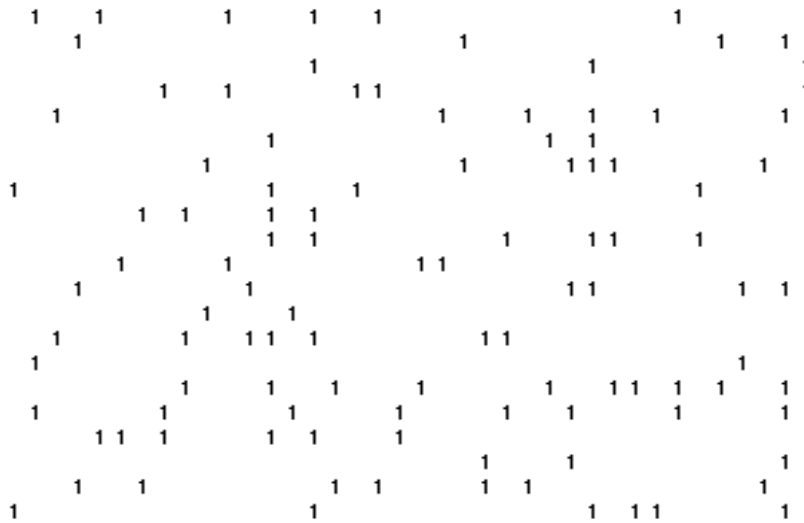


Fig. 3.5 Low density parity check matrix for the half-rate code in the implementation example

each iteration. The first computation is performed at each variable node where the outgoing message is an erasure if all incoming messages are erasures. Otherwise, the outgoing message is equal to common value either 0 or 1. The second computation is performed at each check node where the outgoing message is an erasure if any of the incoming messages is an erasure. Otherwise, the outgoing message is modulo 2 sum of all incoming messages. In a noiseless scenario where only erasures are detected at the receiver, the recovered erasures after each decoding iteration remain unchanged throughout the rest of the decoding iterations. i.e., once an erased variable node is recovered, it remains at that state until the decoder either declares success or failure.

The joint decoding technique consists of two steps: 1) computation of beliefs at the nodes of both sub-graphs, which is independently and individually performed as a single user decoding, 2) erasure recovery at one variable node of a sub-graph results in automatically resolving the corresponding erasure at the other sub-graph. The main idea of the decoding is that the individual Tanner sub-graphs joint efforts to resolve the almost 50% erased bits in the received codeword. Specifically in each iteration, a single user BP decoding is used at each sub-graph to recover some of the erasures

in the variable nodes. In other words, the check nodes compute their beliefs and send them to the variable nodes to independently resolve some of the erasures. Then both sub-graphs exchange the newly recovered erasures using the relation $v_j = u_j + 1$ and proceed to the next iteration. This process continues until either all erasures are recovered or no further erasure recovery progress is made after each iteration. In the next subsection, we illustrate an example to clarify the decoding process.

3.4.3 A Simple Example

To capture the implementation of joint decoding approach over both Tanner sub-graphs for the 2-user MAEC, we illustrate the following example. The parity check matrix H of size $n = 38$ and $m = 21$ with designed rate $R = \frac{17}{38} = 0.4474$, is generated based on an optimized and normalized DDP from a node perspective (L, P) as shown in Fig. 3.5. This DDP is given by the following polynomials [30]:

$$L(x) = 0.6131x^2 + 0.2019x^3 + 0.0576x^4 + 0.0844x^7 + 0.0431x^8 \quad (3.13)$$

$$P(x) = x^6 \quad (3.14)$$

Assume $R_1 = 0.7895$ and $R_2 = 0.6579$ then, $R_1 + R_2 = 1.4474$. Following the individual rates, the splitting process randomly allocate H_1 , $m_1 = \lfloor (1 - R_1)n \rfloor = 8$ rows and allocate H_2 , $m_2 = m - m_1 = 13$ rows. Following the encoding steps in the previous section, we generate the respective codewords

$$u = [01100111011000111010101101001000111001]$$

$$v = [10110001000110000110000101001101110000]$$

At the destination, the received codeword is

$$y = [EE2E0EE20EEEEE0EEEEE20E0E202002E0E22E00E]$$

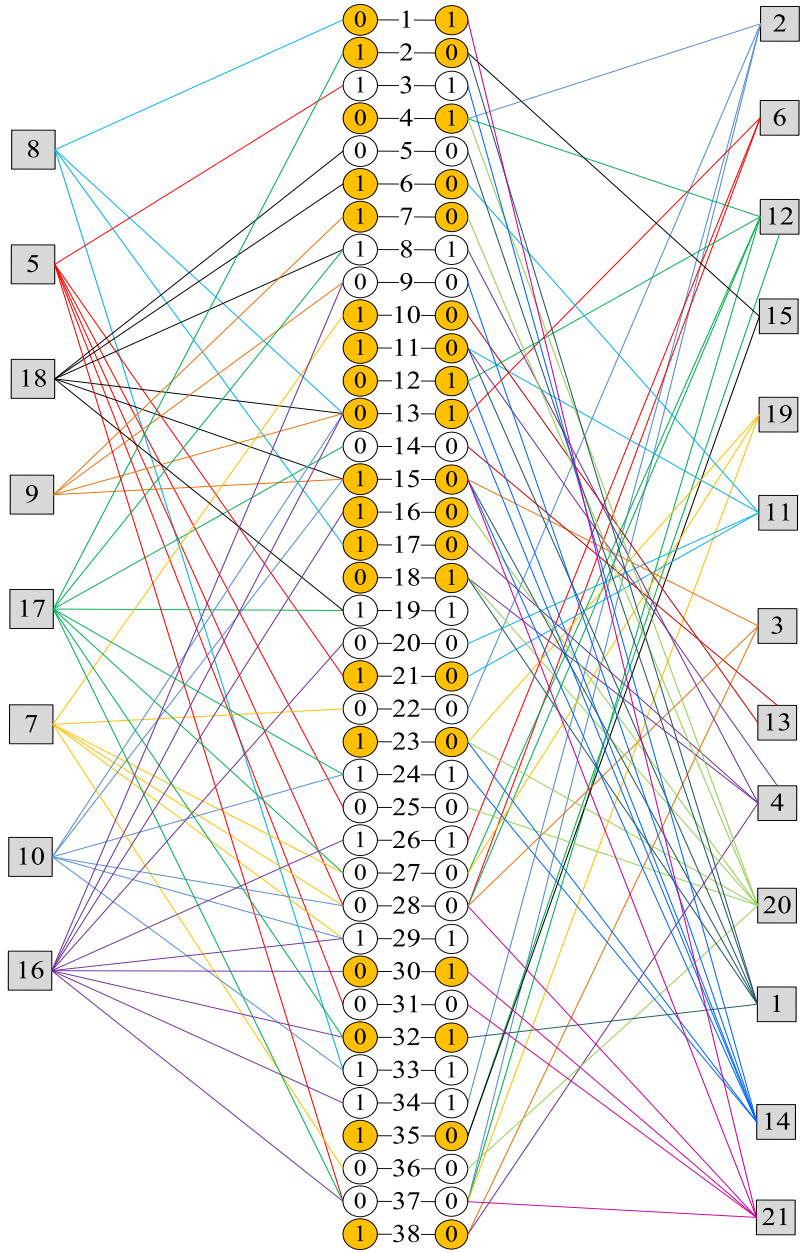


Fig. 3.6 Two-user decoding technique using both Tanner sub-graphs. Erasures are orange variable nodes

The single user BP decoding which is a suboptimal but fast and practical algorithm [30] is used over the individual sub-graphs to recover the erasures. After each iteration, the individual graphs update each other with their respective recovered bits using the relation $v_j = u_j + 1$. Fig. 3.6 illustrates the joint decoding over both sub-graphs. The decoding is completed after 9 iterations

where all erased bits are recovered achieving a rate R close to the capacity boundary region. Table 3.2 illustrates the recovered bits after each iterations. In each iteration, the individual BP decoders independently tries to recover any erasure on the variable nodes. Sometimes they may recover the same erasures. For instance in the first iteration, both BP decoders recovers the erased variable node 10. It is also noted that it only suffices one erasure recovery on either side of the graph to continue the decoding process and not declare decoding failure.

3.5 Simulation Results and Discussion

We evaluate the performance of both coding strategies namely method 1 and method 2 using practical LDPC codes. It is clear that both coding schemes achieve similar rate points on the boundary region. However, the main advantage of using method 2, is that any rate point close to capacity is achievable without time sharing. Then we use some modern coding theory techniques [30] to show the efficiency of the code. Lastly, we draw few remarks.

We first evaluate the performance of both methods using irregular LDPC codes. Particularly, we illustrate how the sum rate $R_1 + R_2$ evolves with the probability of decoding failure. We also show an upper bound on the recoverable erasure for a specific codeword length n . Then we show the gap between the achievable sum rate and the upper bound. Secondly, we evaluate the outage capacity of the system where we show how close the achievable rate pairs (R_1, R_2) to the capacity boundary. Lastly, for the irregular degree distribution used, we show how the probability of erasure evolves with the number of decoding iteration. Furthermore, we illustrate how the maximum tolerable loss evolves with the design rate. The simulation algorithm is presented in details in Alg. 3.1. However, the main steps in producing the results are: 1) Construction of half-rate LDPC matrix, 2) Encoding at both sources, 3) Decoding at the destination.

Table 3.2 Recovered bits after each decoding iteration

<i>Iteration No</i>	<i>Sub-graph1</i>	<i>Sub-graph2</i>
1	$u_{21} = 1, v_{21} = 0$ $u_{10} = 1, v_{10} = 0$	$v_4 = 1, u_4 = 0$ $v_{13} = 1, u_3 = 0$ $v_{23} = 0, u_{23} = 1$ $v_{10} = 0, u_{10} = 1$
2	$u_{15} = 1, v_{15} = 0$	
3	$u_6 = 1, v_6 = 0$ $u_7 = 1, v_7 = 0$	$v_{38} = 0, u_{38} = 1$ $v_{12} = 1, u_{12} = 0$
4		$v_{35} = 0, u_{35} = 1$ $v_{11} = 0, u_{11} = 1$
5		$v_2 = 0, u_2 = 1$
6	$u_{32} = 0, v_{32} = 1$	$v_{18} = 1, u_{18} = 0$
7		
8		$v_{17} = 0, u_{17} = 1$ $v_{16} = 0, u_{16} = 1$
9	$u_1 = 0, v_1 = 1$ $u_{30} = 0, v_{30} = 1$	

3.5.1 Construction of Half-Rate LDPC Matrix

For both coding methods, the key to good code performance is the appropriate design of the parity check matrix H . The starting point in the design of H is to choose the DDP (λ, ρ) that achieves the highest threshold for a given finite codeword length and rate. The authors in [30] used an optimization technique to produce good DDPs. We use their results for the half-rate parity check matrix design. In practice, good performance code is found for a check degree distribution of the form [30]:

$$\rho(x) = ax^{r-1} + (1-a)x^r. \quad (3.15)$$

Assume we choose $a = 1$, $r = 6$, $l_{max} = 8$ and the design rate of one-half. Following the optimization tool in [30], the following right regular DDP are obtained

$$\lambda(x) = 0.4021x + 0.2137x^2 + 0.0768x^3 + 0.3902x^7 \quad (3.16)$$

$$\rho(x) = x^5, \quad (3.17)$$

which yields a design rate of $R(\lambda, \rho) = 1 - \frac{\int_0^1 \rho(x) dx}{\int_0^1 \lambda(x) dx} = 0.5004$ and a threshold $\epsilon^{BP}(\lambda, \rho) =$

0.481. In this chapter and for convenience of notation, we keep referring to H as a half-rate parity check matrix even when the design rate is slightly lower.

Therefore, we first agree on the dimension of H i.e., $m \times n$, then based on a DDP, generate H . The simple way of constructing H starts from an all zero H , then the number of ones that is inserted uniformly in each column is drawn from the variable degree distribution λ . The second step is to check the resulting matrix from the rows perspective to avoid rows with weight $w_r < 2$. The last step is to eliminate length-4 cycles in the equivalent Tanner graph.

In each realization of H , we compute the following: the actual DDP (λ, ρ) , the actual threshold ϵ^{BP} , the actual design rate R , and the evolution of the probability of erasure vs the number of decoding iteration. Then we select the realization that achieves the highest threshold ϵ^{BP} for a given rate. At this stage, H is produced for any method.

Note that the construction of H is done once throughout the simulation algorithm for a specific dimension $m \times n$ and a specific DDP.

3.5.2 Encoding Techniques for Both Methods

Producing the parity bits follows the steps in Section 3.4.1. However, if method 2 is used, then based on the allocated rates for each user, we first randomly distribute the rows over H_1 and H_2 of dimension $m_1 \times n$ and $m_2 \times n$, respectively. Then we generate the codewords u and v to be transmitted over the channel after applying BPSK modulation. If method 1 is used, then one user encodes its data using H and the other user transmits uncoded streams.

Table 3.3 Actual normalized degree distribution pairs for codeword length 10^4

	<i>Rates</i>						
	0.500	0.475	0.450	0.425	0.400	0.375	0.35
λ_2	0.40051466	0.41035256	0.39300935	0.39606974	0.39319233	0.39797144	0.38668728
λ_3	0.20091716	0.20310041	0.21209819	0.20991167	0.20988103	0.21590151	0.21458875
λ_4	0.07310877	0.08089195	0.08127127	0.08032554	0.08631857	0.08821567	0.08590127
λ_5	0.00065983	0.00150668	0.00082593	0.00181957	0.00165235	0.00300280	0.00443977
λ_6	0.00019795				0.00039656		
λ_7	0.20576688	0.19148224	0.20350854	0.19337017	0.19130866	0.18240358	0.17864308
λ_8	0.11824090	0.11115947	0.10571872	0.11433487	0.11368143	0.10649940	0.12234025
λ_9	0.00059384	0.00150668	0.00356801	0.00416846	0.00356907	0.00600561	0.00739961
ρ_2		0.00194194	0.00726816	0.01164522		0.00620579	0.00914263
ρ_3		0.01386145	0.02388582	0.04436431		0.02602429	0.04735752
ρ_4	0.00013197	0.04272274	0.06078827	0.09144143	0.00555188	0.06766315	0.09787220
ρ_5	0.00940253	0.08320220	0.11315207	0.14506898	0.93638467	0.89450153	0.84010261
ρ_6	0.90798720	0.85077175	0.78634907	0.70049955	0.05551884	0.00560523	0.00552504
ρ_7	0.07875029	0.00749992	0.00855661	0.00671585	0.00254461		
ρ_8	0.00343110			0.00026466			
ρ_9	0.00029692						
R	0.500	0.475	0.450	0.425	0.400	0.375	0.35
$1 - R$	0.500	0.525	0.550	0.575	0.600	0.625	0.65
ϵ^{BP}	0.48148490	0.50064714	0.52456507	0.54744148	0.57669850	0.60005343	0.62269565
$\frac{\epsilon^{BP}}{1 - R}$	0.9629698	0.9536136	0.95375467	0.95207213	0.96116416	0.96008548	0.95799330
$1 - \epsilon^{BP}$	0.5185151	0.49935286	0.47543493	0.45255852	0.4233015	0.39994657	0.37730435
δ	0.03570793	0.04876884	0.05349823	0.06089493	0.05504704	0.06237477	0.07236691

3.5.3 Decoding Algorithm for Method 1

At the destination, the receiver first counts the number of erasures e in the received codeword. If $e > m$, then the decoder declares decoding failure. Otherwise, the decoder first computes the LLR of the j^{th} received bit as follows:

$$LLR_j = \begin{cases} -\infty & \text{if } y_i < 0 \\ 0 & \text{if } y_i = 0 \\ \infty & \text{if } y_i > 0 \end{cases} \quad (3.18),$$

then the decoder employs single user BP decoding to first decode the half-rate codeword, then applies SIC to recover the other uncoded stream.

The LLR update rules for single user BP decoding of LDPC code are as in (2.19) and (2.20).

3.5.4 Decoding Algorithm for Method 2

The joint decoding idea used in this method is almost similar to the example given in Section 3.4.3. However, we detail some of the steps. At the destination, the receiver first counts the number of erasures e in the received combined codewords. If $e > m_1 + m_2$, then the decoder declares decoding failure. Otherwise, the joint iterative decoder first computes the initial LLR as in method 1, then each single user BP decoder individually tries to recover some of the erasure on the common variable nodes. At the end of each iteration at both sides of the sub-graphs, each individual BP decoder update the other BP decoder with the newly recovered erasure. This process continues until either all erasures are recovered or no further progress is made on the erasure recovery after the next iteration. In the following we, present the algorithm used for simulation of coding method 2.

Simulation Algorithm for Coding scheme Method 2

- 1: set $n, R_1, R_2, L_{max}, Block_erasure_max$, and (λ, ρ)
- 2: construct H
- 3: split $H = \begin{pmatrix} H_1 \\ H_2 \end{pmatrix}$ to form H_1 and H_2
- 4: initialize $block = 0$, $block_erasures = 0$ counter_upper=0,
- 5: while $block_erasure < Block_erasure_max$ do
- 6: generate s_1 and s_2
- 7: produce codewords u and v
- 8: transmit $y \leftarrow u + v$
- 9: compute e and e_index
- 10: if $e > m_1 + m_2$ then
- 11: counter_upper=counter_upper+1
- 12: $block_erasures = block_erasures + 1$
- 13: end if
- 14: else do
- 15: compute $LLR_1 = LLR_2 = \begin{cases} -\infty & \text{if } y < 0 \\ 0 & \text{if } y = 0 \\ \infty & \text{if } y > 0 \end{cases}$
- 16: while $i < L_{max}$ and $e > 0$ do
- 17: $L_{m1} = DECODER1(LLR_1, H_1, m_1, n)$
- 18: $L_{m2} = DECODER2(LLR_2, H_2, m_2, n)$
- 19: update each individual decoder with recovered erasures
- 20: update e and e_index

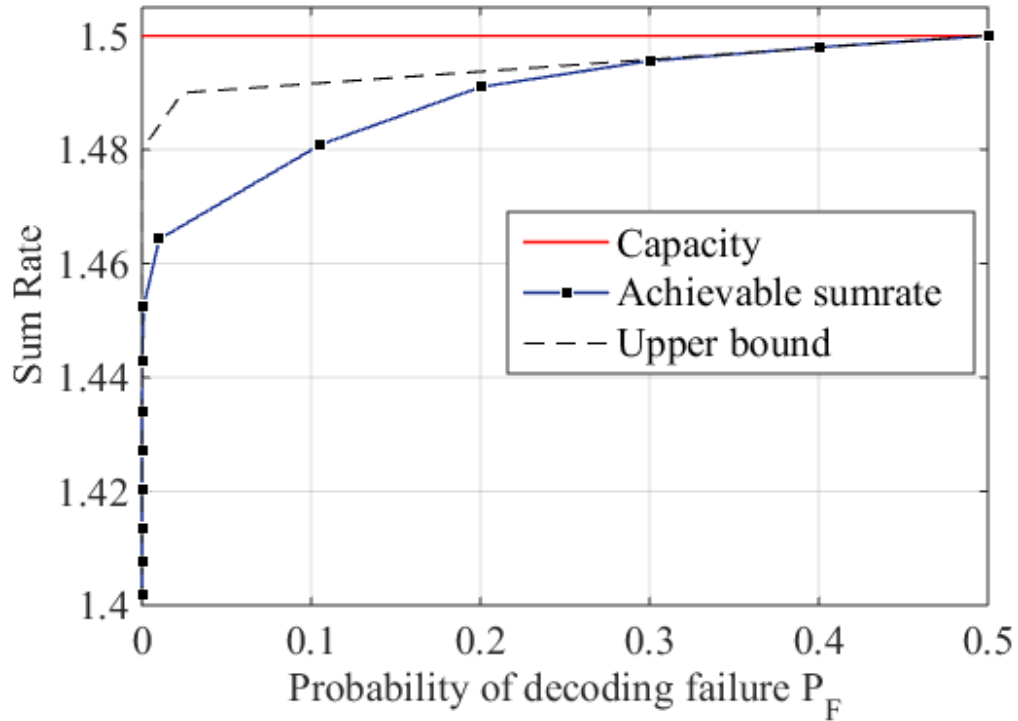


Fig. 3.7 Sum rate as a function of probability of decoding failure. As the sum rate approaches the capacity, the probability of decoding failure dramatically increases.

```

21:     end while
22:     if  $e > 0$  then
23:          $block\_erasures = block\_erasures + 1$ 
24:     end if
25: end else
26: Compute  $P_F = block\_erasures/block$ 
27: Compute  $P_{upper} = counter\_upper/block$ 
28:  $block = block + 1$ 
29: end while

```

Alg. 3.1 Algorithmic presentation of the simulation process for method 2 coding scheme

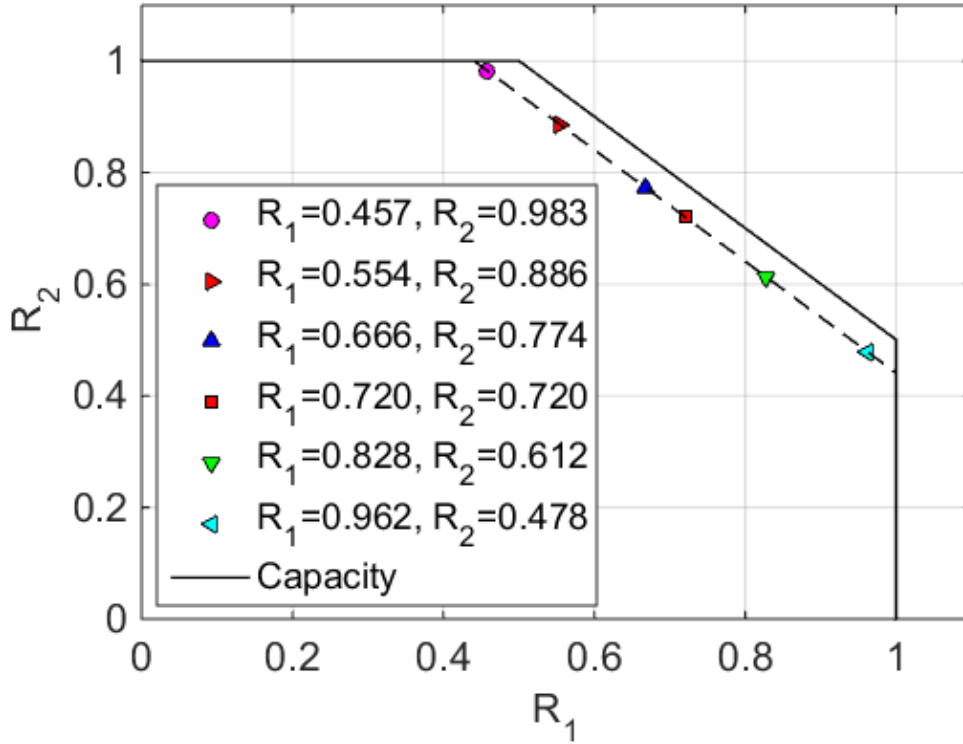


Fig. 3.8 Outage Capacity. The maximum achievable rate for a specific probability of decoding failure 10^{-5}

3.5.5 Simulation Results

In this section, we present the simulation results for the 2-user MAEC. The codeword length used for most of the simulation results is $n = 10^4$. The actual DDP that reflects the constructed parity check matrix H for every rate used in the simulation algorithm is summarized in Table 3.3. Precisely, we illustrate the left and right degree distribution coefficients, the threshold, the design rate, the theoretical threshold, the ratio of threshold and theoretical threshold, and the gap for various rates used in the simulation algorithm.

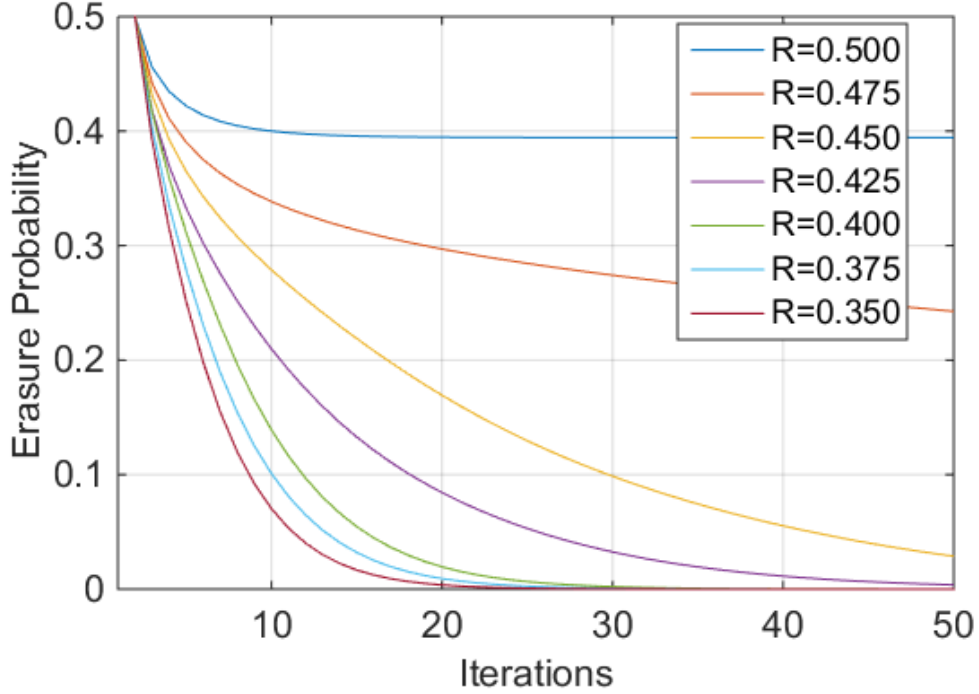


Fig. 3.9 Erasure probability evolving with the number of decoding iterations. The threshold $\epsilon^{BP} = 0.481$. when the rate is greater than the threshold, i.e. $R = 0.5$, the erasure probability never goes to zero even when the number of iterations goes to infinity. However, as the rate goes away below the threshold, the decoder converges faster.

Sum Rate vs. the probability of erasure

Fig. 3.7 illustrates the sum rate as a function of the probability of decoding failure P_F . The capacity which is 1.5 bits per channel use is the red straight solid line. The achievable sum rate is the blue solid line using coding methods 1 or 2. Note that as the sum rate approaches capacity, P_F increases. The upper bound black dashed line is the limit on the possible erasure recovery by the optimal LDPC decoder. However, the gap between the upper bound and the capacity decrease as the codeword length increases. On the other hand, the gap between the achievable sum rate and the upper bound is due to the sub optimality of the decoder and the finite length of the codeword.

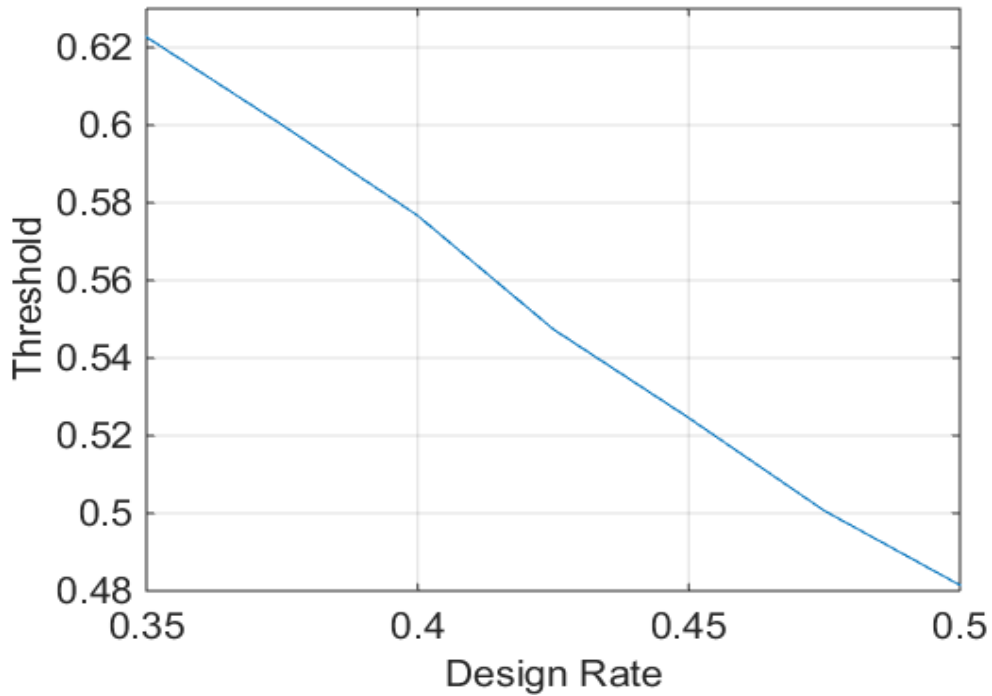


Fig. 3.10 Threshold as a function of the design rate

Outage Capacity

Fig. 3.8 shows the outage capacity for a target probability of decoding failure $P_F \leq 10^{-5}$. Note that the amount of generated parity check equations affect the overall sum rate and not a specific individual rate as this amount of parity check equations is distributed between both encoders such that $R_1 + R_2 \leq 1.5$. The capacity-approaching rate points are the maximum achievable rate pairs (R_1, R_2) for a specific codeword length n , and a target probability of decoding failure P_F . As illustrated in Fig. 3.8, the maximum achievable sum rate $R_1 + R_2 = 1.44$ for a target probability of decoding failure $P_F \leq 10^{-5}$.

Probability of erasure vs. the number of decoding iteration (DE analysis)

Fig. 3.9 illustrates how the probability of erasure evolves with the number of iterations for various design rate R . As the difference between the rate of erasures ϵ in the channel and the threshold ϵ^{BP} increases, the number of decoding iteration decreases and the decoder converges faster. On the otherhand, if $\epsilon > \epsilon^{BP}$ the probability of erasure does not go to zero even if the number of iterations goes to infinity.

Threshold vs. the design rate

Fig. 3.10 illustrates the threshold as a function of the design rate R . As the rate increases the threshold decreases. In the ideal case, the threshold $\epsilon^{BP} = 1 - R$. However this upperbound on the threshold is never achieved in practice. Therefore, as it is shown in Table 2, the ratio $\frac{\epsilon^{BP}}{1-R} < 1$ and $\epsilon^{BP} < 1 - R$ and the loss in capacity is $\delta = 1 - \frac{R}{1-\epsilon^{BP}}$.

3.5.6 Discussion

From the analysis and the simulation results, we draw couple of remarks:

- In a single user half-rate code over the BEC, the received bit stream contains 50% erasures on the average. This requires a half-rate code to recover the erasures. Whereas in the 2-user MAEC coding method 2, the fact that the erasures are common for both individual decoders, makes the decoding efficient in the sense that check node constraints at one sub-graph may recover some erasures that are helpful to carry on the joint decoding process at both sub-graphs. Hence, with relatively small number of constraints from each sub-graph perspective, the coding method 2 can achieve rate pairs (R_1, R_2) close to capacity.

- In the 2-user MAEC coding method 2, the joint iterative decoding process between both sub-graphs does not declare decoding failure if one of the decoders is stuck and unable to further recover some erasures after each iteration. As long as one of the decoders at the corresponding sub-graph is able to recover some of the erasures, the joint decoding process continues to update the other sub-graph with newly recovered erasures. In fact, it may at some point trigger the stuck individual decoder to resume erasure recovery and vice versa. In other words, the individual decoders at each side of the joint graph may be in one of the two states after each iteration: 1) No erasure recovery, 2) Erasure recovery. Note that in the erasure recovery state, some of the recovered erasures may be recovered simultaneously by both constituent decoders within the same decoding iteration. This does not affect the performance of the joint decoder, however, the joint decoder does not declare decoding failure unless the erasure recovery process does not progress at both sides of the joint graph.
- In the 2-user MAEC, the performance of the joint decoder is not affected by the way the matrices H_1 and H_2 are formed nor by the values of the rate pairs (R_1, R_2) . However, the core performance of the joint decoder is only affected by the construction process of H and the codeword length n . As far as n is concerned, the longer the codeword length is the better will the resulting matrix H be translated into a tree like graph [30]. On the other hand, to achieve a highly performant code, H should be constructed from an optimized DDP that results in the highest threshold possible for a given rate. Additionally, H should be as length-4 cycle free as possible.
- The probability of erasure converges faster to zero as the design rate is away below the threshold. Specifically, in the 2-user MAEC iterative decoding process, the number of erasures recovered from one decoding iteration to the other is proportional to how far is the design rate

from the threshold. i.e., the more check nodes constraints at both sides of the graph, the faster the probability of erasure converges to zero.

- The degree distribution coefficients in Table 3.3 illustrate how the right degree coefficients evolves with the design rate. i.e, with increasing the number of rows m in the parity check matrix.

3.6 Conclusion

In this Chapter, we proposed a new practical coding scheme (method 2) for the 2-user MAEC that achieves any rate pair close to the capacity region without time sharing. Specifically, the decoder exploits the fact that when a bit gets erased, sources have transmitted opposite bits. We first showed that when the number of erasures does not exceed the parity check equations at both encoders, the decoder is able to recover both transmitted codewords. Then we computed the probability of decoding failure and the outage capacity. We compared the proposed scheme with the single user decoding scheme (method 1) where one user transmits at half-rate and the other user transmits an uncoded stream with SIC the two corners of the capacity region are achievable, then using time sharing other points on the boundary region are also achieved. We simulated the performance of both methods using LDPC codes for various rate pairs (R_1, R_2) . Additionally, we proposed an efficient approach to construct the LDPC matrices at both encoders. Precisely, we showed that a properly designed half-rate LDPC matrix H achieves rate pair points very close to capacity region on the 2-user MAEC irrespective of the way the rows of H are distributed over the individual parity check matrices H_1 and H_2 . Additionally, we proposed an iterative joint decoding approach for method 2 in which both parts of the graphs employ a single user BP algorithm, then the recovered erasures after each decoding iteration is updated on both sides of the graph before carrying on with

the next iteration. We first showed an upper bound on the achievable sum rate as a function of the probability of decoding failure P_F . Furthermore, we illustrated how the probability of erasure evolves with the decoding iterations. Then we illustrated the outage capacity for a $P_F \leq 10^{-5}$ target. It is clear that both methods perform similarly. However, method 2 achieves any rate pair point without time sharing. Hence, the key element in having good performance in both methods is the appropriate construction of H .

In the next Chapter, we present the second contribution to the thesis where we propose an efficient coding scheme to exchange messages between a large number of MTC devices in the IoT framework. Using Raptor codes, we evaluate the performance of the proposed scheme and compare the results with several relaying strategies.

Chapter 4

A Novel Machine-to-Machine Communication Strategy Using Rateless Coding for the Internet of Things.

4.1 Introduction

In this chapter, we make two major contributions. First, we propose a new cooperative joint network and channel coding strategy for MTC devices in the multicast settings where three or more MTC devices dynamically form a cluster to disseminate messages between themselves. Specifically, in the basic cluster, three MTC devices transmit their respective messages simultaneously to the relay in the first phase. The relay broadcasts back the combined messages to all MTC devices within the basic cluster. Given the fact that each MTC device can remove its own message, the received signal in the second phase is reduced to the combined messages coming from the other two MTC devices. Hence, this results in exploiting the interference caused by one message on the other and therefore improving the bandwidth efficiency. Furthermore, each group of three MTC devices in vicinity can

form a basic cluster for exchanging messages, and the basic scheme extends to N MTC devices. We will detail the extension scheme later in Section 4.3.2.

Second, we implement the proposed scheme employing practical Raptor codes with the use of two relaying schemes namely AF and DNF. We show that with very little processing at the relay using DNF relaying scheme, performance can be further enhanced. We show that the proposed scheme achieves a near optimal sum rate performance. We define the optimal sum rate as the maximum achievable sum rate in such a communication model. Precisely, the optimal sum rate is the summation of all individual rates such that reliable decoding at each MTC device's end is possible. Therefore, the rates configuration, at each MTC device per each TS as shown in Table 4.1, is the optimal configuration to guarantee the decodability constraint (i.e., at least a half-rate message is available at each MTC device's end).

The rest of the chapter is organized as follows. In Section 4.2, we present the system model and define some notations. In Section 4.3, we describe the proposed coding strategy. In Section 4.4, we describe the proposed DNF relaying scheme. In Section 4.5, we present the implementation of the proposed scheme and the simulation results. Section 4.6 concludes the chapter.

4.2 System Model

Consider the scenario where three MTC devices in proximity wish to exchange their messages via a relay R as illustrated in Fig. 4.1. Let D_i denote the i th MTC device with respective message m_i for $i = \{1,2,3\}$. The devices can be any RFID devices, sensors or meters, wireless-enabled consumer electronics, wireless-enabled home appliances, mobile phones or tablets, or any other type of networked MTC devices. The relay can be any repeater, remote radio head (RRH) or another close by MTC device with limited short range transmission to cover three or more devices

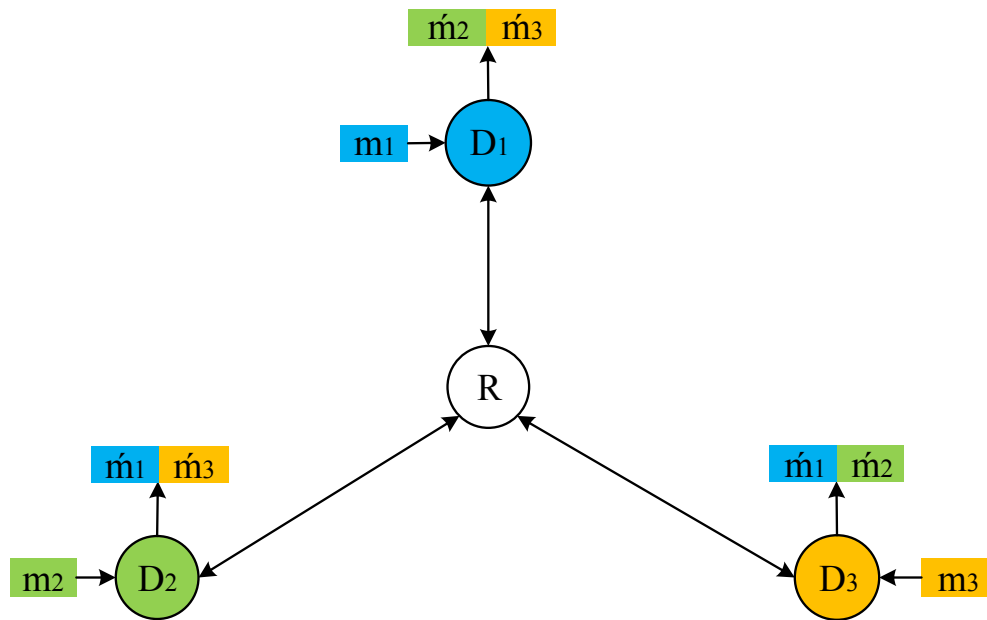


Fig. 4.1 Three MTC devices in proximity exchanging messages via a relay. Each MTC device sends one message and receives two messages. MTC devices are half duplex. \hat{m}_i denotes the decoded message from MTC device i

in proximity forming a cluster. With the rapid grows in chip design and signal processing, highly integrated chips are now available in the market. These powerful chips which are designed for the needs of an increasingly connected world, offer a complete and self-contained Wi-Fi networking solution, allowing them to host applications. Furthermore, these chips have powerful on-board processing and storage capabilities that allow them to be used with sensors and other application-specific devices with minimal development up-front and minimal loading during runtime.

The transmission strategy is over two phases namely MA and broadcast (BC). Note that due to the short distance between MTC devices, the channel in both MA and BC phases is considered as an AWGN channel with equal received power. Additionally, the MTC devices considered are half-duplex for practical reasons; therefore, MTC devices in vicinity cannot directly receive the messages from each other and communication occurs via the relay.

In MA, all MTC devices transmit their respective messages to the relay. The received signal at the relay is characterized by

$$Y_R = X_1 + X_2 + X_3 + Z_R \quad (4.1)$$

where $X_i = \{-1, 1\}$, and Y_i are the channel input from the i th MTC device and the channel output, respectively, in the MA phase. Z_R is a zero mean Gaussian noise with variance σ_R^2 .

In the BC phase, the relay performs AF or DNF to broadcast back the combined messages to MTC devices within the same cluster. The received signal at each MTC device within the cluster is characterized by

$$Y_i = X_R + Z_i \quad (4.2)$$

where X_R is the combined message transmitted from the relay during the BC phase.

At the end of the BC phase, each MTC device removes its own message first (sent during the MA phase), then the remaining received signal consists of the combined messages coming from the other two MTC devices. In the absence of noise, the received signal at MTC device i , Y_i , has three signal levels that correspond to the constellation points [126] d_1 to d_3 : $\{-2, 0, 2\}$ with probabilities $p = \{\frac{1}{4}, \frac{1}{2}, \frac{1}{4}\}$, respectively. In this case, the channel model from each MTC device's perspective reduces to a two-user MAEC [23] over two hops with erasure probability $\alpha = 0.5$. Since all MTC devices transmit equally likely symbols at equal power and same modulation, opposite symbols get erased. Therefore, a half-rate code is required to recover the erased symbols. In Section 4.3, we propose a rateless coding strategy to solve this problem.

4.3 Proposed Coding Strategy for MTC Devices

Use of physical-layer NC in the first phase and the fact that each MTC device can remove its own message in the second phase are the two main components of the proposed coding strategy. Specifically, the core idea of the scheme is to increase the spectral efficiency of the channel by exploiting the interference due to the fact that more than one MTC devices transmit non-orthogonally during the MA phase. The useful interference is strongly coded to recuperate the erased symbols in the received composite signals, and therefore, the key to successful decoding of messages remains in the ability to first recover the erased symbols, then the other message is decoded interference free.

Furthermore, the proposed coding scheme extends to N MTC devices. In the first round, each ensemble of three MTC devices form a basic cluster of order 1 to exchange their messages. In the second round, a logical cluster also consisting of three MTC devices is formed based on the only constraint that each MTC device within the logical cluster of order 2 is randomly selected from one basic cluster of order 1. This way messages are sent from lower order clusters to higher order clusters. This process continues until all $N - 3$ messages are received at the highest order cluster. The last step is to send desired messages from the highest order cluster to lower order clusters and so on until desired messages are received at basic clusters of order 1.

4.3.1 Cluster with Three MTC Devices

Consider the scenario in Fig. 4.1 where one cluster contains three MTC devices in vicinity that want to exchange their messages. In the conventional approach, one MTC device is active at a time while the other two MTC devices are silent. So the conventional scheme requires three TS to multicast 3 bits, hence this scheme is not efficient. On the other hand, in the proposed scheme,

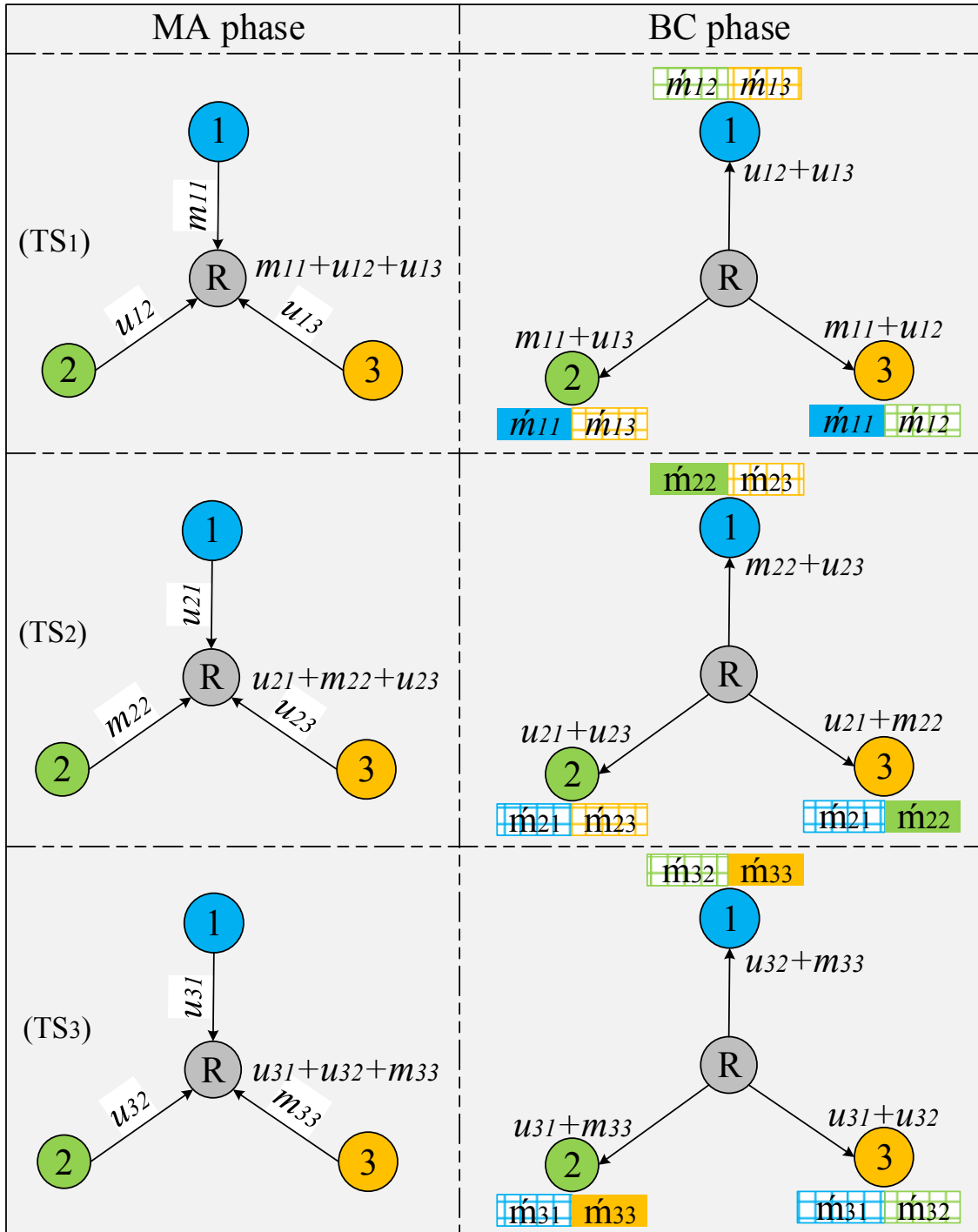


Fig. 4.2 Two phase proposed coding scheme for a cluster with three MTC devices. In the MA phase of the first TS, m_{11} is the unit-rate message sent from MTC device 1 during TS 1, u_{12} is the half-rate coded message sent from MTC device 2 during TS 1, and u_{13} is the half-rate coded message sent from MTC device 3 during TS 1. In the BC phase of the first TS, the first step is that each MTC device removes first its own message, then decodes the half-rate message, applies SIC to decode the unit-rate message if it is available or the other half-rate message. \hat{m}_{11} with solid filled blue color denotes the unit-rate decoded message. \hat{m}_{12} and \hat{m}_{13} with large grid pattern fill green and orange colors denote the half-rate decoded messages.

MTC devices in proximity may exchange messages with each other through a close by relay or another MTC device acting as a relay. The relay is not interested in individual messages, in contrast, it performs AF or DNF to broadcast back the composite signal to the MTC devices.

Let the messages m_{ti} and u_{tj} be row vectors of length k and $\frac{k}{2}$, respectively. The message m_{ti} carries information to be multicast from MTC device i to MTC devices j and l at unit-rate during TS t , where $i, j, l, t \in \{1, 2, 3\}$ and $i \neq j \neq l$. On the other hand, the message u_{tj} carries half-rate coded information to be multicast from MTC device j during TS t . For symmetrical and fair data exchange between MTC devices, we consider three TS-based transmission strategy.

Fig. 4.2 illustrates an example of three consecutive TS. Since half of the bits get erased at each MTC device end, the receiver requires a half-rate coded message to be able to resolve both messages. i.e., the receiver first decodes the half-rate message, then, perform SD to resolve the other message. The main idea of the coding scheme is that one MTC device transmits at a unit-rate whereas the other two MTC devices transmit at half-rate such that in the BC phase (after removing its own message), at least one half-rate message is available at each MTC device to first decode the half-rate message, then removes its effect from the received signal and therefore decode the unit-rate message, or the other half-rate message. In the case where both received messages are at half-rate, the decoder randomly decodes one of the messages first, then decodes the second message in order to preserve fairness. The introduction of TS is to maintain equal average transmission rate at each MTC device. This fairness is guaranteed through the rate configuration in each TS as shown in Table 4.1. Hence, MTC devices in each cluster know at what rate to transmit in each round. Note that a protocol can be devised to choose the rate configuration (selection of a row in Table 4.1) based on the amount of information each MTC device has to share with the other two MTC devices. Next, we describe the example in Fig. 4.2.

Table 4.1 Transmission rates configuration during phase one. The core idea behind such rate distribution is to guarantee that, in any TS, there exists at least one half-rate coded message at each MTC device end, after removing its own message.

Time Slot	MTC device 1	MTC device 2	MTC device 3
1	1	1/2	1/2
2	1/2	1	1/2
3	1/2	1/2	1
Sum rate	2	2	2

MA Phase

In the first TS of the MA phase, all MTC devices within the same cluster transmit simultaneously their corresponding messages m_{1i} , $i = \{1,2,3\}$ at rates 1, $\frac{1}{2}$ and $\frac{1}{2}$ respectively as illustrated in Table 4.1 to a nearby relay. In noiseless scenarios, the received signal Y_{1R} at the relay during the first TS is given by

$$Y_{1R} = m_{11} + u_{12} + u_{13} \quad (4.3)$$

Similarly, in the second and third TS with rate selection from Table 4.1, the received signal at the relay is, respectively, given by

$$Y_{2R} = u_{21} + m_{22} + u_{23} \quad (4.4)$$

$$Y_{3R} = u_{31} + u_{32} + m_{33} \quad (4.5)$$

BC Phase

In the first TS of the BC phase, the relay broadcasts back the composite signal to nearby MTC devices. Each MTC device, removes first its own message, then decodes the two remaining messages from the other two MTC devices. So, each MTC device decodes first half-rate message, applies SIC to decode the unit-rate message or the other half-rate message. Therefore, the received signal at MTC devices 1-3 after removing their own messages is respectively given by

$$Y_{11} = u_{12} + u_{13} \quad (4.6)$$

$$Y_{12} = m_{11} + u_{13} \quad (4.7)$$

$$Y_{13} = m_{11} + u_{12} \quad (4.8)$$

MTC device 1 randomly selects message u_{12} or u_{13} to decode first, then applies SIC to decode the other message. Alternatively, both messages u_{12} and u_{13} can simultaneously be decoded by two independent decoders at the receiver since both are half-rate coded messages. On the other hand, MTC device 2 decodes first the half-rate message u_{13} , then applies SIC to decode the unit-rate message m_{11} . Similarly, MTC device 3 decodes first the half-rate message u_{12} , then applies SIC to decode the unit-rate message m_{11} . Similarly for the remaining TS 2 and 3. Therefore, after three TS, each MTC device has decoded three messages of a sum rate 2. The sum rate of all MTC devices is 6 per 3 TS. That is $\frac{6}{3} = 2$, i.e., $\frac{2}{3}$ per MTC device as shown in Table 4.1.

Note that a ternary channel is assumed in phase 2. Note also that, the relay can be any other additional MTC device in proximity, an AP within the cluster, a RRH, or any type of networked device with in-network processing capabilities.

The advantage of the proposed coding strategy over the conventional scheme is manifold. Due to the short distance between cooperative MTC devices within the cluster, the transmit power is significantly reduced resulting in a major power saving at active MTC devices. Furthermore, less transmitting power usage at MTC devices leads to less interference caused to other MTC devices in neighboring clusters, hence improving frequency reuse factor and increasing network capacity. In addition, directly established links between MTC devices with in-network processing capabilities reduce latency and release radio resources on the core network which also result in increasing network capacity. Moreover, the proposed scheme efficiently uses the spectrum due to the Physical-layer NC which increases the sum rate. Finally, the relay, which can be any device in

vicinity, performs a simple AF or DNF relaying.

Note that for symmetrical data rates, the considered transmission strategy is over three TS in a round robin fashion. However, for asymmetrical data rates between MTC devices, a protocol can be devised to assign transmission rates at each MTC device based on the size of the actual locally available file for sharing. Therefore, each TS (row) of transmission rates configuration in table 4.1, can be more (dynamically) selected based on the available local messages at each MTC device to exchange.

Note also that the set of three MTC devices forming one cluster is the optimal way in terms of the transmission rates. For instance, if we add one more MTC device, so in total we will have four MTC devices such that one MTC device transmits at unit-rate, another MTC device transmits at half-rate and the remaining two MTC devices transmit at quarter-rate each to maintain the decodability constraint. Therefore, the total transmission rate is upper bounded by 2. Hence, by adding one more MTC device, the transmission rate will be distributed between active MTC devices and will never go beyond 2.

4.3.2 Aggregated Cluster with N MTC Devices

The proposed coding strategy extends to N MTC devices in proximity. The extended scheme consists of $\log_3(N)$ rounds each of which is over two phases. In the first round, each three MTC devices in closed vicinity are organized in a basic cluster which results in $\frac{N}{3^d}$ basic clusters of degree $d = 1$, where d is the degree of the cluster. Then, the scheme devised in Section 4.3.1 is applied at each cluster of degree 1. At the end of the first round, each MTC device receives the messages of the other two MTC devices within the same basic cluster of order 1.

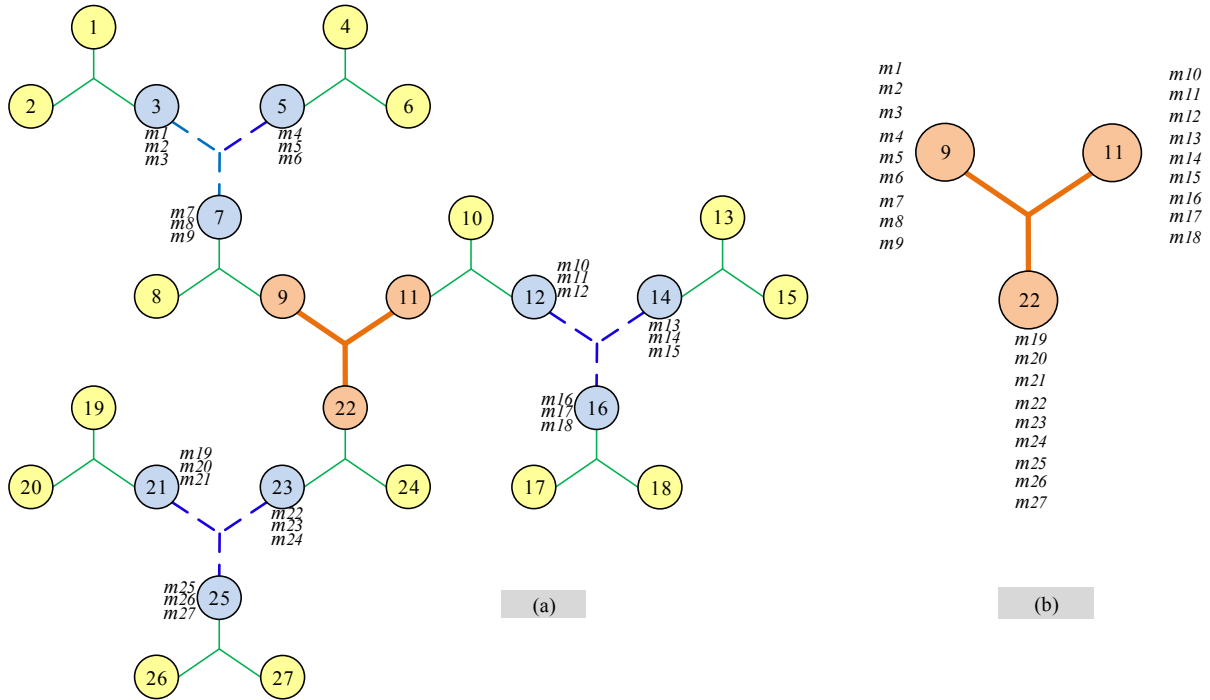


Fig. 4.3 MTC strategy with clustering technique of dimension $N=27$. Clusters with green interconnecting links are of degree 1, clusters with blue interconnecting links are of degree 2 and cluster with orange interconnecting links is of degree 3. In total, we have 9 basic clusters of degree 1, 3 clusters of degree 2, and 1 cluster of degree 3. The blue and orange interconnecting links guarantee dissemination of messages over the entire MTC network. Messages moving across clusters go through interconnecting links based on the scheme devised in Section 4.3.1. Note that the intersecting point that joins three interconnecting links is a relay node regardless the degree of the cluster. (a) illustrates all MTC devices in the network including the interconnecting links for each cluster degree. (b) illustrates the highest degree cluster where all messages are gathered

In the second round, a new logical cluster is formed based on the following constraint. Only one MTC device from a basic cluster of order 1 is allowed to be in the newly formed logical cluster of degree $d = 2$ which results in $\frac{N}{3^d}$ clusters of degree 2. Then, similarly to round 1, the scheme devised in Section 4.3.1 is applied within the logical cluster. In order to disseminate all messages across all MTC devices, this process continues until $d \leq \log_3(N)$. At the end, each MTC device will have received $N - 1$ new messages. Note that each randomly selected MTC device from a cluster of order l contains 3^l exchanged messages within this cluster of order l where $1 \leq l < \lfloor \log_3(N) \rfloor$. Once this procedure reaches the highest logical cluster degree, at this stage, the MTC devices within

Table 4.2 Formation of basic and logical clusters of the example in Fig. 4.3

Cluster Degree No	Cluster Given No	MTC Device No
1	1	1, 2, 3
	2	4, 5, 6
	3	7, 8, 9
	4	10, 11, 12
	5	13, 14, 15
	6	16, 17, 18
	7	19, 20, 21
	8	22, 23, 24
	9	25, 26, 27
2	1	3, 5, 7
	2	12, 14, 16
	3	21, 23, 25
3	1	9, 11, 12

this highest cluster contain all messages in the network. Then, this process continues from the highest order logical cluster downward to basic clusters to only disseminate the wanted messages at each logical cluster of lower degree until reaching each basic cluster of degree 1.

Fig. 4.3 illustrates an example where $N = 27$. In the first round, $\frac{N}{3^d} = \frac{27}{3^1} = 9$ basic clusters of degree 1 (clusters with green interconnecting links in Fig. 4.3) are formed. The formation of basic and logical clusters is described in Table 4.2. In each cluster of degree 1, MTC devices exchange messages as described in Section 4.3.1. For example, in cluster 1 of degree 1, MTC devices 1- 3 exchange their respective messages m_1 - m_3 . In the second round, $\frac{N}{3^d} = \frac{27}{3^2} = 3$ logical clusters of degree 2 (clusters with blue interconnecting dashed links in Fig. 4.3) are formed.

Fig. 4.4 illustrates the logical cluster 1 of degree 2 where one MTC device is randomly selected from each basic cluster of degree 1 (MTC devices 3, 5 and 7) to form the logical cluster of degree 2. At the end of round 2, each MTC device (MTC devices 3, 5, and 7) will have received all messages of MTC devices within the logical cluster 2 as indicated in Fig. 4.4b. Then to disseminate these messages within clusters of lower degree, i.e., degree 1, only messages that are not previously

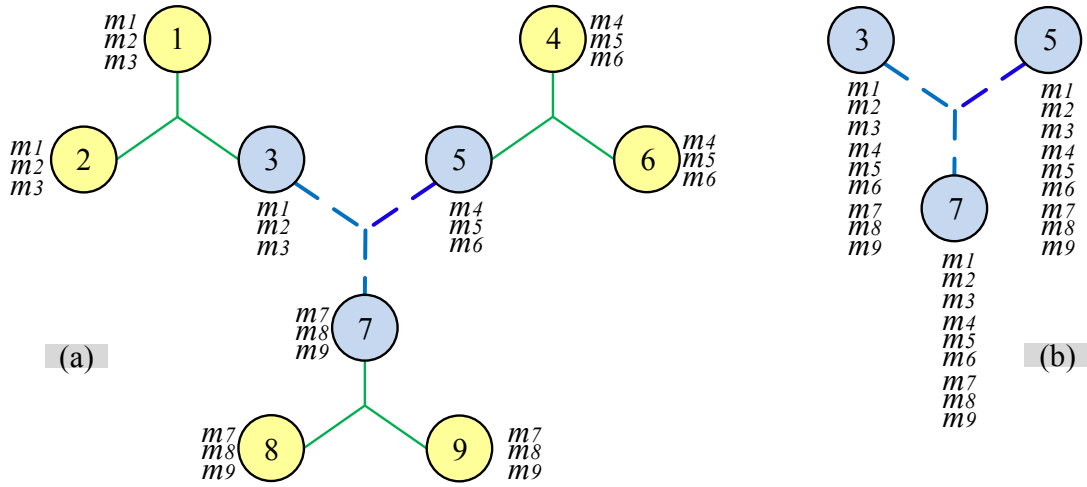


Fig. 4.4 (a) Three clusters of order 1. In each cluster, MTC devices exchange messages. In cluster 1, MTC device 1, 2, and 3 exchange messages m_1 , m_2 , m_3 . Similarly for clusters 2 and 3. In the second round, three MTC devices are randomly selected from three cluster of degree 1 with the constraint that one MTC device is selected from each cluster of degree 1. MTC devices 3, 5 and 7 are selected to form cluster 1 of degree 2. (b) illustrates all the exchanged messages at each MTC device of cluster 1 of degree 2 at the end of the second round

available in each cluster of lower degree are exchanged. For example, in cluster 1 of degree 1 (MTC devices 1-3) messages m_4 - m_9 are only sent downward from higher degree to lower degree.

In the third round where $d \leq \log_3(27) = 3$, $\frac{N}{3^d} = \frac{27}{3^3} = 1$ logical cluster of degree 3 (cluster with thick orange interconnecting links in Fig. 4.3) is formed.

As shown in Fig. 4.3, only one MTC device is randomly selected from each of the three logical clusters of degree 2 (MTC devices 9, 11, and 22). Each MTC device belonging to a logical cluster of degree 2 contains all the messages from that logical cluster of degree 2 to be exchanged with the other two logical clusters of the same degree 2. At the end of round 3, each MTC device will have received $N - 1 = 26$ messages coming from all other devices participating in the MTC network. For example, MTC device 9 has initially message m_9 to exchange with $N - 1 = 26$ MTC devices as illustrated in Fig. 4.3(a). In the first round, MTC device 9 is part of cluster 3 of degree 1 (MTC devices 7-9). At the end of round 1, MTC devices 7-9 contain the messages m_7 - m_9 . In the second

round, MTC device 7 forms a logical cluster of degree 2 with MTC device 3 and 5. At the end of round 2, MTC device 7 contains the messages m_1-m_9 . Newly exchanged messages from this round at MTC device 7 (i.e., m_1-m_6) will be exchanged internally with in the basic cluster 3 and therefore, MTC device 9 will have all the messages of logical cluster 1 of order 2 as illustrated in Fig. 4.3b. In the third round, one logical cluster of order 3 is formed which contains MTC devices 9, 11, and 22 each of which belongs to one logical cluster of order 2 as shown in Fig 4.3a. At the end of this round, each of three MTC devices 9, 11, and 22 will contain all the messages in the network. Finally, only desired messages at each logical cluster of lower order are disseminated. i.e, $m_{10}-m_{27}$ are sent through logical cluster 1 of degree 2 and eventually through basic clusters 1-3 of degree 1.

Note that during the formation process of logical clusters, i.e., clusters of degree $d > 1$, we always select one MTC device from each cluster. However, selected MTC devices for potential formation of logical clusters must be the closest to each other. i.e., we select the i th MTC device from the j th cluster that has the minimum distance with the k th MTC device from the l th cluster.

As per the overhead related to cluster formation, a protocol can be devised to manage MTC devices in vicinity that wish to exchange messages. In such scenarios, the nearest relay receives requests from close by MTC devices wishing to form a group for message sharing. Based on the number of available relays for servicing these MTC devices, the relays agree to allocate each ensemble of three MTC devices to a single relay. Then each relay sends a response message to MTC devices in vicinity to declare the formation of a cluster. Note that the function of a relay in clusters of various degrees (basic or logical clusters) is similar and therefore, clusters are aggregated as shown in Fig. 4.3.

On the other hand, cooperative communication [72] is a key enabling technology for increasing spectral efficiency. The relay plays a vital role in the proposed communication strategy. In domestic

areas, the relay can be a home AP or any other smart device with in-network processing capabilities [127]. The number of MTC devices in a domestic environment is proportionally small and therefore can be served by the home AP which is acting as a relay. However, in larger areas such as malls, universities, airports, and so on, many AP's are deployed all over to ensure nonstop Wi-Fi services in the entire place. While these AP's are mainly used for Wi-Fi access, they can also serve as relays. Let L denote the number of relays required for a given network of N MTC devices. Based on the quality of service and the type of applications, $1 \leq L \leq L_{max}$ where L_{max} denotes the maximum number of relays, as a function of N , required to achieve the best quality of service and is given by

$$L_{max} = \sum_{i=1}^{\log_3 N} \frac{N}{3^i}. \quad (4.9)$$

However, many uncritical applications, such as file sharing, data mirroring and so on, can use any available number of deployed relays in the neighborhood that is $< L_{max}$. When $L = L_{max}$, each cluster is assigned a dedicated relay. When $L < L_{max}$, clusters share relays in time division manner. In the example of Fig. 4.3, $L_{max} = 13$.

As the number of active devices increases, the amount of bandwidth required for disseminating all messages between MTC devices increases. Let B denote the bandwidth allocated to fully exchange messages during the formation of $\frac{N}{3}$ basic clusters of degree $d = 1$. As the degree of clusters increases the number of formed logical clusters decreases by 3^d , however, the amount of required bandwidth is also B since the number of messages to exchange increases as moving to clusters of higher degrees. Therefore, the amount of total bandwidth required to fully exchange messages within a network of N MTC devices is equal to $B[\log_3 N]$. Given the small distance between the nodes, this increase in bandwidth requirement of $O(\log_3 N)$ is affordable. With the small distance

between transmitters and receivers, some of the higher frequency bands such as V-band whose utilization was not feasible due to high attenuation are becoming popular for applications such as the ones suggested in this Chapter [128]. The extremely high bandwidth available in these bands and the short transmission range allow high frequency reuse and very high data rates.

In the example given in Fig. 4.3; note that in the formation of basic clusters, one TS is allocated for all clusters to simultaneously exchange messages as per the proposed scheme in Section 4.3.1. In the formation of logical clusters of degree 2, additional two TSs, that is, three TS in total are required to simultaneously exchange messages as also per the proposed scheme in Section 4.3.1. In the formation of logical cluster of degree 3, six more TSs, that is in total nine TSs, are required to exchange all the messages.

4.4 DNF Relaying Scheme

The DNF scheme is a useful relaying strategy when the relay is not interested in decoding individual messages. The proposed DNF relaying strategy is simple and exhibits lower complexity. The de-noising process consists of mapping the received signal at a relay in vicinity to the nearest constellation point. This process removes the noise propagation to the next hop. However, this process may introduce decision error. By appropriately selecting the decision threshold, we minimize this error.

4.4.1 A Simple De-noising Strategy

In the MA phase, the received signal at the relay in noiseless scenario is the summation of three messages coming from three MTC devices. With the fact that each MTC device utilizes BPSK, this results into four regions symmetric constellation $\{-3, -1, 1, 3\}$ with probabilities $\{1/8, 3/8, 3/8, 1/8\}$

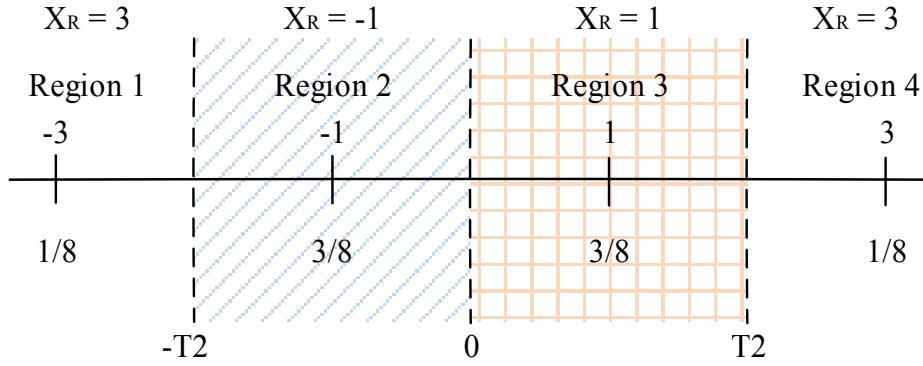


Fig. 4.5 Decision regions and de-noise mapping for the proposed DNF relaying strategy. Received messages that fall in both regions 1 and 4 are considered as reliable information where MTC devices know what each of them sent and therefore can be merged as one region. On the other hand, regions 2 and 3 are not reliable and therefore each region is mapped to a different signal

respectively as shown in Fig. 4.5. The decision rule that minimizes the probability of error is the MAP probability decision rule [129]. Hence, the optimal threshold T_2 is defined as the edge that separates two decision regions in a given constellation [126]. In Fig. 4.5, T_2 is computed as

follows $T_2 = 1 + \frac{(3-1)}{2} + \frac{\sigma_R^2}{2} \ln\left(\frac{3/8}{1/8}\right)$. Therefore, T_2 becomes

$$T_2 = 2 + \frac{\sigma_R^2}{2} \ln(3) \quad (4.10)$$

4.4.2 Decision Regions and De-Noise Mapping

Fig. 4.5 illustrates the decision regions and the per-symbol de-noise mapping applied at the relay. The transmission of $(X_1, X_2, X_3) = (-1, -1, -1)$ and $(X_1, X_2, X_3) = (1, 1, 1)$ are distinctive at the relay and fall in region 1 and 4 respectively. In these two cases the relay knows without ambiguity what each communication device has transmitted. However, the relay is not interested in decoding individual messages, therefore, the relay applies the de-noising process which maps any received signal in the unshaded regions to 3. Actually, when the signal is in either regions 1 or 4 which is considered as reliable information, each MTC device knows what the other MTC devices

transmitted during the MA phase. Therefore, we only require a ternary code to represent the two ambiguous regions (2 and 3) and the clear region (regions 1 and 4).

On the other hand, the transmissions of $(X_1, X_2, X_3) = (-1, -1, 1)$, $(X_1, X_2, X_3) = (-1, 1, -1)$ and $(X_1, X_2, X_3) = (1, -1, -1)$ are indistinguishable at the relay. They all result in the same region 2. Similarly for the other remaining three cases which result in region 3. In those six cases, the relay does not know what exact combination was transmitted during the MA phase; however, the relay removes the AWGN by mapping the signal that falls in the shaded region 2 to -1 and by mapping the signal that falls in the shaded region 3 to 1.

In the BC phase, the relay broadcasts one superimposed/de-noised message to all MTC devices in vicinity. Each MTC device first removes its own message. Then the resulting signaling reduces to the model with constellation regions similar to the one in Fig. 2.10 (three regions constellation). Hence, if the received signal (after removing its own message) falls in either of the unshaded regions 1 and 3, the MTC device knows that the other two MTC devices have sent similar message to his during the MA phase. Otherwise, the received symbols are erased and hence, at least a half-rate code is required to resolve the intended messages for each MTC device.

4.5 Simulation Results and Discussion

We evaluate the performance of the proposed coding strategy with both AF and DNF relaying schemes using Raptor code [18] which is a two layer code, i.e., the pre-code [113] and the LT code [111]. However, the scheme can be evaluated using any half-rate channel code. We first study the performance of the system in the absence of noise, then we consider the presence of noise with both AF and DNF relaying schemes. We perform SD at each MTC device to first decode the lower rate stream, then subtract it from the received signal, then decode the higher rate stream if it is available

Table 4.3 Adaptive rate transmission mechanism between MTC devices. Relay assigns a rate selection scheme (Rows in Table I) based on inputs from MTC devices. However, random selection or equal Average rate selection (default selection code 111) can also be assigned

Broadcast Code by the relay	Selected Rows from Table 4.1
001	Row 3
010	Row 2
011	Row 2, Row 3
100	Row 1
101	Row 1, Row 3
110	Row 1, Row 2
111	Row 1, Row 2, Row 3

or decode the other lower rate stream. Moreover, we evaluate the overheads required for each stream at all MTC devices to achieve a specific BER goal. The pre-code for Raptor code is the LDPC code [113] of rate 0.98 and left degree 4. The number of LDPC decoding iterations is 50 and the number of LT decoding iterations is 300.

The optimized output distribution for Raptor code [114] is given by

$$\begin{aligned} \Omega(x) = & 0.008x + 0.49x^2 + 0.166x^3 + 0.073x^4 + 0.083x^5 + 0.056x^8 + 0.037x^9 \\ & + 0.056x^{19} + 0.025x^{65} + 0.003x^{66}. \end{aligned} \quad (4.11)$$

We consider a block length $k = 65536$ of information bits that are pre-coded with LDPC code at rate 0.98 to generate $k' = 66873$ intermediate bits, then n encoded symbols are generated from the intermediate bits by the LT encoder according to the distribution in (4.11). The relation between the number of produced output symbols n and the overhead ε is given by

$$n = k(1 + \varepsilon) \quad (4.12)$$

The soft decoding process at both layers is completed using the BP decoding algorithm. The LLR update rules for decoding the LT code are as in (2.32) and (2.33). After running the BP decoder enough rounds, the LLR of each input node i is calculated and then is sent to the LDPC belief propagation decoder as a priori LLR of the corresponding symbols. The LLR update rules for decoding the LDPC code are as in (2.19) and (2.20).

4.5.1 Mechanism to Assign Transmission Rates for MTC Devices

The initial step is to decide at what rate each MTC device will transmit. This can be managed by allowing the MTC devices to initially transmit few bits to the relay declaring the amount of data each has to exchange, then the relay selects the rates accordingly by assigning unit-rate to MTC device with the largest file and so on. Alternatively, the relay can randomly pick up any rate combination (any row from Table 4.1) or select the fair combination between the MTC devices (Rows 1- 3 from Table 4.1, in a round robin fashion). Table 4.3 illustrates the various rate allocation schemes and their associated codes. When one single row is selected, i.e., code 001, 010 and 100, each MTC device will transmit at the assigned rate in every TS until an update is received to change the selected rates. On the other hand, when more than one row is selected, the rows are assigned in a round robin fashion. In the equal average rate scenario, i.e., code 111 (default setting), the transmission rates between MTC devices is changed in a round robin fashion as indicated in Table 4.1.

In each TS, one MTC device transmits uncoded source symbols stream while the other two MTC devices transmit n encoded symbols using Raptor code. Encoded symbols from active MTC devices are generated and transmitted until an acknowledgment from respective MTC devices is received at the relay. Then, the relay will send one stop message to both respective encoders. This message can be a 3-bit all zero code (000).

Note that the Raptor code rates are not known a priori. It depends on the channel quality. However, in an erasure channel with 50% of the received symbols are erased on average and links are considered as an AWGN channel, the average number of symbols required at the respective MTC devices is nearly double to be able to resolve the received messages. Therefore, the average rate is around half.

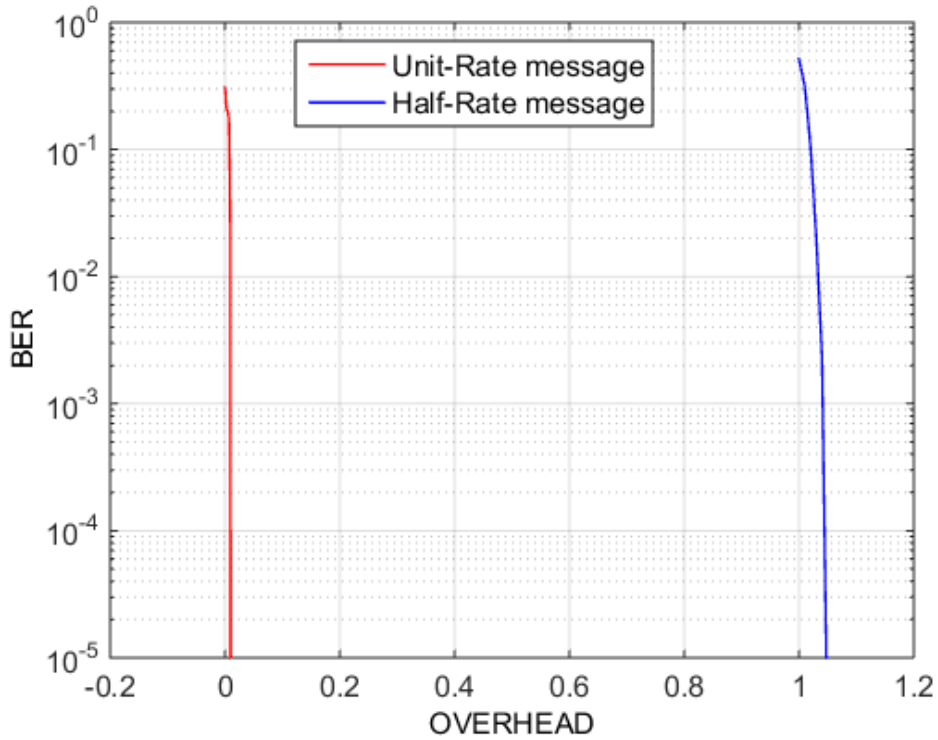


Fig. 4.6 BER vs. overhead for unit-rate and half-rate messages. (Note that for half-rate message, half of the additional coded symbols are erased as well)

4.5.2 System Performance in the Noiseless Scenario

The performance is only affected by the erased symbols. In any TS and at any communication device, the receiver decodes first half-rate message, re-encodes it, and then removes its effect from the received signal to resolve the unit-rate message (where it is available) or the other half-rate message. Theoretically, we need exactly half-rate (twice the number of output symbols) to be able to compensate for the erased symbols and decode the message at the receiver; however, with Raptor code we need a few more reliable symbols to fully resolve the message.

As shown in Fig. 4.6, the overhead required for considerably low BER is $\epsilon_{0.5} = 1.05$ and $\epsilon_1 = 0.01$ for half-rate and unit-rate messages, respectively. In other words, the decoder requires about 1% of additional symbols in the case of unit-rate messages and about 5% of additional symbols

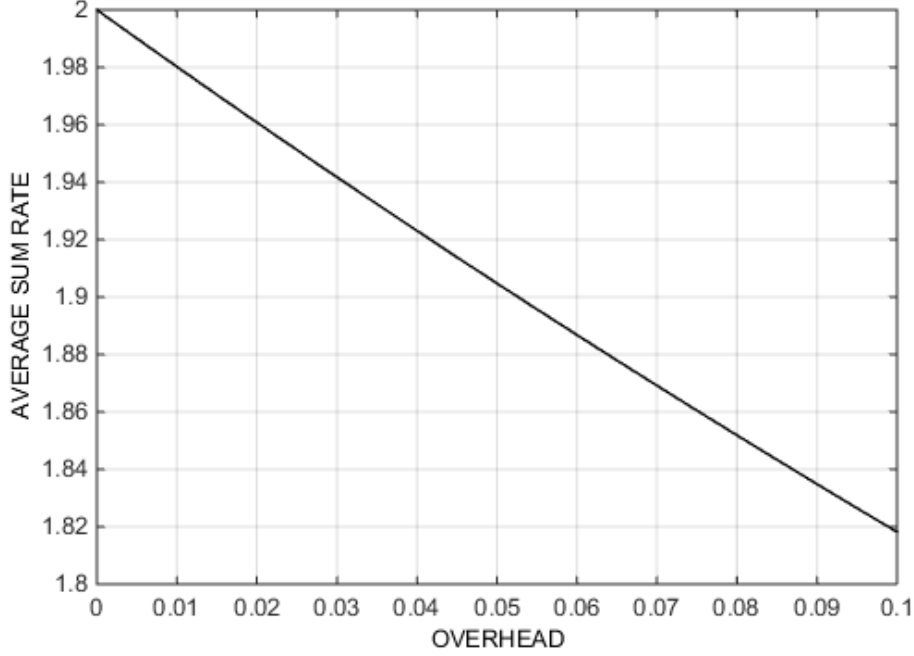


Fig. 4.7 Average sum rate as a function of the simulation overhead ε_{sim} . As the overhead increases, the average sum rate decreases

(on top of the number of symbols that were erased) to fully decode their respective messages. Furthermore, the overhead required for half-rate message is slightly higher compared to unit-rate message since first, half of the additional coded symbols (above overhead 1) are also erased, and second, the distribution in (4.11) is optimized [114] for a block length k and not $\frac{k}{2}$. Consequently, for equal length codewords at all MTC devices, the simulation overhead $\varepsilon_{sim} = 0.025$ as given by the following maximization function

$$\varepsilon_{sim} = \max \left\{ \varepsilon_1, \frac{\varepsilon_{0.5} - 1}{2} \right\} \quad (4.13)$$

Additionally, since the distribution in (4.11) is mainly optimized for block length $k = 65536$, the second term in (4.13) is most likely to dominate. Hence, the average sum rate over three TS is

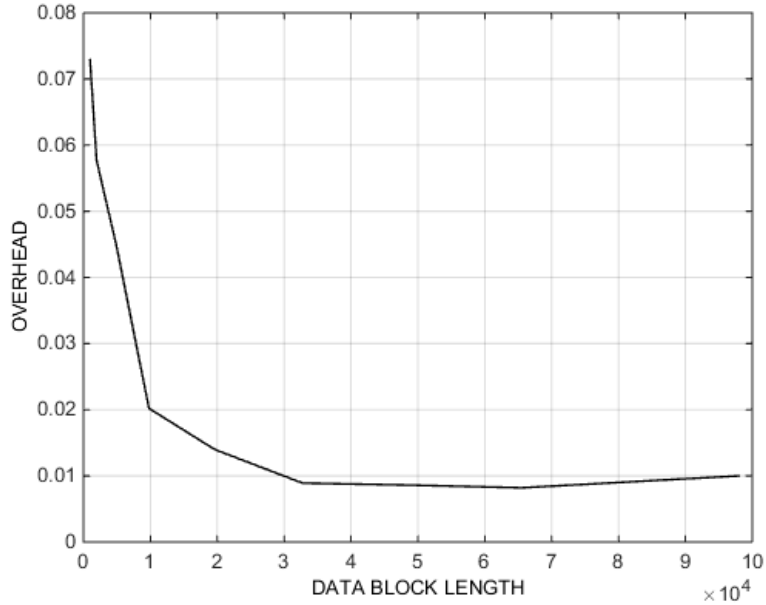


Fig. 4.8 Overhead as a function of the data block length k . The output degree distribution in (11) is optimized for $k = 65536$. Therefore, the lowest overhead is exhibited around this value of k

$R = 1.952$ as given by

$$R = \frac{k}{n} = \frac{2}{(1 + \varepsilon_{sim})} \quad (4.14)$$

The sum rate R decreases as ε_{sim} increases. In the theoretical case, i.e., when $\varepsilon_{sim} = 0$, $R = 2$. Fig. 4.7 illustrates the sum rate as a function of the overhead. Fig. 4.8 shows the overhead as a function of the data block length. Note that the lowest overhead [114] is for block length equal to 65536 since the output distribution in (4.11) is optimized for this value.

4.5.3 System Performance in the Presence of Noise with AF and DNF Relaying Schemes

We consider the performance in the presence of Gaussian noise that is produced at a close by relay and at each MTC device. We assume the same noise variance at all nodes. The received signal at

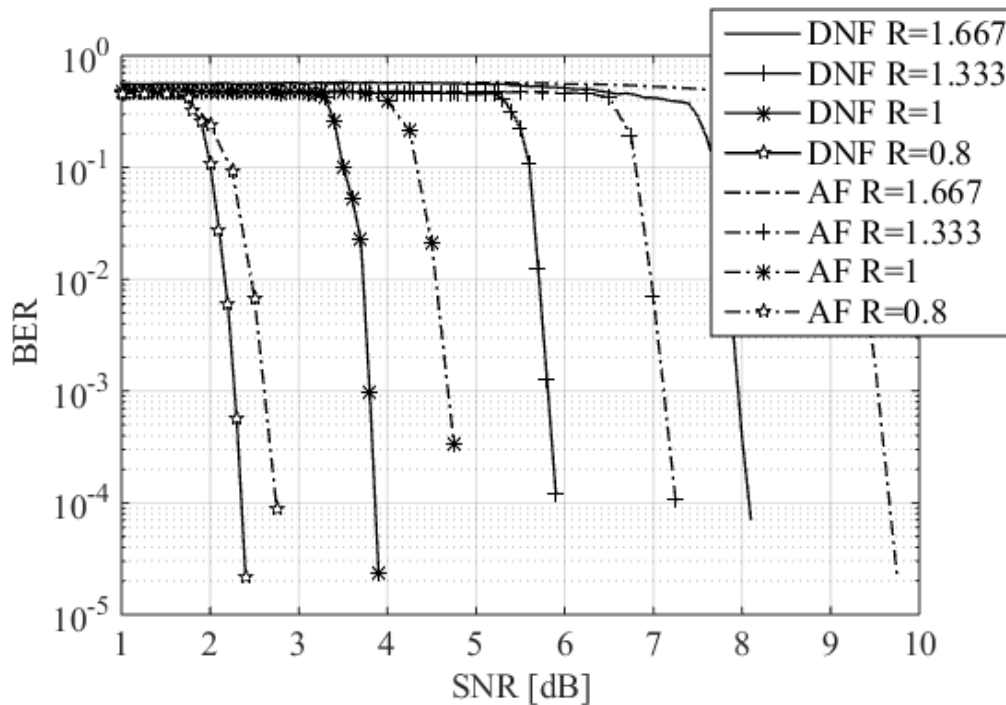


Fig. 4.9 BER as a function of the average SNR for various achievable sum rates R with AF and DNF relaying schemes. The various achievable sum rates reflect the various overheads required at various SNR's. Specifically, for every SNR point, we evaluate the required overhead $\varepsilon_{0.5}$ to achieve a specific BER target $\leq 10^{-5}$. Then using (4.13), we calculate the simulation overhead ε_{sim} , and finally, we calculate the average sum rate using (4.14). On the other hand, the legend can be represented in terms of the overhead $\varepsilon_{0.5}$. i.e., for sum rates $R = 1.667, R = 1.333, R=1$, and $R=0.8$, the $\varepsilon_{0.5}$ overheads are 1.4, 2, 3, and 4, respectively

any MTC device (after removing its own message) is the superposition of two messages coming from the other two MTC devices. Note that, although the unit-rate and half-rate messages are lower than one and half respectively (due to noise), we keep referring to both messages as unit-rate and half-rate for simplicity. The key factor of successful decoding of all messages at any MTC device begins with the ability to decode half-rate message. Note that in the noiseless scenario, the half-rate message requires almost double the transmitted symbols to be able to fully decode the message. Whereas in the noisy scenario, it obviously requires further symbols (more overheads) to compensate for the noise. The unit-rate message is almost surely decodable since ε_{sim} is most likely greater than ε_1 the overhead required for successful decoding of unit-rate message.

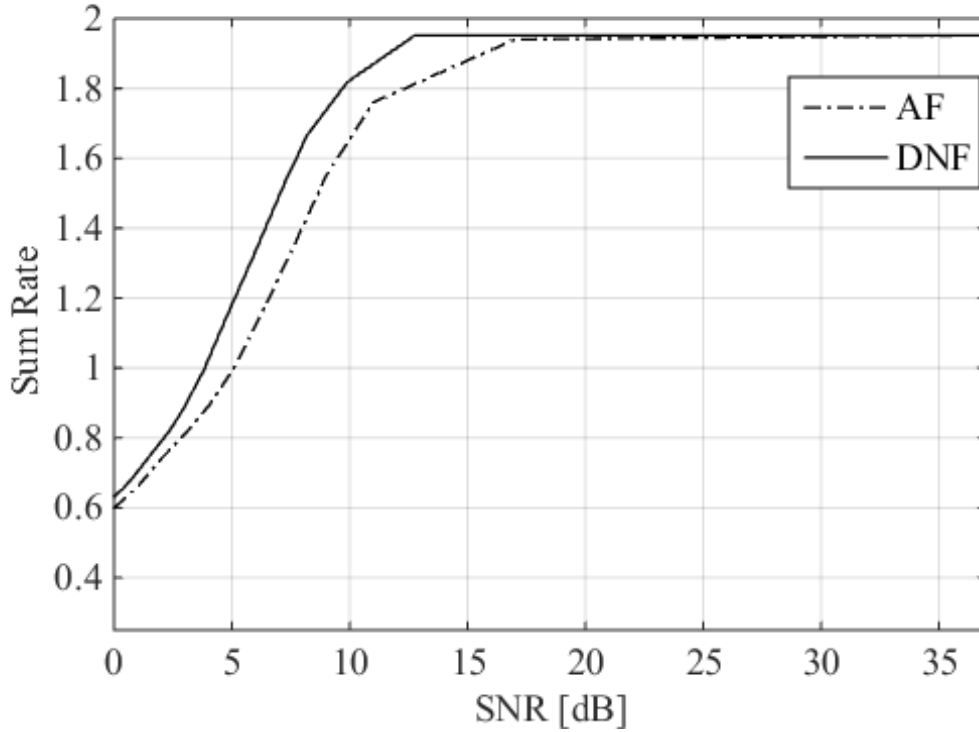


Fig. 4.10 Sum rate as a function of the average SNR with AF and DNF relaying schemes. The overhead required for low SNR increases and therefore results in a lower average sum rate

AF Relaying Scheme

We first consider AF relaying scheme where the relay amplifies the received signal that is received during the MA phase and then broadcasts it to all MTC devices during the BC phase. AF scheme is simple and does not require any processing at the relay. However, due to noise propagation, it performs poorly in the low SNR regime. In the BC phase the relay amplifies the received signal

by a factor $\gamma = \sqrt{\frac{1}{3 + \sigma_R^2}}$ and broadcasts γY_R to MTC devices, where γ is the amplifier gain to maintain the average power constraint at the relay and σ_R^2 is the noise variance.

MTC device i first removes its own message m_i from the received signal. Then, the remaining composite signal at MTC device i is the superposition of the other two messages coming from

MTC devices j and l , plus noise. Assuming that $i = 1$, the remaining messages M_j and M_l have been encoded at half-rate and full-rate respectively (rate selection as Row 3 in Table 4.1). We first decode the half-rate message, then re-encode \hat{X}_j and remove it from the received signal to decode \hat{X}_l interference-free

For every SNR point, we first simulate the amount of overheads required to achieve a BER target less than or equal to 10^{-5} on the half-rate message as shown in Fig. 4.9 (AF). Then, we apply SIC to recover the unit-rate message. The unit-rate message is easily decoded since the simulation overhead ε_{sim} is always greater than the overhead required for decoding unit-rate message ε_1 as illustrated in the maximization function in (4.13). Once this BER target is reached, we note the simulation overhead ε_{sim} and apply (4.14) to compute the sum rate as illustrated in Fig. 4.10 (AF).

DNF Relaying Scheme

In DNF, the relay applies the per-symbol de-noising process at the received signal as follows.

$$X_R^{DNF} = \begin{cases} -1 & \text{if } -T_2 < Y_R < 0 \\ 1 & \text{if } 0 \leq Y_R < T_2 \\ 3 & |Y_R| \geq T_2 \end{cases} \quad (4.15)$$

where Y_R is the received composite signal at the relay during the MA phase, T_2 is the optimal threshold as indicated in (4.10). To maintain the power constraint at the relay, the mapped symbols are also scaled by γ .

Simulation results show that the optimal de-noising threshold T_2 for $SNR \leq 2$ is the MAP [129] as in (4.10). However, for $SNR > 2$, the optimal threshold is fixed to the minimum possible with $T_2 = 2$. Similarly to AF relaying scheme, at each SNR point, we simulate the overheads required to achieve a BER target less or equal to 10^{-5} on the half-rate message as shown in Fig. 4.9 (DNF). Then we apply SIC to recover the unit-rate message. Then after, we note the simulation overhead ε_{sim} and apply (4.14) to compute the sum rate as illustrated in Fig. 4.10 (DNF).

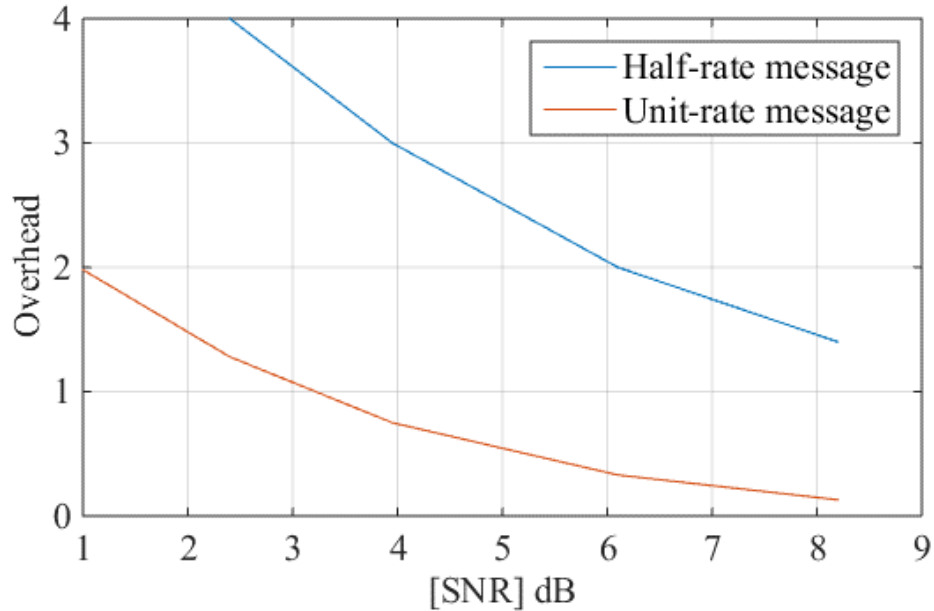


Fig. 4.11 Overhead vs. SNR for half-rate and unit-rate messages. Half-rate message is decoded first

Error free transmission is assumed when $BER \leq 10^{-5}$. To illustrate the importance of the lower rate message, Fig. 4.9 shows the BER as a function of the average SNR for various achievable sum rates with AF and DNF relaying schemes. As SNR increases, the overhead diminishes and therefore the sum rate increases. On the other hand, at very low SNR the sum rate decreases due to the high overhead required to resolve the half-rate message. As illustrated in Fig. 4.9, the performance of DNF outperforms AF for the same amount of overheads.

This Gain in dB for the same overhead is interpreted into higher sum rate. Fig. 4.10 illustrates the average system sum rate over three TS. At lower SNR, the sum rate is bounded by the average overhead required for error free transmission. The dashed line represents the sum rate with AF relaying. It is clearly shown that DNF outperforms AF relaying scheme particularly at low to moderate SNR. Since the performance of both schemes results in the same performance at high SNR, i.e., $SNR > 17$ dB, it is more appropriate to use AF as it is simpler and does not require

further processing. As the overhead increases, the overall sum rate decreases. There is an interesting operational regime in which the sum rate increases linearly with the SNR, i.e. for SNR up to around 12dB. Whereas at higher SNR, the operational sum rate approaches the upper bound. For instance, at 17dB, the sum rate is 1.94. Furthermore, a combined DNF-AF selection relaying scheme can be used with selection SNR threshold to switch between AF and DNF.

Overhead Analysis with DNF Relaying Scheme

In Rateless coding, the overhead at each MTC device depends on the end to end channel quality. In this Chapter, an equal receive signal power is assumed at MTC devices within a cluster. While in a noiseless scenario the overhead required for half-rate messages achieving error free transmission is mainly proportional to the number of erasures (50% on average) in the received combined codeword, the overhead required in the presence of noise is higher to compensate for the errors due to Gaussian noise. Therefore, the overhead experienced at each MTC device is the overhead required to successfully decode both intended messages. For instance, the received signal at MTC device 3 after removing its own message is given by

$$Y_3 = \gamma X_R + Z_3 \quad (4.16)$$

Where X_R is the de-noised combined message at the relay which is a function of the coded messages X_1 and X_2 from respective MTC devices with coding rates as illustrated in Table 4.1. i.e., (X_1, X_2) can take the rate pairs $(1, 0.5)$, $(0.5, 1)$, and $(0.5, 0.5)$.

Using SD, half-rate message is first decoded, subtracted from received signal, then second message is decoded interference free. The overhead vs. SNR is illustrated in Fig. 4.11 for both half-rate and unit-rate messages with DNF relaying scheme. It is clear that the overhead decreases as the SNR increases and the overhead for half-rate message is higher than the overhead for unit-rate message for a given SNR point.

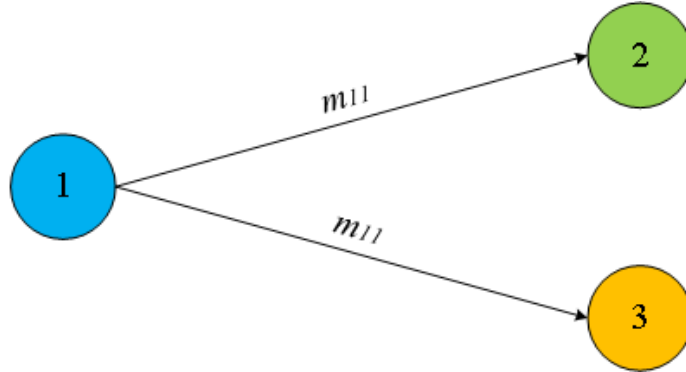


Fig. 4.12 In the first TS, MTC device 1 transmits its message to the other MTC devices 2 and 3. Communication between each active MTC device and the other two MTC devices is interference free. m_i is the unit-rate message sent from MTC device i

4.5.4 Performance Comparison of the Proposed Coding Strategy with Existing Coding Schemes in the Presence of Noise.

In this Section, we compare the performance of the proposed coding strategy with two coding schemes: 1) single device communication where one MTC device is active at a time. 2) Functional decode and forward (FDF) where two MTC devices are active at a time during the MA phase. In the following, we describe and evaluate the performance of both strategies, then we compare them with the proposed scheme.

Traditional Single Device Communication Strategy

In this strategy, one MTC device is active at a time. i.e., one MTC device directly transmits its message to the other two MTC devices (which are in receiving mode). Therefore, in each cluster, three TS are required to exchange three messages between MTC devices. Hence, the sum rate is $\frac{3}{3} = 1$ and therefore, this scheme is not efficient. Fig. 4.12 illustrates the traditional communication strategy over one TS where MTC device 1 is active. The received signal at any of the inactive MTC devices is characterized by

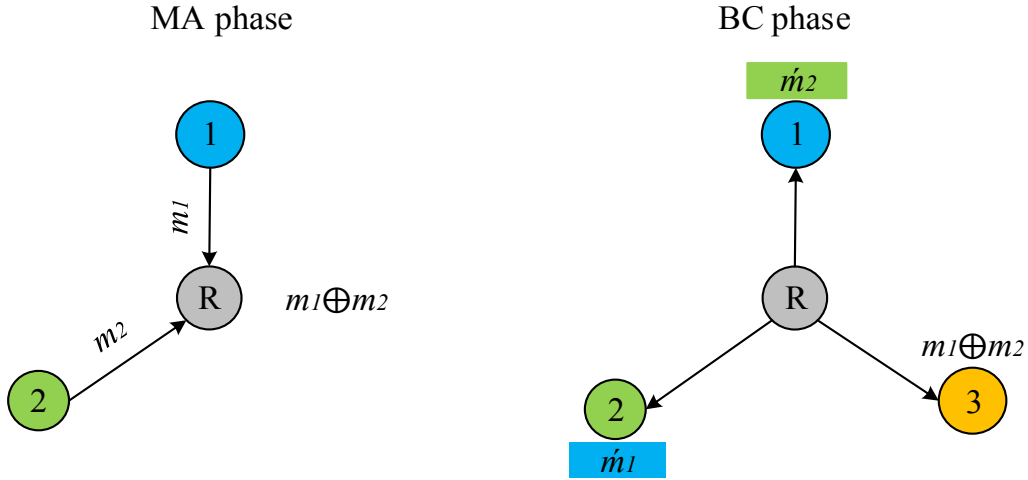


Fig. 4.13 FDF coding scheme for three MTC devices where MTC device 1 and 2 are paired in the MA phase. In the BC phase, MTC device 1 and 2 after removing their own messages, can decode the other MTC device's message interference free. However MTC device 3 cannot decode both messages at this stage and messages are fully resolved in the next TS

$$Y_{tj} = X_i + Z_{tj} \quad (4.17)$$

where X_i is the unit-rate BPSK modulated encoded message, Y_{tj} and Z_{tj} are the received signal and Gaussian noise at MTC device j during TS t , respectively. To compensate for the Gaussian noise at each MTC device end, the messages are Raptor encoded before sent to the other MTC devices. For instance, during the first TS, the received message at MTC device 2 is characterized by

$$Y_{12} = X_1 + Z_{12} \quad (4.18)$$

Since the performance of all messages is similar during any TS, we evaluate the performance of m_1 during the first TS for illustration purposes as indicated in Fig. 4.12. The simulation results are shown in Fig. 4.14, where for every SNR point, we simulate the overhead required to achieve a BER target $\leq 10^{-5}$. Using the following relation, we compute the achievable sum rate

$$R_{TRAD} = \frac{1}{(1 + \epsilon)} \quad (4.19)$$

where ϵ is the required overhead to achieve a specific BER target.

Functional Decode and Forward Scheme

The idea of FDF was initially proposed for two MTC devices in [99] and [130]. Using TDMA and user pairing, this idea was extended to more than two MTC devices in [80]. More specifically, the MA transmission is split into $N - 1$ TSs. In each TS, two MTC devices are active only. For instance when $N = 3$, two TS are required to fully exchange three messages and therefore, the sum rate is $\frac{3}{2}$. Fig. 4.13 illustrates the FDF scheme for three MTC devices during one TS. In this TS, MTC device 1 and 2 are paired during the MA phase. The relay is also not interested in decoding individual messages, however, the relay decodes a function of the received combined messages and transmits it during the BC phase. Then, the paired MTC devices are capable of decoding each other messages from the function message that was received during the BC phase and their own message. The third MTC device is unable to decode the function message at this stage and it will be fully resolved in the next TS. The FDF process avoids the noise propagation at the relay. A simple example of FDF scheme [80] is when the relay uses the XOR function i.e. $m_1 \oplus m_2$. The relay broadcasts $m_1 \oplus m_2$ to all MTC devices within the cluster. Paired MTC devices can decode the exchanged messages by using the XOR function of their own message with the received function message. The received signal at the relay during TS t is characterized by

$$Y_{tR} = X_i + X_j + Z_{tR} \quad (4.20)$$

where X_i and X_j are the unit-rate BPSK modulated encoded message from the paired MTC devices during TS t , respectively. Z_{tR} is the Gaussian noise at the relay during TS t . In the BC phase, the relay broadcasts $X_{tR} = f(Y_{tR})$. The received signal at MTC device j during TS t is characterized by

$$Y_{tj} = X_{tR} + Z_{tj} \quad (4.21)$$

Table 4.4 Comparison between various schemes. Note that the proposed scheme achieves 4% bandwidth saving while it requires 12% of additional Power particularly in the BC phase.

		Traditional	FDF	Proposed
No of TS	MA	3	2	1
	BC	-	2	1
Bandwidth	MA	3	2	1
	BC	-	2	1.56
Power	MA	3P	4P	3P
	BC	-	2P	3/2P
Transmitted messages		3	3	2
Messages / Bandwidth		3/3	3/4	2/2.56
Power / message		P	2P	2.25P

where X_i and X_j are the unit-rate BPSK modulated encoded message from the paired MTC devices during TS t , respectively. Z_{tR} is the Gaussian noise at the relay during TS t . In the BC phase, the relay broadcasts $X_{tR} = f(Y_{tR})$. The received signal at MTC device j during TS t is characterized by

$$Y_{tj} = X_{tR} + Z_{tj} \quad (4.22)$$

The performance of messages at paired MTC devices is similar during any TS. To compensate for the Gaussian noise at the relay and all MTC devices, the messages are Raptor coded before transmitted to the relay. The simulation results are illustrated in Fig. 4.14, where for every SNR point, we simulate the overhead required to achieve BER target $\leq 10^{-5}$. Using the following relation, we compute the achievable sum rate

$$R_{FDF} = \frac{1.5}{(1 + \epsilon)} \quad (4.23)$$

where ϵ is the required overhead to achieve a specific BER target.

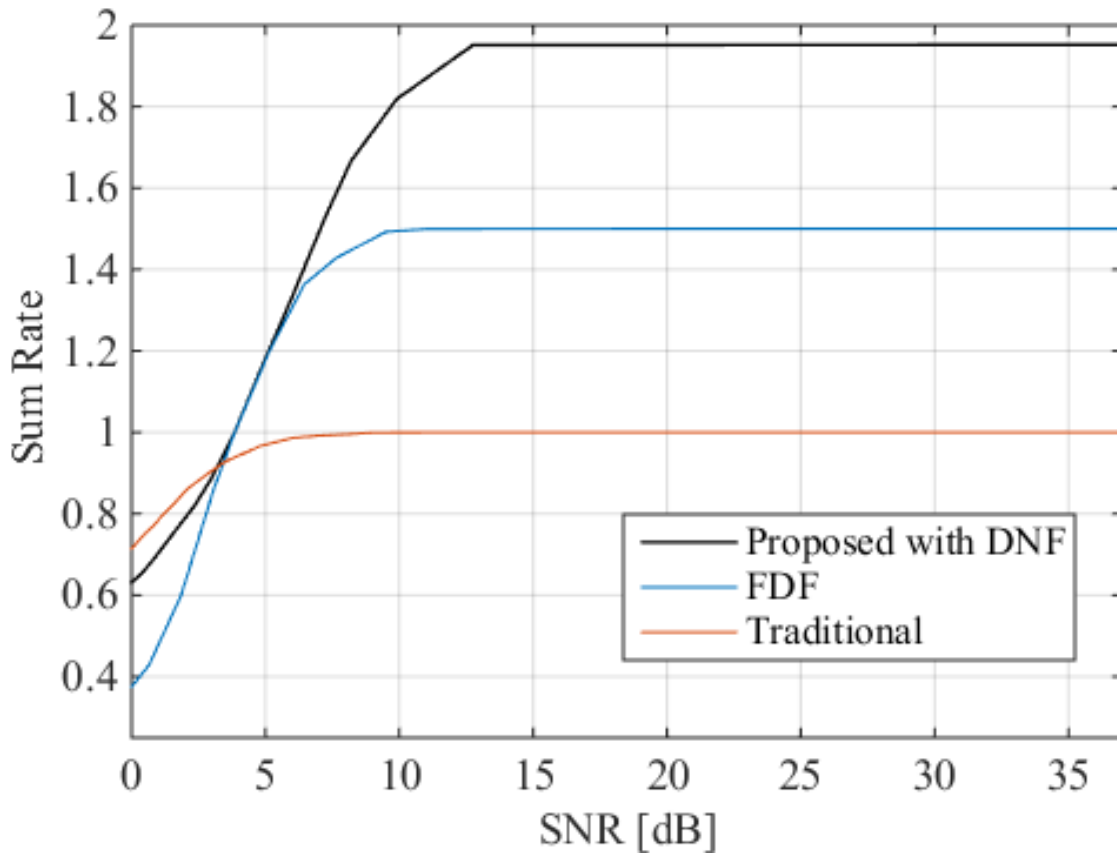


Fig. 4.14 Performance comparison between different schemes. The proposed scheme is the most efficient as it exploits the interference to increase the sum rate. On the other hand, in FDF scheme, messages are decoded interference free with TDMA and pairing. The traditional scheme is the most inefficient and it is used for illustration purposes

Performance Comparison between Proposed and Other Schemes

The performance comparison between the proposed, FDF and traditional coding schemes for the basic cluster (3 MTC devices) is illustrated in Fig. 4.14. However, Table 4.4 shows the comparison in terms of number of TS, bandwidth and power.

4.6 Conclusion and Future Work

In this chapter, we proposed a new cooperative joint network and channel coding strategy for MTC devices in the multicast settings where three or more devices dynamically form a cluster to disseminate messages between them. Specifically, we proposed a coding scheme for MTC devices in proximity to exchange messages via a nearby low cost relay. The key components of the proposed scheme are the use of physical-layer NC in the first phase and the fact that each MTC device removes its own message in the second phase. Additionally, the core idea of the scheme is to increase the spectral efficiency of the channel by exploiting the interference due to the fact that more than one MTC devices transmitting non-orthogonally to the end MTC device. The useful interference is strongly coded to recuperate the erased symbols in the received composite signals, and therefore, the key to successful decoding of messages remains in the ability to first recover the erased symbols, then the other message is decoded interference free. Furthermore, we proposed a systematic approach to extend the scheme to any N MTC devices by employing the concept of clustering. Messages are disseminated first within the basic clusters, then spread out from one layer of logical cluster to another until the last logical layer. Then desired messages within each logical layer are sent from higher logical layer to lower logical layer until the basic clusters.

Additionally, we evaluated the performance of the proposed scheme using practical Raptor codes with two relaying schemes namely AF and DNF. Particularly, we showed that with very little processing at the relay using DNF relaying strategy, performance can be enhanced. In the absence of noise, simulation results showed that a very small overhead is required to fully resolve the messages and hence this represents a small fraction of sum rate loss. Therefore, a sum rate of 1.952 is achievable. Whereas in noisy scenario, simulation results showed that the performance degrades and requires additional overhead to compensate for the errors due to noise at all nodes.

Furthermore, results show that the sum rate increases linearly at low SNR then it saturates close to the upper bound at higher SNR. Moreover, we evaluate the overhead required at each MTC device to successfully decode intended messages. Additionally, we compare the performance of the proposed scheme with FDF and the traditional schemes.

Future work can be directed to propose an optimized power allocation scheme for the unequal received power scenario where Rayleigh fading channel between MTC devices and the relay are considered. In this setup, the CSI are assumed known at MTC devices and can be easily estimated due to the bidirectional aspect of the channel. The aim is to allocate optimal power at each MTC device such that the sum rate is maximized subject to the total power constraint with and without equal rates constraint between MTC devices. The resulting optimized power allocation scheme at each MTC device is a function of the fading channel coefficients and the total power constraint.

In the next Chapter, we present the third contribution to the thesis where we propose a new simple and robust approach to approximating channel coefficients at the receiver without using pilot-aided techniques. Using LDPC and Raptor codes, we evaluate the performance of the proposed scheme in flat correlated Rayleigh fading channel with BP decoders and show that the performance of the proposed scheme is close to optimal case when perfect CSI are assumed available at the receiver.

Chapter 5

Joint Channel Estimation and Raptor Decoding Over Fading Channel

5.1 Introduction

Perfect CSI availability at the receiver is necessary for iterative decoders [16-18] in order to achieve near Shannon capacity limit performance over Rayleigh flat fading channels. Practically, receivers do not possess perfect CSI and consequently some approximation for CSI is required. The optimum technique is to jointly perform channel estimation and decoding. However, this approach exhibits high complexity and delay at the receiver. With the recent advances in iterative decoding algorithms, iterative receivers have been designed to properly perform with reasonable computational complexity on factor graphs [19].

The joint channel estimation and decoding schemes draw a lot of attention among researchers and system designers. One way to estimate the channel is by periodically inserting known pilot symbols in the channel to evaluate the instantaneous state of the communication channel. In this context, several works have been done. Iterative channel estimation and LDPC decoding have been studied in [56] using ML and MAP techniques. Additionally, channel estimation and raptor decoding is

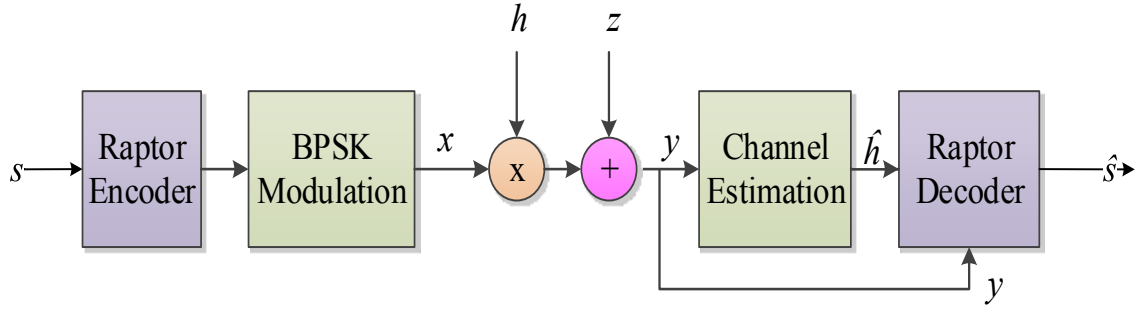


Fig. 5.1 System Model

studied in [64] using minimum mean square error (MMSE) estimate of the channel. These schemes are based on channel estimation and iterative decoding.

In this chapter, we propose a joint channel estimation and decoding scheme over flat Rayleigh fading channel. Specifically, we develop a new simple and robust approach to approximating channel coefficients at the receiver without using pilot-aided techniques. The proposed approach does not exhibit further overhead to the decoder. We evaluate the performance of this estimation scheme over LDPC and Raptor channel codes in flat correlated Rayleigh fading channel and compare our results with other schemes in the literature. Moreover, we illustrate the simulation results, where the channel is on one hand, generated by Jakes' Simulator [131] and on the other hand approximated by a first order AR model [132].

This chapter is organized as follows. In Section 5.2, the channel and the system models are presented. The joint channel estimation and Raptor decoding scheme is investigated in Section 5.3. In section 5.4, we present the simulation results and Section 5.5 concludes the chapter.

5.2 Channel and System Models

The system block diagram is depicted in Fig. 5.1. The source message vector of length k is encoded to produce the codeword vector $u \in \{0,1\}$ of length n . The codeword is binary phase shift keying (BPSK) modulated to generate the vector symbols $x \in \{-1,1\}$ of length n . The modulated symbols are transmitted over a flat fading channel.

The signal is transmitted over a frequency-flat, slow fading channel. The received signal at the destination is given as

$$y = hx + z, \quad (5.1)$$

where z is the independent identically distributed (iid) complex AWGN sample with zero mean and $\sigma_z^2 = \frac{N_0}{2}$ per dimension, and h is the correlated channel fading coefficient with $\sigma_h^2 = E[|h_k|^2] = 1$, modeled as Rayleigh random variables with probability density function (pdf) given by

$$p(h) = \frac{h}{\sigma_h^2} e^{-\frac{h^2}{2\sigma_h^2}}, \quad h \geq 0. \quad (5.2)$$

We consider two channel representations to accurately model the correlation between the channel coefficients, 1) the Jakes' radio channel model [131], and 2) the AR model [132].

In raptor codes, the number of transmitted symbols denoted by n is not fixed a priori. It depends on the channel quality and hence, it requires some overhead to successfully transmit the complete message. Therefore, the number of output symbols is given by

$$n = k(1 + \varepsilon) \quad (5.3)$$

where ε is the overhead. Thus, the rate of a Raptor code is

$$R = \frac{k}{n} = \frac{1}{(1 + \varepsilon)}. \quad (5.4)$$

The soft decoding process at both layers is completed using the BP algorithm. The LLR update rules for decoding the LT code are as in (2.32) and (2.33). After running the decoder enough rounds, the LLR of each input node i is calculated and sent to the LDPC belief propagation decoder as a priori LLR of the corresponding symbols.

The LLR update rules for decoding the LDPC code are as in (2.19) and (2.20).

5.3 Channel Estimation Schemes

In general, the receiver does not have the knowledge of CSI. Therefore, estimation of the channel is required prior to decoding. One way to estimate the channel is by transmitting known pilot symbols at a specific period. This allows the receiver to estimate the channel and eventually to compute the LLR at the decoder. The drawback of such a technique is the overhead incurred from transmission of dummy data known at both sides of the communication link.

Alternatively, the estimation of the CSI at the receiver can be performed using the received information symbols. The main advantage of the latter technique is that it does not need transmission of pilot symbols, nor extra coded bits for yielding the same performance compared to other techniques. Before introducing the new scheme, we briefly describe the ML and MAP techniques.

5.3.1 MAP and ML channel estimation schemes

The approach in these schemes is to estimate the CSI using ML and MAP techniques and subsequently use the estimated CSI in the iterative decoder [56], [64]. The normalized fade rate $f_d T_s$ reflects the degree of correlation in the channel. $\frac{1}{f_d T_s}$, denoted by r , represents the size of a

window through which the channel exhibits a slow fluctuation, i.e., the fading can be considered constant.

Let $L_{x_{ij}}$ be the LLR of i th mapped modulated symbol x_{ij} and define $\hat{x}_{ij} \triangleq \text{sign}(L_{x_{ij}})$. Following the notation in [56], the ML estimation of the channel is given by

$$\hat{h}_{i,ML} = \frac{1}{r} \sum_{j=1}^r y_{ij} \hat{x}_{ij} \quad (5.5)$$

Where x_{ij} and y_{ij} are respectively the i th input and output symbols of the j th window block.

Similarly, the MAP estimation of the channel is given by

$$\hat{h}_{i,MAP} = \frac{\sum_{j=1}^r \frac{y_{ij} \hat{x}_{ij}}{\sigma_z^2} + \sqrt{4 + \frac{2r}{\sigma_z^2} + \left(\sum_{j=1}^r \frac{y_{ij} \hat{x}_{ij}}{\sigma_z^2} \right)^2}}{4 + \frac{2r}{\sigma_z^2}}. \quad (5.6)$$

5.3.2 Proposed channel approximation scheme

This scheme does not require pilot symbols transmission. The estimation is only based on the received signal. Unlike the schemes in references [56] and [64], there is neither hard nor soft decision on received signal y when computing the LLR.

From (5.1), the received signal at the i th time after matched filter is y_i . If we square y_i , and neglect the Gaussian noise, we have

$$y_i^2 = (\hat{h}_{i,APP} x_i + n_i)^2 \cong \hat{h}_{i,APP}^2 x_i^2 = \hat{h}_{i,APP}^2 E_b \quad (5.7)$$

where E_b is the bit energy and $\hat{h}_{i,APP}$ is the approximated CSI at the receiver. The average received signal over a period of r received symbols is given by

$$\bar{y}^2 = \frac{1}{r} \sum_{j=1}^r y_j^2. \quad (5.8)$$

By substituting (5.7) in (5.8), the approximated channel for the i th symbol becomes

$$\hat{h}_{i,APP} = \frac{\bar{y}}{\sqrt{E_b}}. \quad (5.9)$$

Note that $\hat{h}_{i,APP}$ is computed once at the receiver and the same estimated value is used in the iterative decoder. Hence, the decoder will not update this value during the iterative decoding.

One way to enhance the accuracy of $\hat{h}_{i,APP}$ is to slightly vary the window size r around $r \pm \delta$ where $\delta \in \{1, 2 \dots 0.1r\}$. When the fade rate $f_d T_s$ is relatively high, r is small and the average of the received signal over r samples results in a less accurate $\hat{h}_{i,APP}$. However, as the fade rate $f_d T_s$ decreases, no further adjustment of r is required.

The channel LLR of each encoded bit can be expressed as

$$Z_o = \ln \left(\frac{P(o = 0 | y_i, \hat{h}_{i,APP})}{P(o = 1 | y_i, \hat{h}_{i,APP})} \right) = \ln \left(\frac{P(x_i = 1 | y_i, \hat{h}_{i,APP})}{P(x_i = -1 | y_i, \hat{h}_{i,APP})} \right). \quad (5.10)$$

By applying Bayes' rule and using the independence property between x_k and $\hat{h}_{k,APP}$, we obtain

$$Z_o = \ln \left(\frac{P(y_i | \hat{h}_{i,APP}, x_i = 1)}{P(y_i | \hat{h}_{i,APP}, x_i = -1)} \right) + \ln \left(\frac{P(x_i = 1)}{P(x_i = -1)} \right). \quad (5.11)$$

With equal probability channel input x_i , the second term of the right hand side of (5.11) goes to zero. The probability of the matched filter output y_i is expressed as

$$P(y_i | \hat{h}_{i,APP}, x_i = \pm 1) = \frac{1}{\sigma_z \sqrt{2\pi}} e^{-\frac{(y_i \mp \hat{h}_{i,APP})^2}{2\sigma_z^2}}. \quad (5.12)$$

Substituting (5.12) in (5.11), we have

$$Z_o = \frac{2 \hat{h}_{i,APP} y_i}{\sigma_z^2}. \quad (5.13)$$

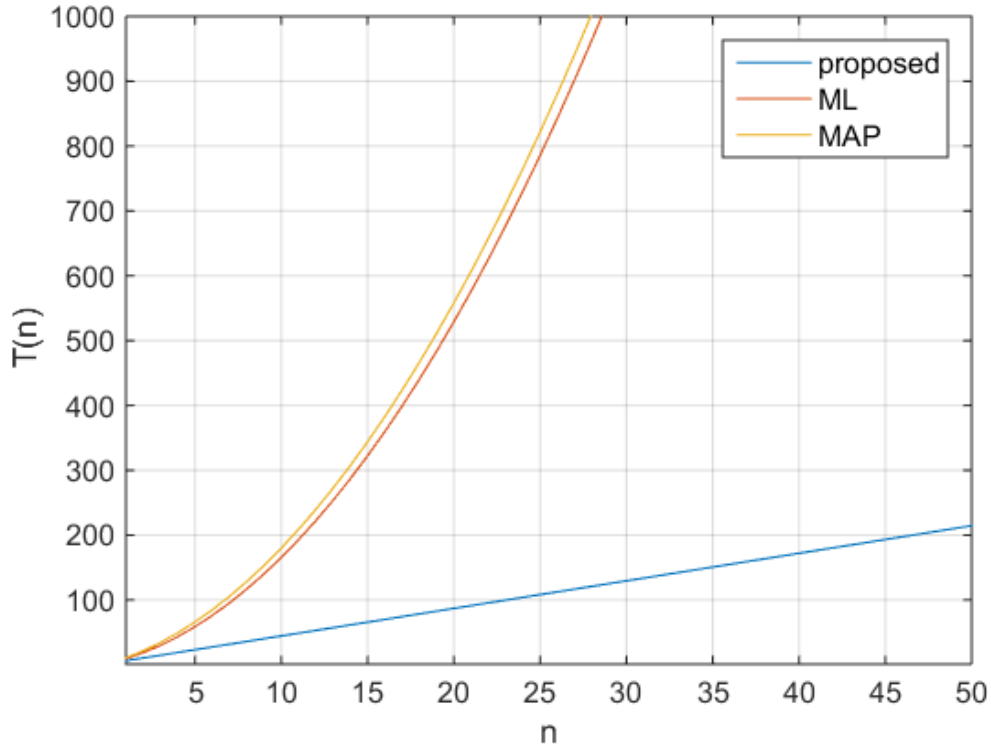


Fig. 5.2 Complexity analysis of proposed scheme vs. existing schemes. The complexity of the proposed scheme is linear with the input size whereas the complexity of existing schemes is quadratic.

5.3.3 Time complexity analysis of proposed and existing schemes

The rate of growth of a function is called the order and is often denoted by the big O notation. When analyzing the proposed approximation scheme, we find that the time it takes to complete the steps in the function with size n is given by

$$T_{APP}(n) = 4n + 5\frac{n}{r} + 2 \quad (5.14)$$

If we ignore constants and slower growing terms, $T_{APP}(n)$ grows at the order of n and hence, $T_{APP}(n) = O(n)$.

On the other hand, the time required to complete the steps in the functions with size n in both existing ML and MAP schemes is respectively given by

$$T_{ML}(n) = n^2 + 6n + 7\frac{n}{r} + 2 \quad (5.15)$$

$$T_{MAP}(n) = n^2 + 6n + 17\frac{n}{r} + 2 \quad (5.16)$$

Therefore, the asymptotic behavior of $T_{ML}(n)$ and $T_{MAP}(n)$ grows at the order of n^2 . Hence, $T_{ML}(n) = O(n^2)$ and $T_{MAP}(n) = O(n^2)$

Fig. 5.2 illustrates a graphic representation of $T_{APP}(n)$, $T_{ML}(n)$, and $T_{MAP}(n)$ relations. It is clear that the running time complexity of the proposed scheme scales linearly with the input size n . Whereas, the running time complexity of the existing schemes is quadratic.

5.4 Simulation Results and Discussion

We evaluate the performance of the proposed scheme using LDPC and Raptor channel codes and compare the simulation results with the other estimation schemes. In the sequel, we consider three modes of operation: perfect CSI, No CSI, and estimated CSI at the receiver. Furthermore, we illustrate the comparison between Jakes' fading channel coefficient simulator and the *AR* approximation models. The number of LDPC decoding iterations is 50 and the number of LT decoding iterations is 300.

5.4.1 Performance Evaluation with LDPC codes

The LDPC code under consideration is a left-regular LDPC code of rate 0.98 and left degree 4 [113]. Fig. 5.3 illustrates the BER performance results of LDPC code in correlated fading channel using Jakes' channel model. For comparison reason, we use similar parameters to [56, Fig. 2], i.e.,

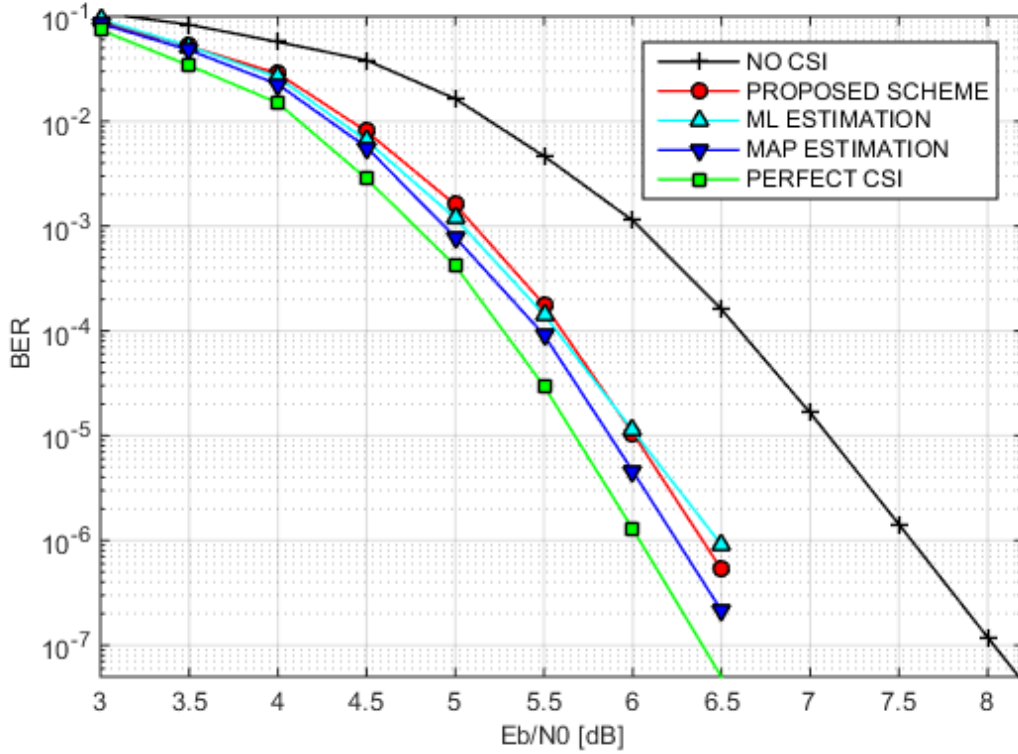


Fig. 5.3 Joint channel estimation and LDPC decoding over block fading channel with $f_d T_s = 0.05$ and $K = 1320$ using Jakes' channel model

the normalized fade rate $f_d T_s = 0.05$, the data block length (DBL) $k = 1320$ information bits and the code rate $R = \frac{k}{n} = 0.5$, where n is the codeword length.

As shown in Fig. 5.3, the performance of the proposed channel approximation scheme is robust and stable. It performs close to ML estimation technique and outperforms it at higher SNR ($\frac{E_b}{N_0} > 6dB$).

At BER of 10^{-5} , the proposed scheme performs about 0.334 dB away from the optimal case (perfect CSI), and about 0.141 dB from the MAP, and 0.001 dB from the ML schemes. The main advantage of the proposed scheme, in contrast with the other schemes in the literature, is that it is simple, efficient and its performance approaches the optimal case.

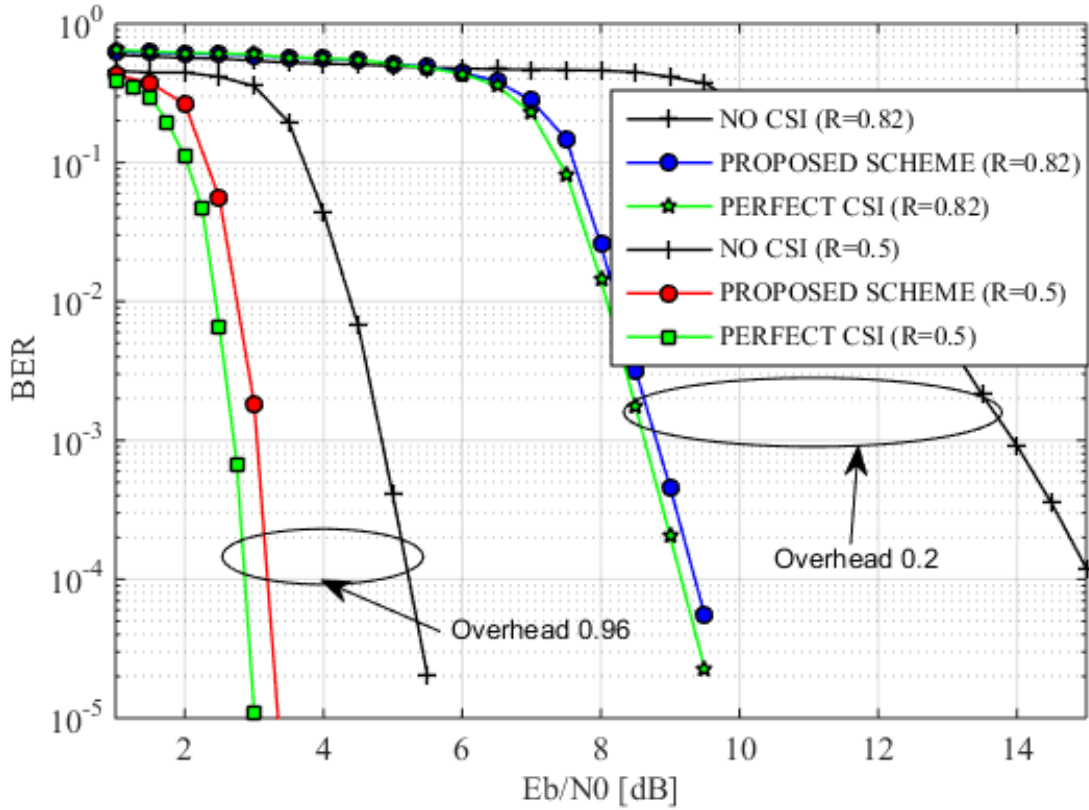


Fig. 5.4 Joint channel estimation and Raptor decoding over block fading channel with $f_d T_s = 0.05$ and $K = 9800$ using Jakes' channel model

5.4.2 Performance Evaluation with Raptor codes

The pre-code for Raptor code is the LDPC code as described in the preceding subsection. We use the optimized output distribution for Raptor code [114].

We evaluate the performance of the proposed channel approximation scheme with Raptor code for different rates using Jakes' and AR channel models. A DBL of 9800 bits is pre-coded by the LDPC pre-code to produce 10000 intermediate bits. Then, using the degree distribution in [114], n encoded bits are generated from the intermediate bits. We consider the system performance for the normalized fade rates of 0.05 and 0.01.

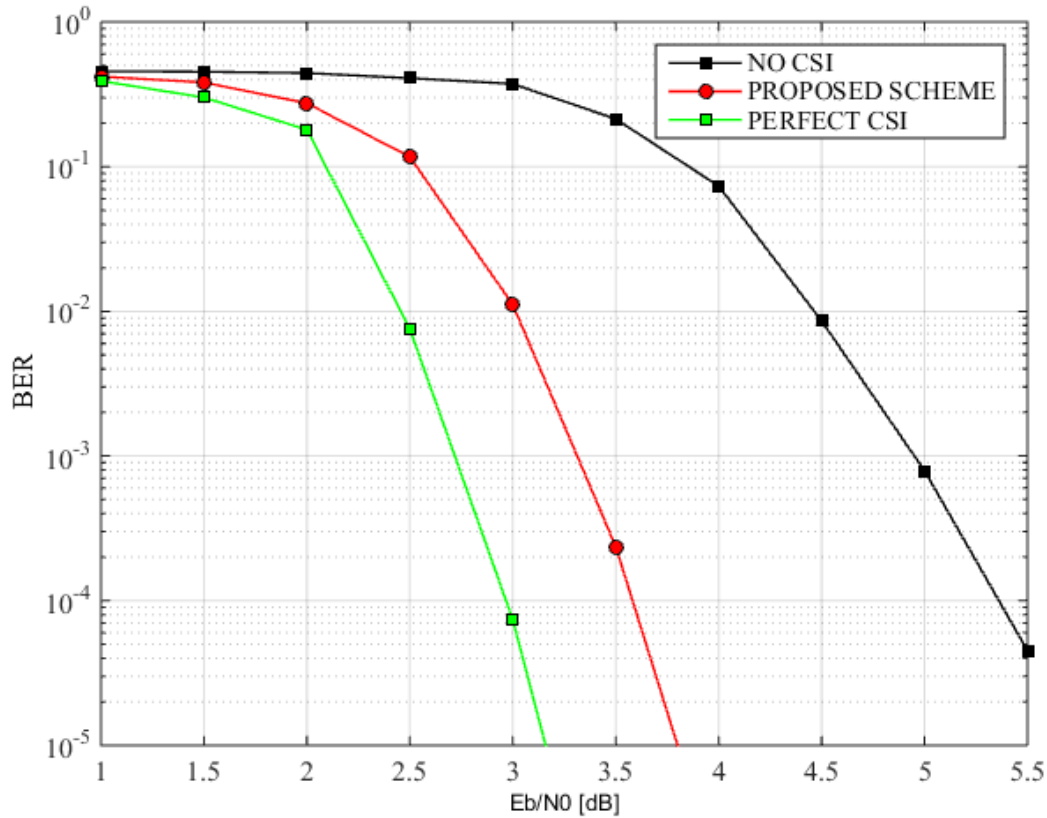


Fig. 5.5 Joint channel estimation and Raptor decoding over block fading channel with $f_d T_s = 0.05$ and $K = 9800$ using AR(1) approximated channel model

Fig. 5.4 illustrates the simulation results of Raptor code with two different rates namely 0.5 and 0.8167. For each rate, we evaluate the proposed scheme along with the perfect and NO CSI cases at the receiver. As shown in Fig. 5.4, at BER 10^{-4} , the performance of the proposed scheme is 0.18 dB away from the perfect CSI at rate 0.8167, while the performance of the proposed scheme is 0.336 dB away from perfect CSI at rate 0.5.

Quite a few observations can be made. First, the higher the SNR, the closer the proposed channel approximation scheme gets to the optimal case. This is also in line with (5.7), i.e., at higher SNR, the signal power increases and the noise power becomes relatively negligible and therefore the

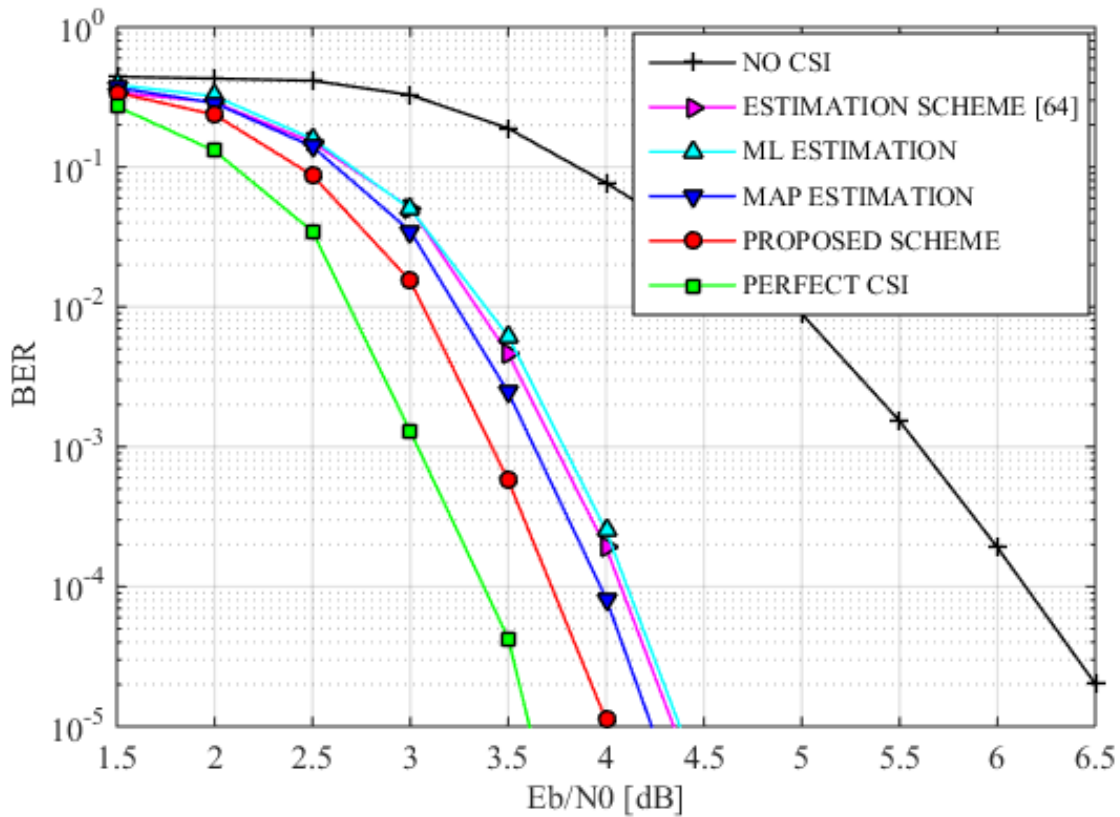


Fig. 5.6 Joint channel estimation and Raptor decoding over block fading channel with $f_d T_s = 0.01$ and $K = 9800$ using Jakes' channel model

proposed approximation scheme approaches the perfect case. Second, the gap between perfect and no CSI, when overhead is 0.2, is greater than the case when overhead is 0.96. This is due to the fact that the code with lower overhead is able to correct fewer errors.

Fig. 5.5 illustrates the performance of Raptor code at rate 0.5, DBL 9800 and normalized fade rate 0.05. we evaluate the proposed scheme in comparison with the cases when No and perfect CSI is available at the receiver using the first order AR(1) channel model. As shown in Fig. 5.5, the performance of the proposed scheme using AR(1) channel model is approximately similar to the

Jakes' channel model. To increase the accuracy of the channel model approximation, a higher order (of order p) AR(p) model can be used at the expense of additional computational complexity [122]. Fig. 5.6 illustrates the simulation results of Raptor codes at rate 0.5, DBL 9800 and normalized fade rate $f_d T_s = 0.01$. We evaluate the performance of the new approximation scheme and compare the results with the other schemes (estimation scheme [64], ML and MAP estimation schemes along with the perfect and no CSI).

As shown in Fig. 5.6, at $BER = 10^{-5}$, the new scheme performs about 0.4 dB away from the optimal case and outperforms all other schemes. Specifically, the new approximation scheme outperforms the MAP, the proposed scheme in [23] and ML schemes of about 0.23, 0.34 and 0.37 dB respectively. The performance of the proposed scheme in reference [23] is about 0.74 dB away from the optimal case which is almost similar to the ML.

5.5 Conclusion and Future Work

In this chapter, we proposed a new simple approximation scheme to estimate the CSI at the receiver when it is not available. The performance of the new scheme was evaluated with LDPC and Raptor channel codes in correlated Rayleigh fading channels. In the simulation, we used the Jakes' channel simulator for different normalized fade rates and we also used the approximated AR channel model.

The results showed that the new approximation scheme performs about 0.375 dB away from the optimal perfect CSI with LDPC code for a specific simulation parameters and it performs about 0.4 dB away from the perfect CSI with Raptor code for different simulation parameters.

In LDPC code, the new scheme performs slightly away from the MAP estimation scheme and it outperforms to some extent the ML scheme. In Raptor code, the new scheme outperforms all other schemes and achieves good performance gain relatively close to the perfect CSI.

The AR(1) approximated channel model performs closely to Jakes' channel simulator. The accuracy of AR model can be enhanced by increasing the order p of the AR(p) model and this gain is at the expense of higher computational complexity.

The main advantages of the new scheme can be summarized as follows. 1) It is simple and efficient in comparison with other schemes in the literature. It does not exhibit high computational complexity. 2) Unlike pilot-aided channel estimation techniques, the new scheme does not require pilot symbols inserted in the data stream to evaluate the CSI at the receiver. Hence, no overhead is necessary. 3) It approaches the optimal case as the SNR increases. The accuracy of the approximation is high as the noise at the receiver is relatively trivial.

The natural extension of this work would be to consider QPSK or other higher order modulation schemes.

Chapter 6

Conclusion and Future Work

6.1 Conclusion

In this thesis, we investigated a number of coding strategies for improving the bandwidth efficiency of multi-user communication channels.

In Chapter three, we proposed a coding strategy for the two user MAEC that achieves any rate pairs close to the capacity boundary region without time sharing nor rate splitting. Specifically, we proposed an encoding approach for two independent sources that want to communicate with a single destination. The key idea behind the proposed scheme is in the fact that when bits get erased, this implies that both sources have transmitted opposite bits. Using LDPC codes, the encoding scheme consists of randomly splitting the rows (constraints) of a half-rate LDPC matrix between both sources 1 and 2. The amount of constraint nodes each constituent (individual) matrix contains is based on the selected rate by each source such that the sum rate is less or equal the capacity of the MAEC which is 1.5 bits per channel use. Then, both codewords are simultaneously transmitted to the destination. On the other hand, the receiver jointly decodes both superimposed codewords using BP decoding. Precisely, the single user decoder independently runs at each constituent sub-graph trying to recover some of the common erasures. After each decoding iteration, the recovered

erasures are updated on both constituent sub-graphs. This process continues until all erasures are recovered or no further erased symbols are being recovered at both constituent decoders. We first showed that when the number of erasures does not exceed the parity check equations at both encoders, the joint decoder is capable of recovering both transmitted codewords. Otherwise the decoder declares failure. Furthermore, we calculated the probability of decoding failure and the outage capacity. We compared the performance of the proposed scheme (method 2) with the known coding scheme (method 1) that achieves the two corners on the capacity region. In method 1, one source is encoded at half-rate while the other source transmits uncoded stream. Using single user decoding at the destination, the receiver decodes the half-rate message first, then using SD to recover the uncoded stream. Other points close to capacity region are also achievable using time sharing. Furthermore, we proposed an efficient approach to construct the LDPC matrices at both encoders. Specifically, we showed that a properly designed half-rate LDPC matrix H achieves rate pair points very close to capacity region on the 2-user MAEC irrespective of the way the rows of H are distributed over the individual parity check matrices H_1 and H_2 . Additionally, we proposed an iterative joint decoding approach for method 2 in which both parts of the graphs employ a single user BP algorithm, then the recovered erasures after each decoding iteration is updated at both sides of the graph before carrying on with the next iteration. We first showed an upper bound on the achievable sum rate as a function of the probability of decoding failure P_F . Furthermore, we illustrated how the probability of erasure evolves with the decoding iterations. Then we illustrated the outage capacity for a $P_F \leq 10^{-5}$ target. We simulated the performance of both methods 1 and 2 using LDPC codes and showed that both schemes achieves similar results. However, the proposed scheme method 2 can achieve any rate pair without time sharing no rate splitting such that the sum rate is less or equal to the capacity.

In Chapter four, we proposed a new cooperative joint network and channel coding strategy for MTC devices in the multicast settings. In this scheme, three or more devices dynamically form a cluster to disseminate messages between them. Specifically, we proposed a coding scheme for MTC devices in proximity to exchange messages via a nearby low cost relay. The key components of the proposed scheme are the use of physical-layer NC in the first phase and the fact that each MTC device removes its own message in the second phase. Additionally, the core idea of the scheme is to increase the spectral efficiency of the channel by exploiting the interference due to the fact that more than one MTC devices transmitting non-orthogonally to the end MTC device. The useful interference is strongly coded to recuperate the erased symbols in the received composite signals, and therefore, the key to successful decoding of messages remains in the ability to first recover the erased symbols, then the other message is decoded interference free. Furthermore, a systematic approach to extend the scheme to any N MTC devices by employing the concept of clustering is proposed. Messages are disseminated first within the basic clusters, then spread out from one layer of logical cluster to another until the last logical layer. Then desired messages within each logical layer are sent from higher logical layer to lower logical layer until the basic clusters.

Additionally, the performance of the proposed scheme using practical Raptor codes with two relaying schemes namely AF and DNF was evaluated. Particularly, it was shown that with very little processing at the relay using DNF relaying strategy, performance can be enhanced. In the absence of noise, simulation results showed that a very small overhead is required to fully resolve the messages and hence this represents a small fraction of sum rate loss. Therefore, a sum rate of 1.952 is achievable. Whereas in noisy scenario, simulation results showed that the performance degrades and requires additional overhead to compensate for the errors due to noise at all nodes.

Furthermore, results show that the sum rate increases linearly at low SNR then it saturates close to the upper bound at higher SNR. Moreover, the overhead required at each MTC device to successfully decode intended messages was evaluated. Additionally, the performance of the proposed scheme was compared with FDF and the traditional schemes.

In Chapter five, we proposed a new simple approximation scheme to estimate the CSI at the. The performance of the new scheme was evaluated with LDPC and Raptor channel codes in correlated Rayleigh fading channels. In the simulation, we used the Jakes' channel simulator for different normalized fade rates and we also used the approximated AR channel model.

The results showed that the proposed approximation scheme performs about 0.375 dB away from the optimal perfect CSI with LDPC code for a specific simulation parameters and it performs about 0.4 dB away from the perfect CSI with Raptor code for different simulation parameters. In LDPC code, the proposed scheme performs slightly away from the MAP estimation scheme and it outperforms to some extent the ML scheme. In Raptor code, the new scheme outperforms all other schemes and achieves good performance gain relatively close to the perfect CSI. The AR(1) approximated channel model performs closely to Jakes' channel simulator. The accuracy of AR model can be enhanced by increasing the order p of the AR(p) model and this gain is at the expense of higher computational complexity. The main advantages of the new scheme can be summarized as follows. 1) It is simple and efficient in comparison with other schemes in the literature. It does not exhibit high computational complexity. 2) Unlike pilot-aided channel estimation techniques, the new scheme does not require pilot symbols inserted in the data stream to evaluate the CSI at the receiver. Hence, no overhead is necessary. 3) It approaches the optimal case as the SNR increases. The accuracy of the approximation is high as the noise at the receiver is relatively trivial.

6.2 Future Directions

The work presented in Chapters three, four and five can be further developed beyond this thesis. In the context of 2-user MAEC, the proposed coding strategy can be further extended to rateless coding using Raptor codes. Another research path within this context, the extension of this work to any number of users. Additionally, one possible extension is to further develop the proposed scheme with higher order modulation. The current scheme uses BPSK, at both sources. The simple starting point may be QPSK or any other higher modulation order. Moreover in this research direction, the current sources transmit at equal power. One interesting and more encountered in practical scenarios is the case with unequal power. In this case, sources transmit with optimal power allocation scheme such that constellation at the destination contains a minimal number of overlapping constellation points. i.e. erasures and minimum distance is maximized. In the proposed scheme, we did not consider the Gaussian noise, nor the Rayleigh fading channel. Another research direction within this context would naturally be the study of the system model in the presence of Gaussian noise and in Rayleigh fading channels. In this scenario, the received power of both sources at the destination varies significantly from one channel realization to another and therefore power allocation with known channel coefficients at the transmitter are required to compensate for the channel variations. In such situations, it is very probable that new schemes have to be proposed.

In the context of M2M communication, we considered the received equal power in both direction of each communication link. However, an interesting and natural extension is to consider the unequal received power. This line of work can be directed to propose an optimized power allocation scheme for the unequal received power scenario where Rayleigh fading channel between MTC devices and the relay are considered. In this setup, the CSI are assumed known at

MTC devices and can be easily estimated due to the bidirectional aspect of the channel. The aim is to allocate optimal power at each MTC device such that the sum rate is maximized subject to the total power constraint with and without equal rates constraint between MTC devices. The resulting optimized power allocation scheme at each MTC device is a function of the fading channel coefficients and the total power constraint.

In both chapters three and four, we considered bandwidth-efficient coding schemes. In this context, multiple devices communicate with a single destination where symbols are assumed synchronized. An interesting direction of research is to study the effect when symbols are not synchronized and how much synchronization offset is tolerable.

Since the relay plays a crucial role in the performance of the coding strategy, another promising research path in this context is the use of multiple relays or relays with multiple antennas. This will increase the DoF at the relay where some space coding techniques can be used to further enhance the relaying approaches. This idea is particularly useful in the case where Rayleigh fading channel is considered.

In the joint channel estimation and Raptor decoding framework, the natural extension would be to consider QPSK or other higher order modulation schemes.

Bibliography

- [1] K. Ashton, "That 'Internet of Things' ", RFID Journal, vol. 22, pp.97-114, Jun. 2009.
- [2] Cisco, "Cisco Visual Networking Index: Global Mobile Data Traffic Forecast Update, 2014-2019", white paper, Feb. 2015.
- [3] Huawei Technologies Co., "Global Connectivity Index", Sep. 2015.
- [4] M. James, M. Chui, P. Bisson, J. Woetzel, R. Dobbs, J. Bughin, and D. Aharon, "The Internet of Things: Mapping the Value Beyond the Hype", McKinsey Global Institute, Jun. 2015.
- [5] FCC, "Spectrum Policy Task Force", ET Docket 02-135, Nov. 2002.
- [6] S. Haykin, "Cognitive radio: Brain-empowered wireless communications", IEEE Journal of Selected Areas in Communications, vol. 23, no. 2, pp. 201-220, Feb. 2005.
- [7] A. Zanella, N. Bui, A. Castellani, L. Vangelista, and M. Zorzi, "Internet of Things for Smart Cities", , IEEE Journal on Internet of Things, vol.1, no.1, pp.22-32, Feb. 2014.
- [8] M. Dohler and C. Anton-Haro, "Machine-to-Machine communications Architecture, performance and applications", Woodhead Publishing, Jan. 2015.
- [9] I. Stojmenovic, "Machine-to-Machine Communications With In-Network Data Aggregation, Processing, and Actuation for Large-Scale Cyber-Physical Systems", IEEE Journal on Internet of Things, vol.1, no.2, pp.122-128, Apr. 2014.
- [10] F. Ghavimi, and C. Hsiao-Hwa, "M2M Communications in 3GPP LTE/LTE-A Networks: Architectures, Service Requirements, Challenges, and Applications", IEEE Transactions on Communications Surveys & Tutorials, vol.17, no.2, pp.525-549, 2nd quarter 2015.
- [11] <http://www.3gpp.org/specifications/releases/68-release-12>

- [12] X. Lin et al., "An overview of 3GPP device-to-device proximity services", *IEEE Communication Magazine*, vol. 52, pp. 40–48, 2014.
- [13] C. Yu et al., "On the performance of device-to-device underlay communication with simple power control", *Proceedings IEEE Vehicular Technology Conference, VTC Spring*, pp. 1–5, Apr. 2009.
- [14] T. Peng et al., "Interference avoidance mechanisms in the hybrid cellular and device-to-device systems", *Proceedings IEEE PIMRC*, pp. 617–621, 2009.
- [15] Z. Zhou et al., "Energy efficiency and spectral efficiency tradeoff in device-to-device (D2D) communications", *IEEE Wireless Communications Letter*, pp. 485–488, 2014.
- [16] C. Berrou, A. Glavieux, and P. Thitimajshima, "Near Shannon limit error-correcting coding and decoding: Turbo-codes", *Proceedings IEEE International Conference on Communications*, pp.1064 -1070 1993.
- [17] R. G. Gallager, *Low-Density Parity-Check Codes*. Cambridge, MA: MIT Press, 1963
- [18] A. Shokrollahi, "Raptor codes", *IEEE Transactions on Information Theory*, vol. 52, no. 6, pp. 2551–2567, Jun. 2006.
- [19] A. P. Worthen and W. E. Stark, "Unified design of iterative receivers using factor graphs", *IEEE Transactions Information Theory*, vol. 47, no. 2, pp. 843-849, Feb. 2001.
- [20] F. R. Kschischang, B. J. Frey, and H.-A. Loeliger, "Factor graphs and the sum–product algorithm", *IEEE Transactions Information Theory*, vol. 47, no. 2, pp. 498–519, Feb. 2001.
- [21] H. A. Loeliger, "Some remarks on factor graphs", in *Proceedings 3rd International Symposium on Turbo Codes and Related Topics, Brest, France*, pp. 111-115, 1-5, Sep. 2003.

- [22] H. A. Loeliger, "An introduction to factor graphs", IEEE Signal Proceedings Magazine, vol. 21, No. 1, pp. 28-41, Jan. 2004.
- [23] T. Cover and J. Thomas, "Elements of Information Theory", 2006, Wiley-Interscience
- [24] A. Carleial, "A case where interference does not reduce capacity", IEEE Transactions on Information Theory, vol.21, no.5, pp.569,570, Sep. 1975.
- [25] S. Verdú, Multiuser Detection, Cambridge: Cambridge University Press, 1998
- [26] D. Tse and P. Viswanath, "Fundamentals of Wireless Communication", New York, NY: Cambridge University Press, 2005.
- [27] B. Rimoldi and R. Urbanke, "A rate-splitting approach to the Gaussian multiple-access channel", IEEE Transactions on Information Theory, vol. 42, no. 2, pp. 364–375, Feb. 1996.
- [28] P. Elias, "Coding for two noisy channels", in Proceedings 3rd London Symposium on Information Theory, London, U.K., pp. 61–76, 1955.
- [29] S. Lin and D. J. Costello Error Control Coding: Fundamentals and Applications, Prentice-Hall, 2004.
- [30] T. Richardson and R. Urbanke, "Modern Coding Theory", Cambridge University Press, 2008.
- [31] J.W. Lee, R. Urbanke, R.E. Blahut, "On the performance of turbo codes over the binary erasure channel", IEEE Communications Letters, vol.11, no.1, pp.67,69, Jan. 2007.
- [32] G. Kraidy, and V. Savin, "Irregular turbo code design for the binary erasure channel", 5th International Symposium on Turbo Codes and Related Topics, vol., no., pp.277-282, Sept. 2008.

- [33] T.J. Richardson, R.L. Urbanke, "Efficient encoding of low-density parity-check codes", IEEE Transactions on Information Theory, vol.47, no.2, pp.638,656, Feb. 2001.
- [34] H. Pishro-Nik, F. Fekri, "On decoding of low-density parity-check codes over the binary erasure channel", IEEE Transactions on Information Theory, vol.50, no.3, pp.439,454, Mar. 2004.
- [35] L. Xiao, T. Fuja, J. Kliewer and D. Costello, "Nested Codes with Multiple Interpretations", 40th Annual Conference on Information Sciences and Systems, Mar. 2006.
- [36] M. Hagh and M. R. Soleymani, "Raptor Coding for Non-Orthogonal Multiple Access Channels", IEEE International Conference on Communications, vol., no., pp.1–6, Jun. 2011.
- [37] G. Wu, S. Talwar, K. Johnsson, N. Himayat, and K. Johnson, "M2M: From mobile to embedded Internet", IEEE Communications Magazine, vol. 49, no. 4, pp. 36–43, Apr. 2011.
- [38] C. Perera, A. Zaslavsky, P. Christen, and D. Georgakopoulos, "Context aware computing for the Internet of Things: A survey", IEEE Communication Surveys Tutorials, vol. 16, no. 1, pp. 414–454, First Quarter 2014.
- [39] P. Mach, Z. Becvar, T. Vanek, "In-Band Device-to-Device Communication in OFDMA Cellular Networks: A Survey and Challenges", IEEE Communications Surveys & Tutorials, vol.PP, no.99, 2015.
- [40] A. Asadi, Q. Wang, V. Mancuso, "A Survey on Device-to-Device Communication in Cellular Networks", IEEE Communications Surveys & Tutorials, vol.16, no.4, pp.1801-1819, Fourth quarter 2014.

- [41] S. Sun, Q. Gao, W. Chen, R. Zhao, Y. Peng, "Recent progress of long-term evolution device-to-device in third-generation partnership project standardisation", IET on Communications, vol.9, no.3, pp.412-420, 2015.
- [42] X. Cheng, Y. Li, B. Ai, X. Yin, Q. Wang, "Device-to-device channel measurements and models: a survey", IET on Communications, vol.9, no.3, pp.312-325, 2015.
- [43] D. Feng, L. Lu, Y. Yuan-Wu, L. G. Shaoqian Li, G. Feng, "Device-to-device communications in cellular networks", IEEE Communications Magazine, vol.52, no.4, pp.49,55, Apr. 2014.
- [44] T. Koskela, S. Hakola, T. Chen, J. Lehtomäki, "Clustering Concept Using Device-To-Device Communication in Cellular System", IEEE Wireless Communications and Networking Conference (WCNC), 2010, vol., no., pp.1,6, 18-21 Apr. 2010.
- [45] B. Zhou, H. Hu, S. Huang, H. Chen, "Intracluster Device-to-Device Relay Algorithm With Optimal Resource Utilization", IEEE Transactions On Vehicular Technology, vol.62, no.5, pp.2315,2326, Jun. 2013.
- [46] B. Peng, T. Peng, Z. Liu, Y. Yang, C. Hu, "Cluster-Based Multicast Transmission for Device-to-Device Communication", IEEE 78th Vehicular Technology Conference (VTC Fall), 2013, vol., no., pp.1,5, 2-5 Sep. 2013.
- [47] M. Du, X. Wang, D. Wang, Y. Wang, "Device-to-Device Dynamic Clustering Algorithm in Multicast Communication", IEEE 11th international conference on Dependable, Autonomic and Secure Computing (DASC), vol., no., pp.578,582, 21-22 Dec. 2013.
- [48] M. Condoluci, L. Militano, G. Araniti, A. Molinaro, A. Iera, "Multicasting in LTE-A networks enhanced by device-to-device communications", IEEE Globecom Workshops, vol., no., pp.567,572, 9-13 Dec. 2013.

- [49] X. Wu, Y. Chen, X. Yuan, M. Mkiramweni, "Joint resource allocation and power control for cellular and device-to-device multicast based on cognitive radio", *IET on Communications*, vol.8, no.16, pp.2805-2813, 2014.
- [50] Y. Xu, Y. Liu, D. Li, "Resource management for interference mitigation in device-to-device communication", *IET on Communications*, vol.9, no.9, pp.1199-1207, 2015.
- [51] J. Zheng, R. Chen, Y. Zhang, "Dynamic resource allocation based on service time prediction for device-to-device communication underlying cellular networks", *IET on Communications*, vol.9, no.3, pp.350-358, 2015.
- [52] T. Zhou, B. Xu, T. Xu, H. Hu, L. Xiong, "User-specific link adaptation scheme for device-to-device network coding multicast", *IET on Communications*, vol.9, no.3, pp.367-374, 2015.
- [53] B. W. Khoueiry and M. R. Soleymani, "Destination cooperation in interference channels", in *Proceedings IEEE International Conference on Consumer Electronics*, Las Vegas, USA, Jan. 2012.
- [54] B. W. Khoueiry and M. R. Soleymani, "A novel destination cooperation scheme in interference channels", in *Proceedings IEEE Vehicular Technology Conference*, Vancouver, Canada, Sep. 2014.
- [55] B. W. Khoueiry and M. R. Soleymani, "A novel coding strategy for device-to-device communications", *12th Annual IEEE on Consumer Communications and Networking Conference (CCNC)*, vol., no., pp.200-205, 9-12 Jan. 2015.
- [56] X. Jin, A. W. Eckford, and T. E. Fuja, "Analysis of Joint Channel Estimation and LDPC Decoding on Block Fading Channels", in *Proceedings ISITA*, Parma, Italy, Oct. 2004.

- [57] H. Niu, M. Shen, J. A. Ritcey, and H. Liu, "A factor graph approach to iterative channel estimation and LDPC decoding over fading channels", *IEEE Transactions Wireless Communications*, Vol. 4, No. 4, pp. 1345-1350, Jul. 2005.
- [58] Z. Lin, Z. Yang, C. Pan, "Low-Complexity Joint Channel Estimation and LDPC Decoding for Block Fading Channel", *Asia-Pacific Conference on Communications, APCC* pp. 1–5, 2006.
- [59] I. Andriyanova, E. Biglieri, D. Declercq, "Joint Channel Estimation and Decoding of Root-LDPC Codes in Block-Fading Channels", *IEEE Global Communications Conference*, pp. 1 – 4, 2011.
- [60] T. J. Richardson and R. Urbanke, "The capacity of low-density parity check codes under message-passing decoding", *IEEE Transactions Information Theory*, vol. 47, no. 2, pp. 599–618, Feb. 2001.
- [61] Y. Zhu, D. Guo, M.L. Honig, "A message-passing approach for joint channel estimation, interference mitigation, and decoding", *IEEE Transactions on Wireless Communications*, pp. 6008 - 6018 Vol. 8, Issue 12, Dec. 2009.
- [62] M. Valenti and B. Woerner, "Iterative channel estimation and decoding of pilot symbol assisted Turbo codes over flat-fading channels", *IEEE Journal on Selected Areas Communications*, vol. 19, no. 9, pp.1697 -1705 2001.
- [63] M. Kwon, Y. H. Lee, M.-K. Oh, and H. D.-J. Park, "Iterative channel estimation and LDPC decoding with encoded pilots", *IEEE Transactions on Vehicular Technology*, vol. 57, pp. 273-285, Jan. 2008.

- [64] S. Majumder and S. Verma, "Joint channel estimation and decoding of Raptor code on fading channel", *Indian Journal of Computer Science and Engineering* vol.4, no.2, pp. 168-173, May 2013.
- [65] C. E. Shannon, "A mathematical theory of communication", in *Bell System Technical Journal*, The , vol.27, no.3, pp.379-423, Jul. 1948.
- [66] P. Wang, J. Xiao and L. Ping "Comparison of orthogonal and non-orthogonal approaches to future wireless cellular systems", *IEEE Vehicular Technology Magazine*, vol. 1, no. 3, pp.4-11 2006.
- [67] K.S. Gilhousen, I.M. Jacobs, R. Padovani, A.J. Viterbi, L.A. Weaver, Jr., and C.E. Wheatley, III, "On the capacity of a cellular CDMA system", *IEEE Transactions Vehicular Technology*, vol. 40, no. 2, pp. 303–312, May 1991.
- [68] F. Brannstrom, T.M. Aulin, and L.K. Rasmussen, "Iterative detectors for trellis-code multiple-access", *IEEE Transactions on Communications*, vol. 50, no. 9, pp. 1478–1485, Sep. 2002.
- [69] L. Liu, J. Tong, and Li Ping, "Analysis and optimization of CDMA systems with chip-level interleavers", *IEEE Journal on Selected Areas in Communications*, vol. 24, no. 1, pp. 141–150, Jan. 2006.
- [70] E. C. Van Der Meulen, "Three-terminal communication channels", *Advances in Applied Probability*, pp. 120–154, 1971.
- [71] T. Cover and A. El-Gamal, "Capacity theorems for the relay channel", *IEEE Trabsactions on Information Theory*, pp. 572 – 584, Sep. 1979.
- [72] G. Kramer, I. Maric and R. D. Yates "Cooperative communications", *Found. Trends Networking*, vol.1, no. 3, pp.271-425, 2006.

- [73] J. N. Laneman, D. N. C. Tse, and G. W. Wornell, "Cooperative diversity in wireless networks: Efficient protocols and outage behavior", *IEEE Transactions on Information Theory*, vol. 50, no. 12, pp. 3062-3080, Dec. 2004.
- [74] B. Schein and R. Gallager, "The gaussian parallel relay network", *Proceedings IEEE International Symposium on Information Theory*, pp. 22, 2000.
- [75] B. E. Schein, "Distributed coordination in network information theory", PhD thesis, Massachusetts Institute of Technology, 2001.
- [76] S.S.C. Rezaei, S.O. Gharan, and A.K. Khandani, "A new achievable rate for the Gaussian parallel relay channel", *IEEE International Symposium on Information Theory*, pp. 194–198, 2009.
- [77] P. Popovski and H. Yomo, "The anti-packets can increase the achievable throughput of a wireless multi-hop network, " in *Proceedings IEEE International Conference on Communications*, Istanbul, Turkey, pp. 3885-3890, Jun. 2006.
- [78] S. Katti, H. Rahul, W. Hu, D. Katabi, M. Médard, and J. Crowcroft, "XORs in the air: practical wireless network coding", in *Proceedings Conference on Applications, Technologies, Architectures, and Protocols for Computer Communications (SIGCOMM)*, Pisa, Italy, pp. 397–408, Sep. 2006.
- [79] S. Zhang, S. Liew, and P. P. Lam, "Physical-layer network coding", in *Proceedings 12th Annual International Conference on Mobile Computing and Networking (MobiCom)*, Los Angeles, CA, pp. 358–365, Sep. 2006.
- [80] L. Ong , S. J. Johnson and C. M. Kellett "An optimal coding strategy for the binary multiway relay channel", *IEEE Communication Letter*, vol. 14, no. 4, pp.330 -332, 2010.

- [81] A. El-Gamal and M. Aref, "The capacity of the semideterministic relay channel", IEEE Transactions on Information Theory, pp.536 – 536, May 1982.
- [82] A. Reznik, S.R. Kulkarni, and S. Verdu, "Degraded gaussian multirelay channel: capacity and optimal power allocation", IEEE Transactions on Information Theory, pp.3037– 3046, 2004.
- [83] L.-L. Xie and P.R. Kumar, "An achievable rate for the multiple-level relay channel", IEEE Transactions on Information Theory, pp. 1348 –1358, 2005.
- [84] A. El Gamal and S. Zahedi, "Capacity of a class of relay channels with orthogonal components", IEEE Transactions on Information Theory, pp.1815 –1817, May 2005.
- [85] A. El Gamal, M. Mohseni, and S. Zahedi, "Bounds on capacity and minimum energy-perbit for awgn relay channels", IEEE Transactions on Information Theory, pp.1545– 1561, 2006.
- [86] A.D. Wyner and J. Ziv, "The rate-distortion function for source coding with side information at the decoder", IEEE Transactions on Information Theory, pp.1–10, 1976.
- [87] Y. Liang, V.V. Veeravalli, and H.V. Poor, "Resource allocation for wireless fading relay channels: Max-min solution", IEEE Transactions on Information Theory, pp. 3432 –3453, 2007.
- [88] A. Host-Madsen and Junshan Zhang, "Capacity bounds and power allocation for wireless relay channels", IEEE Transactions on Information Theory, pp. 2020–2040, 2005.
- [89] G. Kramer, M. Gastpar, and P. Gupta, "Cooperative strategies and capacity theorems for relay networks", IEEE Transactions on Information Theory, pp. 3037 – 3063, 2005.
- [90] T.M. Cover and Y. Kim, "Capacity of a class of deterministic relay channels", IEEE International Symposium on Information Theory, pp. 591–595, 2007.

- [91] Y. Kim, "Capacity of a class of deterministic relay channels", IEEE Transactions on information Theory, pp.1328–1329, 2008.
- [92] P. Mitran, H. Ochiari, and Vahid Tarokh, "Space-time diversity enhancements using collaborative communications", IEEE Transactions on information Theory, pp. 2041–2057, 2005.
- [93] D. Slepian and J.K. Wolf, "Noiseless coding of correlated information sources", IEEE Transactions on information Theory, pp. 471–480, 1973.
- [94] D. Gunduz, A. Yener, A. Goldsmith and H. Poor "The multiway relay channel", IEEE Transactions on Information Theory, vol. 59, no. 1, pp.51-63, 2013.
- [95] B. Rankov and A. Wittneben, "Spectral efficient protocols for half-duplex fading relay channels", IEEE Journal on Selected Areas in Communications, vol.25, no.2, pp.379-389, 2007.
- [96] R. Ahlswede, N. Cai, S. R. Li and R. W. Yeung, "Network information flow", IEEE Transactions on Information Theory, vol. 46, no. 4, pp.1204 -1216, 2000.
- [97] D. S. Lun, M. Médard, and R. Koetter, "Efficient operation of wireless packet networks using network coding", in Proceedings International Workshop on Convergent Technologies (IWCT), 2005.
- [98] Y. Wu, P. A. Chou and S. Kung "Information exchange in wireless networks with network coding and physical-layer broadcast", Proceedings. Conference on Information Science and Systems, 2005.
- [99] S. Zhang, S. C. Liew, P. P. Lam, "Hot Topic: Physical-layer Network Coding", ACM Proceedings of the 12th annual international conference on Mobile computing and networking, pp. 358-365, 2006.

- [100] B. Nazer and M. Gastpar, "Computing over multiple-access channels with connections to wireless network coding", Proceedings IEEE International Symposium Information Theory, pp.1354 -1358, 2006.
- [101] B. Nazer and M. Gastpar, "Reliable physical layer network coding", Proceedings IEEE, pp.438 -460, 2011.
- [102] D. J. C. MacKay, and R. M. Neal, "Near Shannon limit performance of low density parity check codes", Electronics Letters , vol.33, no.6, pp.457–458, Mar. 1997.
- [103] T.J. Richardson, M.A. Shokrollahi, R.L. Urbanke, "Design of capacity-approaching irregular low-density parity-check codes", IEEE Transactions on Information Theory, vol.47, no.2, pp.619–637, Feb. 2001.
- [104] C. Berrou, A. Glavieux, "Near optimum error correcting coding and decoding: turbo-codes", IEEE Transactions on Communications, vol.44, no.10, pp.1261–1271, Oct. 1996.
- [105] J.W. Lee, R. Urbanke, R.E. Blahut, "On the performance of turbo codes over the binary erasure channel", IEEE Communications Letters, vol.11, no.1, pp.67–69, Jan. 2007
- [106] G. Kraidy, V. Savin, "Capacity-Approaching Irregular Turbo Codes for the Binary Erasure Channel", IEEE Transactions on Communications, vol.58, no.9, pp.2516–2524, Sep. 2010.
- [107] M. Tanner, "A recursive approach to low complexity codes", IEEE Transactions on Information Theory, vol. IT-27, pp.533–547, 1981.
- [108] A. Shokrollahi, "New sequences of linear time erasure codes approaching the channel capacity", Proceedings 13th Conference Applied Algebra and Error Correcting Codes, no.1719, pp.65–76, 1999.
- [109] J. Byers, M. Luby, M. Mitzenmacher, and A. Rege, "A digital fountain approach to reliable distribution of bulk data", Proceedings ACM SIGCOMM'98, 2–4 Sep. 1998.

- [110] M. Luby, M. Mitzenmacher, A. Shokrollahi, D. Spielman, "Efficient Error Correcting Codes", IEEE Transactions on Information Theory, Vol. 47, Issue 2, pp. 569-584, Feb. 2001.
- [111] M. Luby, "LT codes", in Proceedings 43rd. Annu. IEEE Symposium Found. Computer Science, Vancouver, BC, Canada, pp. 271-280, Nov. 2002.
- [112] A. Shokrollahi and M. Luby, "Raptor Codes", Foundations and Trends in Communications and Information Theory, vol. 6, no. 3-4, pp. 213-322, 2009.
- [113] A. Shokrollahi, "LDPC Codes: An Introduction, in Coding, Cryptography and Combinatorics", Computer Science & Applied Logic, pp. 85-110, 2004.
- [114] O. Etesami and A. Shokrollahi, "Raptor codes on binary memoryless symmetric channels", IEEE Transactions Information Theory, 52(5):2033-2051, May 2006.
- [115] ETSI TR 102 935 V2.1.1, "Machine-to-Machine communications: Applicability of M2M architecture to Smart Grid Networks; Impact of Smart Grids on M2M platform", Technical Report, 2012.
- [116] A. Zanella, N. Bui, A. Castellani, L. Vangelista, and M. Zorzi, "Internet of Things for Smart Cities", IEEE Journal on Internet of Things, vol.1, no.1, pp.22-32, Feb. 2014.
- [117] N. Skeledzija, J. Cesic, E. Koco, V. Bachler, H. N. Vucemilo, H. Dzapo, "Smart home automation system for energy efficient housing", in Information and Communication Technology, Electronics and Microelectronics (MIPRO), 2014 37th International Convention on , vol., no., pp.166-171, 26-30, May 2014.
- [118] K. Chen, "Machine-to-Machine Communications for Healthcare", Journal of Computing Science and Eng., Vol. 6, No. 2, pp. 119-126, Jun. 2012.

- [119] R. Leeb, L. Tonin, M. Rohm, L. Desideri, T. Carlson, and J.D.R. Millan, "Towards Independence: A BCI Telepresence Robot for People With Severe Motor Disabilities", IEEE Proceedings, vol.103, no.6, pp.969-982, Jun. 2015.
- [120] Z. Yongjun, Z. Xueli, Z. Shuxian and G. shenghui, "Intelligent transportation system based on Internet of Things", in World Automation Congress (WAC), 2012 , vol., no., pp.1-3, 24-28 Jun. 2012.
- [121] L. Zhang, J. Liu, and H. Jiang, "Energy-efficient location tracking with smartphones for IoT", IEEE conference on Sensors, vol., no., pp.1-4, 28-31 Oct. 2012.
- [122] H. Tschofenig, et al., "Architectural Considerations in Smart Object Networking", Technology no. RFC 7452. Internet Architecture Board, Mar. 2015.
- [123] www.bluetooth.com.
- [124] www.zigbee.org.
- [125] www.z-wave.com.
- [126] J. Proakis and M. Salehi, "Digital Communications", McGraw-Hill, New York, USA, 5th edition, 2008.
- [127] M. Hasan and E. Hossain, "Resource allocation for network-integrated device-to-device communications using smart relays", in Proceedings IEEE Globecom workshop, pp. 597–602, 2013.
- [128] T.S. Rappaport, J.N. Murdock, F. Gutierrez, "State of the Art in 60-GHz Integrated Circuits and Systems for Wireless Communications", in Proceedings of the IEEE , vol.99, no.8, pp.1390-1436, Aug. 2011.
- [129] H. V. Poor, "An Introduction to Signal Detection and Estimation", 2nd Edition, Springer, 1998.

- [130] S. Katti, H. Rahul, H. Wenjun; D. Katabi, M. Medard, J. Crowcroft, "XORs in the Air: Practical Wireless Network Coding", in IEEE/ACM Transactions on Networking, vol.16, no.3, pp.497-510, Jun. 2008.
- [131] W. C. Jakes, Microwave Mobile Communications, :Wiley, 1974.
- [132] K. Baddour and N. Beaulieu "Autoregressive modeling for fading channel simulation", in IEEE Transactions on Wireless Communications, vol. 4, pp.1650 -1662, 2005.